

---

# Field control of magnonic heat flow in square lattice Heisenberg antiferromagnets

Von der Fakultät für Elektrotechnik, Informationstechnik,  
Physik der Technischen Universität Carolo-Wilhelmina zu  
Braunschweig

zur Erlangung des Grades eines Doktors der  
Naturwissenschaften (Dr. rer. nat.)  
genehmigte Dissertation

von

Benjamin Köhler

aus Leipzig

**eingereicht am:** 01.08.2022

**Disputation am:** 26.01.2023

**1. Referent:** Prof. Dr. Wolfram Brenig

**2. Referentin:** Prof. Dr. Gertrud Zwicknagl

**Druckjahr** 2023







---

**Köhler, Benjamin**

Field control of magnonic heat flow in square lattice Heisenberg antiferromagnets, Institute for Theoretical Physics

Technische Universität Braunschweig, February 2023

*Dedicated to my best friends Franz Albert Eysoldt (1990-2016) and my father Frank-Martin Köhler (1962-2016) who unfortunately did not see the end of this work*



# Acknowledgement

It is said that it takes a village to raise a child. This is definitely true for finishing a Ph.D. Although I had to write this text on my own, many people supported me in this process. This is the place where I want to take the opportunity to thank the most important people.

My advisor Prof. Dr. Wolfram Brenig gave me the opportunity and supported me in my ambition to start working in a completely new field of physics. He accelerated my learning with numerous early meetings where I was allowed to ask many questions and where he guided me to the most relevant topics. I admire his ability to explain complicated issues only using basic concepts of physics. I profited from this ability many times when we were discussing my results. When I left the university to start a new position in industry, I realised how much I took from my time working under the supervision of Prof. Brenig. I tried to adopt his way of finding a way into the thoughts of someone else by asking simple questions and getting to the bottom of the issue. He also taught me many polite ways to disagree with someone. I have grown very much as a person and a physicist because of him. This is a very wonderful gift for which I am extremely thankful.

I owe a big thank you to every member of Prof. Brenig's condensed matter theory group. Each one of them was open to discuss my or their work. During my first year in Braunschweig, Boris Celan helped me to understand the basic principles of spin wave theory and diagrammatic methods to evaluate correlation functions. Despite being busy finishing his own thesis, he never sent me away. This kindness helped me set foot in my new environment.

When I had a question or idea that was not developed enough to present to Prof. Brenig, Dr. Alexandros Metavitsiadis was my go-to person. His open and friendly manner allows anyone to be unafraid to approach him. He listened to my worries many times and he ensured me that such things are normal during a Ph.D.

Dr. Niklas Casper visited me in my office many times while getting coffee. It is rare to find someone as down-to-earth and funny in theoretical physics as him. He made me smile many times when I had been upset just moments ago. I value him being honest to admit when he is unsure how to solve a problem and asking for help and being very generous with his profound knowledge. Together we learned

many new things because our skill sets complemented each other and we are like-minded. I especially thank him for always resolving my IT-related problems fast and without any ridicule.

During my last year in Braunschweig, I shared my office with Alexander Schwenke. His company made the days run by fast. I liked to have someone to discuss ideas with. I hope he profited from this opportunity as much as I did.

Erik Wagner's comments during our practise talks and poster presentations were always very insightful. He is very diligent with his work. Everything he says and does is well thought about. His ability to pick up the ideas of others is outstanding.

Finally, I want to thank Miss Baron who manages the theoretical physicists that deal with things below and beyond the Van Allen belt. Her help with the bureaucracy did not just enable me to get back to the work I love so much, but also everyone else.

A sound mind needs a sound body. My friends Dr. Savutjan Sidik and Evrard-Ouicem Eljaouhari accompanied me to the pool every Friday evening after work. I needed this motivation to do something other than running. The evenings when we cooked dinner for each other or visited the best falafel place in Braunschweig and exchanged war stories have been a wonderful conclusion to the week of working in the office and start to working at home. I hope our friendship remains for the rest of our lives.

After I left the university, I found two of the most amazing colleagues in Susanne Arndt and Hagen Borstell. Both welcomed me very warmly, helped me find my place in the company, and enabled me to contribute to many interesting projects. During the two years we have been through many tough situations and have solved many problems as a team. I was always able to count on their support. Many times they helped me to make my ideas become reality and even though they might not have understood all of my thought process, they trusted me. I think that our relationship went beyond what is usual for people working together. Without Susann and Hagen I would not have the strength to work on the thesis after the week at the company. Hopefully, they enjoyed working with me as much as I did with them.

The seven years it took me to finish this work have been the hardest ones for me on a personal level too. I am very thankful to my family. My mother is a constant source of encouragement. I know it has been a very tough time for her too and I am glad that she did not despair despite our mutual misfortune. I tried my best to support her too, but she surely did much more for me. Without her, I could not have come so far. I will probably never be able to pay her back, but I know that seeing me finish this thesis means at least as much to her as it means to me.

My sister is the person after me who read this thesis the most times. For someone

---

who has no deep knowledge in theoretical physics and probably no interest to acquire one, this is a feat in itself. I thank her for never complaining and always giving me her feedback on the language very fast. The thesis became much better and more readable thanks to her comments. I think that I have the best big sister in the world. From my childhood on, I am proud to have such an intelligent, funny, and kind sister. I hope we will be close for the rest of my life.

My sister also introduced me to my nephew Milan. He is in my life for as long as I am a Ph.D. student. While I am leaving my academic career, his has just started. I hope to be able to help him through it so that it will not be as hard for him as it has been for me. Whatever profession he pursues, he can count on my help.

—

# Abstract

The utilisation of the spin degree of freedom for the transfer of information has become a key interest in modern microtechnology. In this work I investigate the influence of magnetic and electric fields on the spin system's ability to transport heat. I consider a two-dimensional square lattice with nearest neighbour antiferromagnetic Heisenberg interaction. Using a Green's function approach and the Kubo formula, I derive expressions which relate the thermal conductivity to the magnetic excitation's mobility, heat capacity, and their lifetime. All three of these properties are affected by the external fields which I consider. The fields break  $SU(2)$  symmetry, so that one of the acoustic branches becomes a gapped optical one. This energy gap is the most significant contribution to the alteration of the thermal conductivity in the low-temperature limit, where the optical modes can not be excited and the thermal transport is carried by acoustic magnons. For a higher temperature, other parts of the magnon spectrum become important. Then the momentum-dependence of the magnons' lifetime as well as the effect of the field on the magnon dispersion is crucial for the evolution of the thermal transport.

In the first part of this work I consider a magnetic field which is homogeneously applied to the system. I focus on the effect of field-induced inter-magnon scattering which reduces their lifetime. I find that the temperature-independent spontaneous decay processes drastically reduce the magnetic thermal conductivity. Such processes occur only beyond a specific strength of the field. Spontaneous magnon decay reduces the lifetime of a large proportion of magnon modes and, as a result, also the thermal conductivity. The effects of spontaneous magnon decay can be expected to be experimentally observable for materials with a high contribution of magnetic excitations to the thermal transport. In the second part of this thesis I consider the effect of an electric field which is applied homogeneously to the whole system and only to a finite spatial region. Because the electric field leads to the emergence of an additional Dzyaloshinskii-Moriya (DM) interaction, it can be used to change the magnetic order, too. The DM-vectors caused by the electric field are anisotropic, i.e. their direction is different for the individual crystallographic directions. This anisotropy is also observed in the magnetic order of the

classical ground state, the magnon spectrum, as well as in the thermal conductivity. Due to the broken translational invariance in the inhomogeneous setup, linear spin wave theory has to be used in real- instead of in momentum-space to obtain the magnon spectrum. I use numerical procedures to determine the thermal conductivity on a finite lattice. My results show that the inhomogeneity introduces additional scattering. This reduces the conductivity further with respect to the homogeneous setup. It turns out that, because the gap opens for short-wavelength magnons, the size of the region where the field applied to is more or less inessential. It is therefore possible to control the thermal transport by the electric field's strength. These results might be interesting for the further development of spintronic applications.

# Zusammenfassung

In dieser Arbeit habe ich den Einfluss von magnetischen und elektrischen Feldern auf die Fähigkeit des Spinsystems Wärme zu leiten untersucht. Ich habe ein zweidimensionales Quadratgitter mit antiferromagnetischer nächstnachbar Heisenberg-Wechselwirkung betrachtet. Durch Anwendung von Green's-Funktionen und der Kubo-Formel konnte ich Beziehungen herleiten, die die thermische Leitfähigkeit mit charakteristischen Eigenschaften der magnetischen Anregungen in Zusammenhang bringen. Diese Eigenschaften können mit den untersuchten externen Feldern beeinflusst werden. Sie heben die Entartung zwischen zwei akustischen Magnonästen auf. Aus einem wird ein optischer Ast mit feldabhängiger Energielücke und aus dem anderen ein akustischer mit feldabhängiger Geschwindigkeit. Letztere hat den größten Einfluss auf die thermische Leitfähigkeit im Grenzfall niedriger Temperaturen, bei dem die optischen Moden noch nicht angeregt werden können und der Großteil des Wärmetransportes von akustischen Anregungen getragen wird. Bei höheren Temperaturen ist die Impulsabhängigkeit der Magnonlebenszeit sowie der Effekt des Feldes auf die Dispersion in anderen Regionen entscheidend dafür, wie sich die thermische Leitfähigkeit entwickelt.

Im ersten Teil der Arbeit habe ich den Effekt eines magnetischen Feldes untersucht, welches homogen im gesamten System angelegt wird. Hier wurden Magnon-Magnon-Streuprozesse berücksichtigt, die durch das Magnetfeld verursacht werden und die Magnonlebensdauer senken. Ich habe ermittelt, dass die temperaturunabhängigen spontanen Zerfallsprozesse die thermische Leitfähigkeit drastisch reduzieren. Diese Prozesse treten jedoch erst oberhalb einer spezifischen Magnetfeldstärke auf. Durch spontane Zerfallsprozesse, welche erst ab einer kritischen Feldstärke stattfinden, sinkt die Lebensdauer einer Vielzahl von Magnonmoden und damit auch die thermische Leitfähigkeit. Der zweite Teil dieser Arbeit betrachtet die Auswirkungen eines elektrischen Feldes auf die thermische Leitfähigkeit. Da dieses Feld zum Auftreten einer zusätzlichen Dzyaloshinskii-Moriya (DM)-Wechselwirkung führt, ist es geeignet, die magnetische Ordnung zu beeinflussen. Die DM-Vektoren zeigen in unterschiedliche Richtungen. Die hiermit einhergehende Anisotropie hat Auswirkungen auf die thermische Leitfähigkeit. Für den Fall gebrochener Translationsinvarianz führte ich die lineare Spinwellen-

theorie im Real- statt im Impulsraum durch. Ich wandte numerische Verfahren an, um die thermische Leitfähigkeit auf einem endlichen Gitter zu berechnen. Meine Resultate zeigen, dass durch Anlegen des elektrischen Feldes in einem räumlich beschränkten Bereich eine zusätzliche Quelle für Streuung entsteht, was im Vergleich zum homogenen Fall die thermische Leitfähigkeit noch weiter reduziert. Es zeigt sich, dass das elektrische Feld nur in einer kleinen Region angelegt werden muss, um die selben Effekte wie für das homogene System zu erreichen. Damit kann der Wärmetransport in einem magnetischen Material durch Anlegen eines elektrischen Feldes in einer kleinen Region gesteuert werden. Dies ist insbesondere für die Weiterentwicklung spintronischer Anwendungen interessant.

# Contents

1. Introduction	1
<b>I. Preliminaries</b>	<b>9</b>
2. Thermal transport	11
2.1. Principle of thermal transport measurements . . . . .	11
2.2. Thermal transport in magnetic materials . . . . .	13
3. Quantum magnetism	17
3.1. The Hubbard and the Heisenberg model . . . . .	18
3.2. Magnetic order in the Heisenberg model . . . . .	24
4. Linear response theory and transport coefficients	29
<b>II. Field control of magnonic heat flow</b>	<b>35</b>
5. Control of magnonic heat flow by a magnetic field	37
5.1. General theory of magnonic thermal conductivity . . . . .	38
5.1.1. Linear spin-wave theory . . . . .	38
5.1.2. Linear response theory . . . . .	43
5.2. Thermal conductivity using empiric lifetimes . . . . .	48
5.2.1. Contribution of acoustic and optic modes as a function of the magnetic field . . . . .	48
5.2.2. Thermal conductivity with temperature-independent scat- tering . . . . .	52
5.2.3. Thermal conductivity with magnon-phonon scattering . .	57
5.3. Considering magnon-magnon scattering rates . . . . .	62
5.3.1. Leading 1/S corrections . . . . .	63
5.3.2. Spontaneous magnon decay . . . . .	67

---

5.3.3. Finite temperature decay . . . . .	73
5.3.4. Resulting magnonic thermal conductivity . . . . .	75
5.4. Summary . . . . .	81
<b>6. Electric field control of the magnetic thermal conductivity</b>	<b>85</b>
6.1. Homogeneous electric field in entire system . . . . .	87
6.1.1. Magnetic ground state . . . . .	87
6.1.2. Magnetic excitation spectrum . . . . .	91
6.1.3. Thermal conductivity . . . . .	93
6.2. Electric field in finite region . . . . .	97
6.2.1. Magnetic ground state and spectrum . . . . .	98
6.2.2. Thermal conductivity . . . . .	100
6.3. Summary . . . . .	112
<b>7. Conclusion</b>	<b>115</b>

### **III. Appendix** **123**

<b>A. Matsubara-Green's functions</b>	<b>125</b>
A.1. Definition . . . . .	125
A.2. Wick's theorem and diagrammatic evaluation . . . . .	127
A.3. Real-time Green's functions and transport coefficients . . . . .	131
<b>B. Current operator from the energy density for an electric field induced Dzyaloshinskii-Moriya interaction</b>	<b>133</b>
<b>C. Influence of the Dzyaloshinskii-Moriya interaction on the magnonic heat flow</b>	<b>137</b>
C.1. Magnonic thermal conductivity in a system with homogeneous Dzyaloshinskii-Moriya interaction . . . . .	138
C.1.1. Magnetic ground state . . . . .	138
C.1.2. Magnetic excitations . . . . .	140
C.1.3. Current operator . . . . .	143
C.1.4. Thermal conductivity . . . . .	143
C.2. Magnonic thermal conductivity in a system with a spatially confined Dzyaloshinskii-Moriya interaction . . . . .	146
C.3. Summary . . . . .	153

# List of Figures

2.1.	Sketch of thermal transport measurement . . . . .	12
2.2.	Sketch of the qualitative temperature dependence of the thermal conductivity due to magnons . . . . .	15
3.1.	Sketch of kinetic exchange and superexchange processes . . . . .	22
3.2.	Sketch of superexchange leading to a finite Dzyaloshinskii-Moriya interaction and its control by an electric field . . . . .	23
3.3.	Goldstone modes in systems with and without a finite magnetic field	26
4.1.	The relaxation of a current and the relation to transport coefficients	32
4.2.	Diagrammatic representation of the transport bubble . . . . .	33
5.1.	The spin configuration of a Heisenberg antiferromagnet in the presence of a magnetic field with minimal classical energy . . . . .	41
5.2.	Magnon dispersion for different magnetic fields . . . . .	44
5.3.	Contour for the evaluation of the Matsubara sum . . . . .	46
5.4.	Heat capacity $c_k$ of a single magnon mode in the optical approximation . . . . .	50
5.5.	Contribution of an acoustic mode to the thermal transport as a function of its velocity . . . . .	51
5.6.	Contribution of acoustic magnons to the thermal transport as a function of the external magnetic field . . . . .	52
5.7.	Thermal conductivity as a function of temperature for different values of the external magnetic field . . . . .	54
5.8.	Reduced thermal conductivity around the $M$ -point and around the $\Gamma$ -point for different magnetic fields . . . . .	55
5.9.	Thermal conductivity as a function of the external magnetic field with impurity scattering only . . . . .	57
5.10.	Thermal conductivity over temperature with empiric expressions for grain-boundary and magnon-phonon scattering for different external magnetic fields . . . . .	59

5.11.	The maximum of the thermal conductivity with empiric expressions for grain-boundary and magnon-phonon scattering and the temperature at which it is reached in as a function of the external magnetic field . . . . .	61
5.12.	Frequency-independent renormalisation of the canting angle and the magnon spectrum due to cubic terms . . . . .	66
5.13.	Spontaneous magnon decay processes . . . . .	68
5.14.	Region of unstable magnon modes for different magnetic fields . .	69
5.15.	The free magnon dispersion and the scattering rate from spontaneous magnon decay . . . . .	70
5.16.	Rates of spontaneous magnon decay at different magnetic fields . .	71
5.17.	Temperature-dependent magnon scattering process . . . . .	73
5.18.	Magnon scattering rates at different magnetic fields . . . . .	74
5.19.	Full magnon-magnon scattering rate for different temperatures, the grain-boundary scattering rate, and the magnon dispersion along a specific path through the first Brillouin zone . . . . .	76
5.20.	Thermal conductivity taking into account magnon-magnon scattering as a function of temperature for different external magnetic fields . . . . .	77
5.21.	Thermal conductivity as a function of the external magnetic field with and without magnon-magnon scattering at different temperatures . . . . .	79
6.1.	Distribution of the Dzyaloshinskii-Moriya vectors for a system with an electric field in z-direction . . . . .	88
6.2.	Comparison of the ground state energy $E_g$ of different spin textures as a function of the electric field . . . . .	90
6.3.	Magnon dispersion for different electric fields . . . . .	92
6.4.	Reduced thermal conductivity for different electric fields . . . . .	95
6.5.	Thermal conductivity as a function of temperature for different electric fields . . . . .	96
6.6.	Thermal conductivity as a function of the electric field's strength for different temperatures . . . . .	97
6.7.	Schematic sketch of magnetic thermal field effect transistor . . . . .	98
6.8.	Spin texture of magnetic ground state in electric field heterostructure	99
6.9.	Density of states for different system geometries and strengths of the electric field . . . . .	103
6.10.	Frequency dependence of the thermal conductivity for different system sizes . . . . .	106

6.11.	Thermal conductivity in a inhomogeneous system as a function of the area an electric field is applied to . . . . .	108
6.12.	Electric field dependence of the thermal conductivity in a inhomogeneous system . . . . .	110
6.13.	Temperature dependence of the thermal conductivity in a inhomogeneous system . . . . .	111
A.1.	Contour integration for the evaluation of Matsubara sums . . . . .	130
C.1.	Configuration of the atoms involved in the superexchange process leading to staggered Dzyaloshinskii-Moriya vectors . . . . .	139
C.2.	Magnon dispersion for different strengths of the Dzyalo-shinskii-Moriya interaction . . . . .	141
C.3.	Comparison of the Dzyaloshinskii-Moriya interaction related energy gap in a system with staggered order and a system spiral order	143
C.4.	Thermal conductivity as a function of the intrinsic Dzyaloshinskii-Moriya interaction and of the ambient temperature . . . . .	144
C.5.	Thermal conductivity perpendicular to a barrier as a function of the latter's length at different temperatures . . . . .	147
C.6.	Thermal conductivity as a function of frequency for different sizes of the intermediate barrier . . . . .	149
C.7.	Thermal conductivity as a function of the length of the intermediate barrier at different temperatures . . . . .	150
C.8.	Thermal conductivity as a function of the Dzyaloshinkii-Moriya-interaction's strength for different lengths of the intermediate barrier	151
C.9.	Thermal conductivity as a function of temperature for different magnitudes of the Dzyaloshinskii-Moriya-interaction's strength in a inhomogeneous system . . . . .	152



# 1. Introduction

Solid state systems are the foundation of modern technology. They created unprecedented comfort and the possibility of quickly exchanging information. This was made possible by the utilisation of the electron's charge degree freedom. It allows to transport energy from one place to another via wires, communicate over longer distances with telegraphs, telephones, and the internet, store information on hard drives and build powerful computers that can help with tedious tasks. Without doubt, the use of electronics improved living conditions. At the same time, the high energy consumption of those devices is an issue. Increasing their efficiency even slightly means a great advancement.

To achieve this goal and keep the functionality of the existing technology, quantum mechanics needs to be employed. Here, one finds interesting and useful effects such as the tunnelling of particles into classically forbidden regions or the observation of quantised measurement results. Such quantum effects do not usually appear in systems of macroscopic size, but on a nanometer-scale or below. The functionality of these small systems can not be based on mechanical manipulation. Instead, microscopic contacts are used which allow for fields or injected currents to ensure the desired effect. Applications with new functionalities can be developed with a deeper understanding of the interaction of the systems with these contacts. There are many interesting quantum systems with low dimension such as quantum dots and nanowires, and systems with a quasi two-dimensional interaction. Among the many quantum degrees of freedom that can be found in these systems, the spin is interesting in particular: There is no known classical analogue for it and it is involved in many exciting phenomena in aforementioned systems.

From a technological standpoint, considering the spin-degree of freedom is beneficial, too. Although electronic logic parts have become smaller over time allowing Moore's law to hold over a respectable period, the energy consumption of those parts has, on the other hand, skyrocketed. A well known issue therefore is that the inevitably produced heat can not be kept at or conducted to a region where it is usable or can be stored. Using the spin instead of the charge degree of freedom can be an considerable improvement [1]: Firstly, spintronic transport can be controlled

by a lower switching voltage and switching energy in comparison to electronic transport. This leads to a much higher possible switching frequency and energy efficiency while a spintronic device is in operation or in stand by mode. Secondly, the logic density of spintronic devices is much higher. Hence, spintronic devices allow for a faster and more energy-efficient way to switch their densely packed logic gates. Replacing electronics with spintronics appears to be a step to not just faster technology, but also to more energy efficiency. This includes practical fields like sensors, communication and medical technology.

Although the main focus is on systems with itinerant magnetism today, using insulating materials with localised magnetic moments is feasible, too. In fact, the first use of spin for technological purposes was for  $\text{Y}_3\text{Fe}_5\text{O}_{12}$  (YIG) [2]. This material is an insulator with localised magnetic moments and a low damping of their excitations. As a result the propagation of spin-waves can be observed over centimetre distances which makes the material ideal for microwave magnetic technologies and, hence, YIG is the go-to material to explore the basic functionalities and possible realisations of so-called magnonic devices [2]. These applications include, e.g. the magnon transistor and logic gate [2–4]. Magnonic devices can be integrated into electronic as well as photonic technologies and allow for fast reprogramming [5]. The information carrying spins can be manipulated without a current [2]. It is possible to realise magnonic logic gates [6, 7] that recreate their electric counterparts while at the same time having a lower energy consumption or allowing for conversion of waste heat into electric voltages [8, 9], having a high potential for miniaturisation [10], and giving access to more potent wave-based computing concepts [11]. All this makes magnonic devices a possible key technology for the future.

The improvement of the quality of YIG samples and the integration into different substrates is subject of ongoing research [12, 13]. Unfortunately, high-quality YIG-films can not be grown on silicon and therefore integration of magnonic YIG-devices into semiconductor technology is complicated [14]. Hence, new substrates or magnonic materials are needed. Antiferromagnetic materials are discussed as such materials as they allow to use a higher spin-wave frequency and, hence, faster processing and storage of the information [15]. To make use of the advantages, new ways to manipulate spin-waves in antiferromagnets need to be developed and the micromagnetic modelling has to be extended beyond the classical Landau-Lifshitz-Gilbert equation [16] to take into account quantum-mechanical effects and coupling to other excitations [5]. In this thesis, I investigate such possibilities by looking at materials with localised magnetic moments and a small spin quantum number, so that the quantum nature of the spin plays an important role. The main idea is to control their contribution with an external field by changing their

mobility and scattering. The control of such a magnetic contribution to thermal transport might open new paths to technological applications.

An important question is whether the contribution of magnetic excitations in quantum magnets is a factor that needs to be regarded as important for the overall thermal transport. Usually, the contribution of magnetic excitations is small compared to the electronic or lattice contribution. In the material class of cuprates, the spin-excitation spectrum is well described by several different spin models. Low-dimensional spin-systems like spin-chains, -ladders, and -planes are realised where the contribution of magnetic excitations is large and can exceed the thermal conductivity of metals [17]. An antiferromagnetic square lattice is realised, e.g. in  $\text{La}_2\text{CuO}_4$  where many thermal transport measurements have been performed and a high contribution of magnetic excitations has been observed [18–23].

For such materials where the magnetic thermal transport is comparable to other contributions, one might be interested in manipulating the properties of the magnetic excitation. On the one hand, this can have technological reasons. It is conceivable that, e.g. by complicating their propagation, the materials' properties can be controlled. On the other hand, additional information can be gained about the fundamental properties of the excitations, most importantly their interactions, and indirectly about their wavelength or velocities. A simple approach to affect the magnetic thermal transport might be to use the anisotropy in low-dimensional systems or to exchange the magnetic atoms with non-magnetic ones by doping. In contrast to this, by using an external field, the ability of the material to transport energy can be quickly and reversibly changed. There are early works studying the effect of a magnetic field on the thermal conductivity of ferromagnetic materials as a result of enhanced magnon-phonon interaction [24] or insulators doped with magnetic impurities [25]. The idea proposed in this thesis of using the field to actively control the thermal transport in magnetic materials, however, is new.

There are more fundamental reasons for studying thermal transport beside the interest in technological progress. It was studied from the beginning of modern solid state theory for phonons and electrons [26, 27]. Valuable information has been revealed about the generation, mobility, scattering, and dissipation of those (quasi-)particles. The contribution of the magnon as another quasiparticle to the thermal transport was predicted in 1936 [28]. Convincing experimental evidence was found in the 60s [29–32]. These experiments mainly focused on the mere identification of magnetic heat transport at low temperatures ( $T < 10\text{K}$ ) when the material is in a magnetically ordered phase. The first signature of magnetic thermal conductivity above the ordering temperature was found in a quasi-one-dimensional antiferromagnetic material. This result proved that no magnetic order is necessary in order to have magnetic contributions to the thermal conductivity. Ballistic heat

transport was predicted in spin-1/2 chains [33] and a huge magnetic contribution was found in quantum two-leg spin-1/2 ladders [34–36]. Most recently, fractionalised excitations which are signatures of topological order, such as spinons [37–39], monopoles [40], and itinerant Majorana fermions [41, 42] have been detected. The contribution of these new found excitations to the thermal transport in quantum magnets is an interesting field for technological as well as fundamental research.

The assumption of the magnon being a weakly interacting and long-lived excitation is justified for quantum magnets with collinear magnetic order [43, 44]. Because terms describing interactions between the magnons are quartic, the former are usually weak and terms beyond the harmonic order can be neglected. For systems with non-collinear order, cubic terms arise which are related to magnon scattering processes that can persist down to zero-temperature and as a result strong corrections to the harmonic picture are observable [45]. Although this is a general many-body effect, which is observed e.g. in anharmonic crystals [46] or superfluid liquids and gases [47, 48], these processes have a special role for quantum magnets. The effects are stronger for quantum magnets and there is a larger range of available options, such as the lattice geometry and external fields to adjust. Therefore, this effect can be studied much more closely in experiments on magnetic systems, resulting in the experimental observation of theoretically proposed signatures [49–55]. The term ‘spontaneous magnon decay’ was coined [45]. Interestingly, an external magnetic field can be used to induce non-collinear magnetic order and by this allowing spontaneous magnon decay [21, 51, 55–63]. The properties of the magnetic excitations can be manipulated by the magnetic field in this way. It is reasonable to assume that a control of the magnetic thermal transport is also possible. This allows for tunable magnetic thermal transport discussed before.

Surprisingly an electric field can be of interest for the control of magnetic thermal transport, too. Materials with a strong spin-orbit interaction and broken inversion symmetry contain an additional asymmetric term in the effective Hamiltonian of the magnetic system [64]. This is the well-known Dzyaloshinskii-Moriya interaction [65, 66]. Generally it is known that in antiferromagnetic materials, the magnetic order is altered by this interaction [67–70] and they become weak ferromagnets. Furthermore, it causes gaps to open at high-symmetry points in the magnetic excitation spectrum [68, 71]. An electric field can be used to change the strength of the Dzyaloshinskii-Moriya interaction [68, 72]. Many ideas have been proposed to utilise this property for applications in spintronics [64, 73, 74]. It also presents an alternative way to control magnetic thermal transport which has not been discussed so far.

In summary: Modern experimental methods are able to resolve, detect, and verify that magnetic excitations can be of equal importance as electrons and lattice

vibrations for the thermal transport in certain materials [17]. There is a substantial knowledge about the effects of external fields on magnetic excitations. The magnon's propagation and interaction is well understood. Putting those two together, one can gain new and deeper insights both into interesting novel many-body effects as well as potential utilisation of these discoveries for applications. Field control of magnonic heat flow is therefore a promising field both for fundamental and application-oriented research.

**Thesis overview** I start my thesis with part I, which introduces basic notions. Chapter 2 gives an overview over thermal transport and the thermal conductivity as its characteristic quantity. I describe how the thermal conductivity is measured experimentally and what has been found for materials with magnetic order. I discuss the temperature dependence of the magnetic contribution on the thermal conductivity, which follows from the kinetic theory and qualitative expressions for the most important scattering processes in the high- and low-temperature limit, respectively.

Chapter 3 is an introduction to the field of quantum magnetism. I begin by motivating the Hubbard model as a simple description of the behaviour of valence electrons in solids. I demonstrate how antiferromagnetic order can arise in the atomic limit. I show how the Heisenberg model can be obtained using the band limit and assuming half-filling of the Hubbard model. The Heisenberg model is an effective model for the electron spins' interaction. The additional terms that arise in the presence of an external magnetic and an electric field are discussed as well. I discuss the consequences of a broken symmetry in the system's Hamiltonian by its ground state, i.e. the occurrence of gapless modes. By the same mechanism, these gapless modes can disappear when a symmetry of the Hamiltonian is lifted by an external field. In this manner, the fields can be used to control the transport. Quantities that characterise the transport can be calculated via linear response theory.

In the last chapter 4 of part I, I give an introduction to linear response theory in spin systems. Linear response describes the influence of a weak field on a system's properties. I focus on the temperature and a magnetic field as these are the most important ones for technology. I introduce the Kubo formula to express the transport coefficients as current-current correlation functions. The thermal conductivity is one of the transport coefficients that appear. I show how the correlation functions can be evaluated using Matsubara-Green's functions which are described in appendix A.

In the main part of this thesis, I present the results for a square lattice Heisen-

berg antiferromagnet subjected to external fields. I start with a magnetic field in chapter 5. In section 5.1 I describe a general approach to determine the magnon spectrum from linear spin-wave theory and an expression for the thermal conductivity from linear response theory. I show that the dependence of the spectrum on the magnetic field can be understood from a simple classical picture. I also demonstrate that the kinetic expression for the thermal conductivity is regained and give an intuitive interpretation.

I continue with section 5.2 where I calculate the thermal conductivity from effective expressions for the scattering of the magnons with grain-boundaries and phonons. In the low-temperature limit, the thermal conductivity's dependence on the magnetic field's strength is determined by acoustic magnons with a linear dispersion and optic magnons with an excitation gap. Both the velocity of the acoustic as well as the size of the gap for the optic magnons depends on the magnetic field's strength. I therefore check how the contribution of the acoustic and optic magnons changes when the velocity of the former and the gap of the latter changes, respectively. I identify a simple mechanism for the thermal conductivity's field dependence from this idealised scenario. The results I obtain using the full magnon spectrum in the calculation of the thermal conductivity corroborate these insights.

After that, I present a calculation of magnon-magnon scattering rates from the leading terms beyond linear spin-wave theory in section 5.3. The topic of spontaneous magnon decay is discussed for the square lattice in the literature [61]. I include the most important steps of the calculation in the main part. I include an additional temperature-dependent interaction among magnons that was not previously considered. I show that there is a threshold field for these scattering processes to occur. I put an emphasis on the evolution of the scattering rates in momentum-space as a function of the magnetic field's strength. At the end of the chapter, I discuss the resulting thermal conductivity with the magnon-magnon scattering rates obtained from the spin-wave theory as a function of the magnetic field's magnitude and of the ambient temperature.

In chapter 6, I investigate the influence of an electric field on the magnetic thermal transport. The electric field enhances the strength of a specific type of spin-spin interaction (Dzyaloshinskii-Moriya interaction)<sup>1</sup> and changes the magnon spectrum. An electric field can be confined to a small region in space, e.g. by

---

<sup>1</sup>In the appendix C, I investigate the effect of the Dzyaloshinskii-Moriya interaction on the thermal transport when this interaction is not introduced by an external field, but is present intrinsically in the material. The associated Dzyaloshinskii-Moriya vectors are mono-directional which eases the determination of the spin ground state. The results of chapter 6 and appendix C can be compared to each other.

parallel plates of a capacitor. This is interesting for spintronic applications where the spin degree of freedom is used for transport and manipulated by external fields. The region of the material that is partially subjected to the electric field can be seen as a simple spintronic device. I investigate how the thermal transport is changed by the electric field as a function of ambient temperature and of the electric field's strength. Additionally, I investigate the relevance of the length over which the field is supplied.

I begin chapter 6 with a discussion of the homogeneous system where the system is completely subjected to the electric field in section 6.1. Because of peculiarities of the corresponding Dzyaloshinskii-Moriya vectors, determining the spin ground state is non-trivial. I find that a spin-spiral along one of the crystallographic directions minimises the energy. The spiral's pitch vector depends on the electric field's strength. At a finite electric field, the magnon spectrum has an acoustic and an optic branch, again. I find that there is an anisotropy of the magnon dispersion with respect to the direction along the spin-spiral and in the direction perpendicular to it. I investigate how this affects the thermal conductivity in the low-temperature limit.

In the following section 6.2, I look at the inhomogeneous setup where the electric field is only non-zero in a finite region. As momentum is then no longer a good quantum number, all calculations have to be carried out in real-space. There is, however, no common way to apply linear spin-wave theory in real-space. I therefore introduce a numerical procedure to calculate the resulting magnon spectrum as well as the energy current operators. Both are necessary for the evaluation of the thermal conductivity. As for the magnetic field, the thermal conductivity depends on the magnitude of the field as well as on the ambient temperature. I discuss both of these dependencies in the remainder of the chapter considering effective scattering rates. Additionally, I present results for the influence of the region's length where the electric field is applied to. With the help of results from the homogeneous system and a rough estimation of the wavelength of the magnons excited at a certain temperature, I present an interpretation for all these dependencies. At the end, I give an estimation of the necessary experimental requirements to obtain the presented results, the material's thickness and the voltage between the capacitor's plates in particular.

The thesis ends with the concluding chapter 7. I give a summary of the results both for the magnetic and the electric field, first. For both types of field I discuss the dependence of the thermal conductivity on temperature and magnitude of the fields. For the electric field, I additionally discuss the dependence on the intermediate layer's length in the inhomogeneous system. I also give an estimate of to what amount the thermal conductivity can realistically be reduced to for both

fields. I discuss the implications for future applications, too.

**Part I.**

**Preliminaries**



# 2. Thermal transport

I consider magnetic thermal conductivity in insulators in this work. This chapter is about thermal conductivity in general in order to be able to put latter results in context. First, I describe the basic principle of thermal measurements, i.e. the quantities that are relevant and how they can be determined experimentally. Next, I summarise results for thermal transport measurements in insulators and the influence of magnetism in those experiments. After this discussion from a more experimental point of view, I look at the contribution of magnetic excitations to the thermal conductivity in the low- and high-temperature limit according to a kinetic equation in section 2.2.

## 2.1. Principle of thermal transport measurements

Thermal transport experiments measure the amount of heat per time that flows through a material, i.e. the heat current  $j_Q$ . A system in equilibrium does not have a finite current in either direction. If there is a temperature gradient, there is a flow of heat in order to re-establish thermal equilibrium. For this reason, thermal transport is inherently associated with non-equilibrium<sup>1</sup>. For small temperature gradients  $\nabla T$ , the heat current  $j_Q$  and the latter are linearly related by Fourier's law

$$j_Q = -\kappa \nabla T \tag{2.1}$$

via the second rank thermal conductivity tensor  $\kappa$ . The minus sign ensures that heat always flows from the hot to the cold end of a material.

Experimentally, a setup like the one sketched in Figure 2.1 is used to determine the thermal conductivity of a material. First, one measures the heat  $Q$  injected at one end of a sample with cross-sectional area  $A$ . This can be done by heating

---

<sup>1</sup>In the sense that although the system is in a steady state, i.e. there is no time-variation of physical variables, some currents are non-zero and there is entropy production.

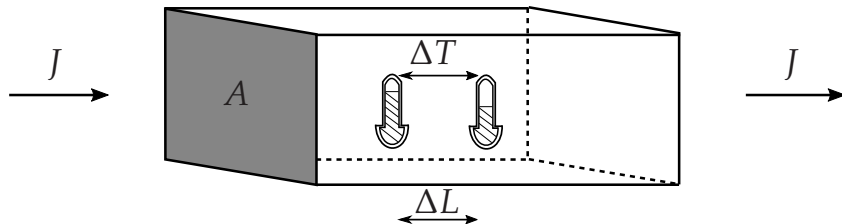


**Figure 2.1.:** Sketch of thermal transport measurement: a heat current  $J$  is injected at one end of the probe leading to a temperature difference  $\Delta T$  over a distance  $\Delta L$ . From these quantities, the thermal conductivity  $\kappa$  can be calculated according to equation (2.2).

this end with a constant or periodic rate  $J = Q/t$ . The temperature drops by  $\Delta T$  over a distance  $\Delta L$ . One measures this with two thermometers. Compared to the ambient temperature  $T$ , the temperature difference  $\Delta T$  should not be too large. The relative error in the thermal conductivity  $\Delta\kappa/\kappa$  is proportional to  $(\Delta T/T)^2$  at small ambient temperature in regular materials<sup>2</sup> [26, 27]. Of course, it must be ensured that the main process of heat transport is due to conduction through the material and not other processes like radiation or convection. This limits the accessible temperatures at which the experiments can be carried out. The better the thermal conductor, the higher the ambient temperature can be. Therefore, especially for thermal insulators, proper heat shielding and other precautions are necessary to ensure reliable results. If the sample is heated at a steady rate, the experimental thermal conductivity is determined by

$$\kappa_{\text{exp}} = \frac{J\Delta L}{A\Delta T}. \quad (2.2)$$

When the sample is heated at a periodic rate, the temperature distribution is time-dependent. The thermal conductivity can then be determined in two ways: either by measuring the attenuation  $1/\Lambda$  or the lag  $\Psi$ . The attenuation is related to the imaginary part of the conductivity tensor in frequency-space, while the lag is related to its real part (see chapter 4). Both are depending on the thermal diffusivity  $D$  which is a ratio of thermal conductivity  $\kappa$  and the heat capacity  $C$  per unit volume [26]. Theoretically, the temperature can be assumed to be a function of distance

<sup>2</sup>In three-dimensional crystals with particles dominating the thermal transport which have a linear dispersion  $\kappa \propto T^3$ . The overall heat flow is  $J = -\int_T^{T+\Delta T} \kappa dT$  and according to equation (2.2) the experimental conductivity is  $\kappa_{\text{exp}} \propto \frac{1}{4} ((T + \Delta T)^4 - T^4) / \Delta T$ . The true conductivity in the middle of the sample is  $\kappa_{\text{true}} = \kappa(T + \Delta T/2) \propto (T + \Delta T/2)^3$ . The relative error is  $\Delta\kappa/\kappa \propto (\kappa_{\text{true}} - \kappa_{\text{exp}})/T^3 = \frac{1}{4} (\frac{\Delta T}{T})^2$ .

from the point where the sample is heated  $x$  and time  $t$  [26]

$$T(x, t) = T_0 \exp\left(-\sqrt{\frac{\omega}{2D}} x\right) \sin\left(\omega t - \sqrt{\frac{\omega}{2D}} x\right). \quad (2.3)$$

Here  $\omega$  is the frequency with which the heat is applied to the system. It follows from this that the diffusivity is

$$D = \frac{\omega x^2}{2 \ln^2 \Lambda} = \frac{\omega x^2}{2\Psi^2} \quad (2.4)$$

by either measuring the attenuation or the lag, respectively. Due to heat losses, none of the above mentioned relationships might hold, strictly speaking. By measuring both the lag and the attenuation at the same time, the experimental results become much more reliable [26]. The thermal diffusivity is then

$$D = \frac{\omega x^2}{2\Psi \ln \Lambda}. \quad (2.5)$$

If the heat capacity  $C$  is measured as well, the thermal conductivity is

$$\kappa = DC. \quad (2.6)$$

## 2.2. Thermal transport in magnetic materials

Materials can have a contribution of the atoms' spin degrees of freedom to the thermal transport. The spin system can either transport heat by itself or act as an additional source of phonon scattering in insulating, magnetically ordered crystals. A phonon can be absorbed in order to excite a spin and at a later time this spin might relax and emit another phonon in a different direction to the initial phonon. The process of a spin excitation being absorbed by a phonon and emitted again in a different direction is possible, as well. Hence, the thermal conductivity behaves differently depending on the material being in a magnetically ordered state (below the Néel temperature) or in the paramagnetic state [75]. The thermal conductivity is increasing more slowly with temperature in the former case than in the latter, because there is an additional channel for phonon scattering. The differences in the thermal conductivity when a material is doped by non-magnetic atoms and when the atoms are magnetic are considered, e.g. in [76]. The thermal conductivity decreases much more when the impurities are magnetic than it does when they are non-magnetic, although the mass difference suggests the opposite. The influence of a magnetic field on the thermal conductivity which is the object

of this work, is considered too [77, 78]. The thermal conductivity changes by up to 10% [79] which can be explained by a simple model [80]: the magnetic field causes a splitting of the spin-doublet changing the energy of the phonons which couple different modes of spin excitations. Such a process reduces the contribution of the involved phonons to the thermal transport. The magnetic field can be used to shift the spin-phonon scattering to phonon modes with a higher energy which alters the thermal conductivity at a fixed temperature [24, 29, 30, 81]. Contributions of the magnetic excitations to the thermal transport need to be taken into account, too. The treatment of phonons and spin excitations as a coupled mode oftentimes achieves better agreement with experiments than a separate treatment of both [31].

The thermal conductivity's behaviour is qualitatively well-described by a kinetic theory for bosonic excitations, e.g. magnons and phonons. The respective expression for it is [26]

$$\begin{aligned} \kappa &= \frac{1}{2\pi^2} \int_0^{q_{\max}} \frac{q^4 v^4 \tau(q)}{k_B T^2} \frac{v q / k_B T}{(e^{vq/k_B T} - 1)^2} dq \\ &= \frac{k_B^4}{2\pi^2} \frac{T^3}{v} \int_0^{\xi_{\max}} \tau(\xi(q)) \frac{\xi^4 e^\xi}{(e^\xi - 1)^2} d\xi \\ &= \frac{1}{3} v^2 \int_0^{\theta/k_B T} \tau(\xi(q)) C(\xi) d\xi, \end{aligned} \quad (2.7)$$

I have switched to a dimensionless variable  $\xi = \frac{vq}{k_B T}$  and assumed a linear magnon dispersion  $\epsilon(q) = v|q|$  in all three dimensions up to a characteristic momentum  $\epsilon(q_{\max}) = \theta$  and zero above that. The contribution from modes in the range  $x$  to  $x + dx$  is denoted by

$$C(\xi) d\xi = \frac{3k_B^4}{2\pi^2 v^3} T^3 \frac{\xi^4 \exp(\xi)}{(\exp(\xi) - 1)^2} d\xi.$$

This quantity has its maximum at  $\xi \approx 3.8$ , meaning that the greatest contribution to the thermal conductivity at a given temperature is from magnons with energy  $\epsilon = 4k_B T$ . The approximation of mere magnons with a linear dispersion contributing, is only good for temperatures where not too many optical modes are excited. Because the latter's modes' dispersion is flat, they mainly affect the thermal transport indirectly by scattering with the acoustic modes. The temperature dependence of the relaxation time then determines the one of the thermal conductivity in equation (2.8).

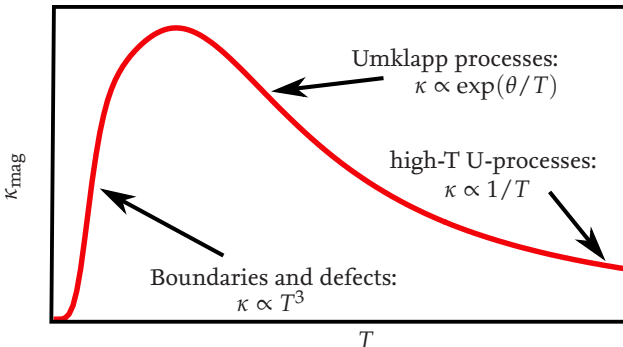


**Figure 2.2.:** Sketch of the contribution of magnons to the thermal conductivity  $\kappa_{\text{mag}}$  as a function of the external temperature  $T$  with an indication of the dominant scattering processes for a material with a three-dimensional magnon dispersion.  $\theta$  is a characteristic temperature for magnon excitation.

It follows from equation (2.8) that at low temperature, mainly the low-energy (acoustic) modes contribute to the thermal transport. This means that only low-energy modes which have small momenta are important. The processes do not involve large  $|q|$  and the proportion of inter-particle scattering processes, e.g. magnon-phonon or magnon-magnon, decreases. Therefore, at low  $T$ , scattering events with the boundary or impurities dominate. The rates of these scattering events are unaffected by the external temperature. The number of excited magnons increases, however. This means that the magnon's heat capacity increases due to the proliferation of acoustic magnons. It is clear from equation (2.8) that the thermal conductivity is proportional to  $T^3$  in the low-temperature limit<sup>3</sup>. The interaction of magnons with each other and other quasi-particles grows as more magnons, especially optical ones, are excited. Relaxation times of these processes are similar to the ones for phonons in the high-temperature limit [82, 83]

$$\tau \propto \exp\left(\frac{\theta}{T}\right). \quad (2.8)$$

As can be seen from the first expression on the right side of equation (2.8), the thermal conductivity goes to zero as  $1/T$  in the high-temperature limit. In Figure 2.2 one can see a sketch of the qualitative behaviour of the thermal conductivity as a function of the external temperature.

In the next chapter 3, I describe the origin of magnetic order in insulating materials. Excitations of this order, the already discussed magnons, can be manipulated

<sup>3</sup>This result is valid for a three-dimensional magnon dispersion. I show in the main part of this work, that for magnons on the two-dimensional square lattice  $\lim_{T \rightarrow 0} \kappa \propto T^2$ .

by external fields and utilised for information or energy exchange. Chapter 4 introduces the theory of how to systematically calculate characteristic quantities such as the thermal conductivity when the external fields are small enough so that the system is still close to equilibrium.

# 3. Quantum magnetism

I give an introduction to thermal transport in the previous chapter. There, I mention that materials with magnetic properties allow for thermal transport due to the spin degree of freedom. In this chapter, I illustrate the necessary foundation to describe the interactions leading to the magnetic properties in insulating materials. The insights are used in chapter 4 to describe the aforementioned spin-related transport.

I start with the Hubbard model in section 3.1 and show how, in principle, magnetic order can arise from this simple effective microscopic model of electrons in solids. The first part motivates how the two terms in the Hubbard model arise from the electrons' kinetic energy and their Coulomb interaction. Afterwards, I discuss the atomic limit of the Hubbard model at half-filling. I show that in the limit of large on-site interaction, the electronic Hamiltonian reduces to an effective interaction between the electrons' spins. This leads to the Heisenberg Hamiltonian which is the model I use in my work. I discuss the kinetic exchange and the super-exchange interaction. Both can lead to antiferromagnetic order of the electrons' spins.

Spin-orbit interaction and a possible magnetic field can be incorporated into the Hubbard model, too. I show that the resulting terms can be written in terms of spin operators as well. The electric field can be used to change the importance of the term related to spin-orbit interaction. The control of the energy transport via the magnetic and the electric field are the subject of my thesis.

In section 3.2, I describe how magnetic order can arise in the Heisenberg model despite the inherent  $SU(2)$  symmetry due to spontaneous symmetry breaking. Furthermore, I discuss the peculiarity of magnetic order in low-dimensional spin models and how the lattice and interactions can affect the former. At the end of the section, I illustrate the consequences of the magnetic order on the excitation spectrum. The latter can be controlled by the external fields and with it the thermal transport by these excitations.

## 3.1. The Hubbard and the Heisenberg model

Quantum magnetism does not arise directly from the movement of the electron, but from its quantum statistical properties. Because of their fermionic nature, two electrons can not occupy the same quantum mechanical state. The energy scales of the electronic system are determined by the spatial degrees of freedom, i.e. by the kinetic energy and the Coulomb interaction. A spin configuration restricts the range of possible spatial configurations which can have different energies, leading to energy differences associated with different spin configurations. The system can try to minimise its potential energy by reducing the overlap of wavefunctions, i.e. antisymmetric wavefunctions and symmetric spin functions. Hence, this process leads to interactions favouring parallel spin configuration. The system can alternatively minimise the kinetic energy, i.e. the gradients of wavefunctions. This delocalisation of the electrons means symmetric spatial superpositions and antisymmetric spin functions. This process then leads to interactions where anti-parallel spin orientation is energetically beneficial. The competition between the kinetic and the potential energy can, therefore, be decisive of the spin-spin interaction's character. Throughout a material, the spin degree of freedom of the atoms' unpaired electrons can be ordered over macroscopic distances.

The simplest model that can capture this behaviour is the Hubbard model [84–91]. It takes into account that screening causes the Coulomb interaction to exponentially decrease with the spatial distance between two electrons. Effectively, they only interact when they are at the same site when the orbitals are localised like e.g. d-orbitals. The strength of the corresponding on-site interaction  $U_{i,\sigma\sigma'}^{\alpha\beta}$  is [92]

$$U_{i,\sigma\sigma'}^{\alpha\beta} = \frac{1}{2} \int v(x - x') \phi_{i,\sigma,\alpha}^*(x) \phi_{i,\sigma',\beta}^*(x') \phi_{i,\sigma',\beta}(x') \phi_{i,\sigma,\alpha}(x) d^3x d^3x'. \quad (3.1)$$

Here the indices  $\sigma/\sigma'$ ,  $\alpha/\beta$ , and  $i$  of the wavefunctions  $\phi$  refer to their spin, atomic orbital, and the atom at lattice position  $x$ ; they are localised at. The function  $v$  is an effective screened potential. Kinetic energy is expressed by the hopping matrix elements  $t_{ij}^\alpha$  [92]

$$t_{ij}^\alpha = \sum_\sigma \int \phi_{i,\sigma,\alpha}^*(x) \left[ -\frac{\hbar^2}{2m} \nabla^2 \right] \phi_{j,\sigma,\alpha}(x) d^3x. \quad (3.2)$$

For the moment, I do not consider spin-orbit interaction. Angular momentum is conserved and, as a result, electrons can only hop between the same orbitals of two different atoms. At the end of this chapter, I include spin-orbit interaction and show that it leads to an additional term in the effective spin-spin interaction.

The complete many-band Hubbard Hamiltonian with both of these interactions is [92]

$$H = \sum_{i,\sigma,\sigma',\alpha,\beta} U_{i,\sigma\sigma'}^{\alpha\beta} c_{i,\sigma,\alpha}^\dagger c_{i,\sigma',\beta}^\dagger c_{i,\sigma',\beta} c_{i,\sigma,\alpha} - \sum_{i,j,\alpha,\sigma} t_{ij}^\alpha c_{i,\sigma,\alpha}^\dagger c_{j,\sigma,\alpha} + \text{h.c.} \quad (3.3)$$

The first sum runs over all sites  $i$  of the lattice and additionally over the spin orientations  $\sigma, \sigma' = \uparrow, \downarrow$  of two valence electrons in the orbitals  $\alpha$  and  $\beta$ , respectively. Terms with  $\alpha = \beta$  and  $\sigma = \sigma'$  vanish due to  $c_i^\dagger c_i^\dagger = c_i c_i = 0$  which follows from the fermionic anti-commutators. The second sum runs over sites  $i$  and  $j$  an electron can hop from one into the other. The operators  $c_i, c_i^\dagger$  are fermionic annihilation and creation operators of an electronic state.

The Hubbard Hamiltonian allows for a variety of magnetically ordered states. I consider the atomic limit, i.e.  $U \gg t$ , throughout my thesis. Correlation effects are most pronounced in this limit. The assumption of delocalised electron bands does not hold then. Electrons avoid double occupation of orbitals at the same site. The Pauli exclusion principle forbids that an electron can gain energy by hopping into an orbital already occupied by another electron of the same spin-polarisation. As the ratio of electrons in the system to the number of available electron states increases, correlation effects, i.e. how much the spin-polarisation of nearby electrons matters, become important. When there are as many electrons as there are atoms, there is one electron at every atom to minimise potential energy. Electrons are free to hop from one site to the other in principle, but this is prevented by the large on-site interaction. Although there is one free electron per site, the material is not a conductor but an insulator. Those types of insulators are called Mott-insulators [93–97]. It turns out that Mott-insulators are magnets [98] due to the correlation effects. Whether neighbouring spins favour ferromagnetic or antiferromagnetic orientation depends on the energy difference between the different atomic orbitals.

When the orbitals are non-degenerate and energetically well separated, only the orbital closest to the Fermi-energy of the atom is relevant. The many-band Hamiltonian in equation (3.3) then reduces to the single-band Hubbard model

$$H = \sum_i U_i c_{i,\uparrow}^\dagger c_{i,\downarrow}^\dagger c_{i,\downarrow} c_{i,\uparrow} - \sum_{i,j,\sigma} t_{ij} c_{i,\sigma}^\dagger c_{j,\sigma} + \text{h.c.} \quad (3.4)$$

I assume half-filling, i.e. one electron per atom and use Brillouin-Wigner perturbation theory [99] to derive an effective Hamiltonian for the sector of single occupation. The Hamiltonian is split into

$$H = H_0 + H_I \quad (3.5)$$

where  $H_0$  contains the on-site interaction and  $H_I$  the hopping terms. Using the projectors  $P$  onto the eigenstates of  $H_0$  with the lowest energy and  $Q$  projecting onto the rest of the describing excitations of former states allows to decompose any state  $|\Psi\rangle$  in the following way

$$|\Psi\rangle = P|\Psi\rangle + Q|\Psi\rangle = |\Phi\rangle_{\text{GS}} + |\Phi\rangle_{\text{ex}} \quad (3.6)$$

into its ground state portion  $|\Phi\rangle_{\text{GS}}$  and the excitation portion  $|\Phi\rangle_{\text{ex}}$ . The Schrödinger equation multiplied by  $P$  and  $Q$ , respectively, leads to the following two equations

$$PH_0P|\Phi\rangle_{\text{GS}} + PH_IQ|\Phi\rangle_{\text{ex}} = E|\Phi\rangle_{\text{GS}}, \quad (3.7)$$

$$QH_IP|\Phi\rangle_{\text{GS}} + QH_0Q|\Phi\rangle_{\text{ex}} = E|\Phi\rangle_{\text{ex}}, \quad (3.8)$$

the last of which can be resolved for  $|\Phi\rangle_{\text{ex}}$  so that it can be eliminated in the first equation. The result

$$\left[ PH_0P + PH_IQ(E - H_0)^{-1}QH_IP \right] |\Phi\rangle_{\text{GS}} = H|\Phi\rangle_{\text{GS}} = E|\Phi\rangle_{\text{GS}} \quad (3.9)$$

defines the Hamiltonian acting on the low-energy part in state space. Because the eigenenergy  $E$  of the full Hamiltonian occurs on both sides, the Schrödinger equation needs to be solved self-consistently. This leads to a series expansion in  $H_I$ . Up to second order one obtains

$$H_{\text{eff}}^{(2)} = PH_0P + PH_IQ(E_0 - H_0)^{-1}QH_IP \quad (3.10)$$

where  $E_0 = PH_0P$  which is an effective Hamiltonian for the low-energy states. As shown in the last section, the ground state portion of the on-site interaction is a composition of two-spin states, i.e.

$$\begin{aligned} P = & \sum_{i,j} |\uparrow\rangle_i |\uparrow\rangle_j \langle \uparrow|_i \langle \uparrow|_j + |\uparrow\rangle_i |\downarrow\rangle_j \langle \uparrow|_i \langle \downarrow|_j \\ & + |\downarrow\rangle_i |\uparrow\rangle_j \langle \downarrow|_i \langle \uparrow|_j + |\downarrow\rangle_i |\downarrow\rangle_j \langle \downarrow|_i \langle \downarrow|_j. \end{aligned} \quad (3.11)$$

This projection operator can be explicitly inserted into equation (3.10). The following relations for the perturbed and unperturbed part of the Hamiltonian when

acting on all the two-site spin states

$$H_I |\uparrow\rangle_i |\downarrow\rangle_j = -t_{ij} |\uparrow\downarrow\rangle_i |0\rangle_j + t_{ij} |0\rangle_i |\uparrow\downarrow\rangle_j \quad (3.12)$$

$$H_I |\downarrow\rangle_i |\uparrow\rangle_j = +t_{ij} |\uparrow\downarrow\rangle_i |0\rangle_j - t_{ij} |0\rangle_i |\uparrow\downarrow\rangle_j \quad (3.13)$$

$$H_I |\uparrow\rangle_i |\uparrow\rangle_j = 0 \quad (3.14)$$

$$H_I |\downarrow\rangle_i |\downarrow\rangle_j = 0 \quad (3.15)$$

$$H_I |\uparrow\downarrow\rangle_i |0\rangle_j = -t_{ij} |\uparrow\rangle_i |\downarrow\rangle_j - t_{ij} |\downarrow\rangle_i |\uparrow\rangle_j \quad (3.16)$$

$$(E_0 - H_0)^{-1} |\uparrow\downarrow\rangle_i |0\rangle_j = -\frac{1}{U} |\uparrow\downarrow\rangle_i |0\rangle_j \quad (3.17)$$

can be used to find

$$\begin{aligned} H_{\text{eff}}^{(2)} = & \frac{2t_{ij}^2}{U} \sum_{ij} |\uparrow\rangle_i |\downarrow\rangle_j \langle \downarrow|_i \langle \uparrow|_j - |\uparrow\rangle_i |\downarrow\rangle_j \langle \uparrow|_i \langle \downarrow|_j \\ & + |\downarrow\rangle_i |\uparrow\rangle_j \langle \uparrow|_i \langle \downarrow|_j - |\downarrow\rangle_i |\uparrow\rangle_j \langle \downarrow|_i \langle \uparrow|_j. \end{aligned} \quad (3.18)$$

This expression can be written in terms of spin operators

$$H_{\text{eff}}^{(2)} = \sum_{ij} J_{ij} S_i^z S_j^z + \frac{J_{ij}}{2} \left( S_i^+ S_j^- + S_i^- S_j^+ \right) - \frac{J_{ij}}{4} \quad (3.19)$$

where  $J_{ij} = \frac{4t_{ij}^2}{U}$  is called the exchange interaction and

$$S_i^z |\uparrow\rangle_i = \frac{1}{2} |\uparrow\rangle_i, \quad (3.20)$$

$$S_i^z |\downarrow\rangle_i = -\frac{1}{2} |\downarrow\rangle_i, \quad (3.21)$$

$$S_i^- |\uparrow\rangle_i = |\downarrow\rangle_i, \quad (3.22)$$

$$S_i^+ |\downarrow\rangle_i = |\uparrow\rangle_i, \quad (3.23)$$

$$S_i^- |\downarrow\rangle_i = S_i^+ |\uparrow\rangle_i = 0. \quad (3.24)$$

The constant  $\sum_{ij} J_{ij}/4$  in equation (3.19) can be left out, which corresponds to the Heisenberg Hamiltonian

$$H = \sum_{ij} J_{ij} \mathbf{S}_i \cdot \mathbf{S}_j \quad (3.25)$$

with the operators  $S^x = \frac{1}{2}(S^+ + S^-)$  and  $S^y = \frac{1}{2i}(S^+ - S^-)$ . Because  $J > 0$  the spins' interaction is antiferromagnetic.

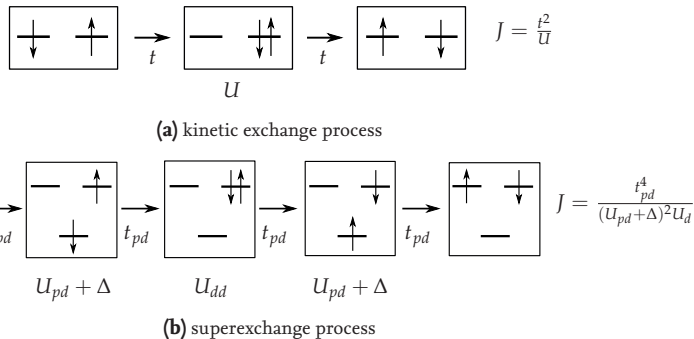


**Figure 3.1.:** Sketch of exchange processes which lead to antiferromagnetic interactions: (a) in a kinetic exchange process and the superexchange process in (b)

The exchange process discussed before is referred to as kinetic exchange and is depicted and described in Figure 3.1a. In this exchange process, an electron first hops from one site to another (only possible when both electrons have opposite spin). This releases energy  $t$  due to the hopping, but also costs energy  $U$  due to the on-site interaction. At last, the other spin hops into the unoccupied site. The energy difference between the parallel and the antiparallel spin orientation is  $J = \frac{t^2}{U}$ .

Such a process is rare as materials are, usually, a composition with more than one kind of atom. While for some of the atoms the orbital closest to the Fermi-energy is filled, for some there are unpaired electrons. Other exchange processes which can be interpreted as effective interactions between the unpaired electrons' spins are still possible. The superexchange process is the most relevant for the materials I consider in my thesis. Superexchange [95, 100] refers to the process of (indirect) interaction of two spins via intermediate ligands, e.g. oxygen in transition-metal oxides. The lowest-order correction that lifts the spin-degeneracy is fourth-order [92]. The respective process is illustrated in Figure 3.1b. In this process (here between two  $d$ - and a  $p$  orbital), an electron from a filled orbital hops into one of two half-filled orbitals. The resulting state has a higher energy due to the difference ( $\Delta$ ) and the Coulomb interaction  $U_{pd}$  between both orbitals. Next, the remaining electron of the initially filled orbital hops into the remaining half-filled orbital (only possible when both initially unpaired electrons have opposite spin). The energy difference to the initial state is  $U_{dd}$  due to the on-site interaction. In the next step, the other initially unpaired electron hops into the empty ( $p$ -)orbital. This state has an energy which is higher by  $U_{pd} + \Delta$  with respect to the initial state, again. At last, an electron hops back into the initially full orbital so that the initially half-filled orbitals are half-filled again. Every hopping process releases energy  $t_{pd}$ . The energy difference between the parallel and the antiparallel spin orientation

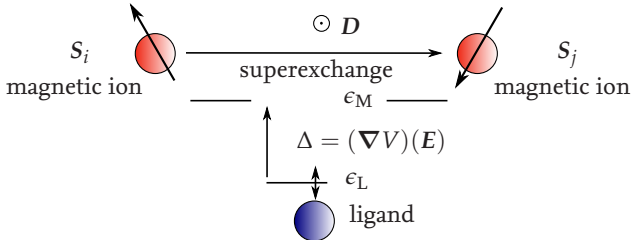


**Figure 3.2.:** Superexchange interaction between the spins  $S_i$  and  $S_j$  of two magnetic ions via a ligand. An electric field  $E$  changes the local one electron potential  $V$  between the ligand and the magnetic ion orbitals. As a result, the strength of the Dzyaloshinskii-Moriya interaction  $D$  changes, which arises due to a superexchange process with spin-orbit interaction (see equation (3.29)).

is  $J = \frac{t_{pd}^4}{(U_{pd} + \Delta)^2 U_{dd}}$ . Therefore, there is an effective antiferromagnetic spin-spin interaction.

In the presence of external fields, additional terms arise in the Heisenberg Hamiltonian. A magnetic field directly couples to the spin degree of freedom, reducing or increasing the system's energy by the Zeeman energy. Therefore, the term

$$H_Z = -B_z \sum_{i,\sigma} c_{i,\sigma}^\dagger c_{i,\sigma} = -\mathbf{B} \cdot \sum_i \mathbf{S}_i \quad (3.26)$$

needs to be added to equation (3.25).

The electric field can affect an additional term which can be seen by the inclusion of spin-orbit coupling. This interaction is omitted in the derivation of the Hubbard Hamiltonian before. It is described by a hopping term connecting states with different spin polarisation [101, 102]:

$$H_{SO} = \sum_{\langle i,j \rangle} \sum_{\alpha,\alpha'} c_{i,\alpha}^\dagger \left( i\lambda \frac{(\nabla V \times \mathbf{p})_{ij} \cdot \sigma_{\alpha\alpha'}}{2} \right) c_{j,\alpha'} + \text{h.c.} \quad (3.27)$$

Here  $V$  is the one electron potential,  $\mathbf{p}$  the momentum operator and  $(\nabla V \times \mathbf{p})_{ij}$  is the matrix element between the orbital wavefunctions on site  $i$  and  $j$  of this vector product.  $\lambda$  is a parameter that depends on the spin-orbit interaction. The term in equation (3.27) is equivalent to a spin-dependent vector potential. This effectively adds a complex phase  $\alpha$  proportional to the spin-orbit interaction to the hopping parameter [72]

$$H_t = - \sum_{i,j,\sigma} t_{ij} \left( e^{i\alpha\sigma} c_{i,\sigma}^\dagger c_{j,\sigma} + \text{h.c.} \right). \quad (3.28)$$

The higher the spin-orbit interaction is, the more the spin rotates while hopping from one site to the other. This changes the superexchange process as it is de-

scribed before. It leads to the emergence of an additional anisotropic exchange term [64]:

$$H_{\text{DMI}} = \sum_{\langle i,j \rangle} \mathbf{D}_{ij} \cdot (\mathbf{s}_i \times \mathbf{s}_j) \quad (3.29)$$

with  $\mathbf{D}_{ij} = -J \frac{ea}{\lambda} \nabla_i V \times (\mathbf{e}_i - \mathbf{e}_j)$

where  $D$  is called the Dzyaloshinskii-Moriya vector which depends on the distance of the two magnetic ions  $a$  and an energy parameter  $\lambda$  stemming from spin-orbit interaction [72]

$$\lambda = \frac{243 t_{ij} a}{64 a_B} \frac{(Z_O/2 + Z_M/3)^6}{Z_O^{5/2} Z_M^{7/2}} \quad (3.30)$$

where  $Z_O, Z_M$  are the atomic numbers of the ligand and the magnetic ions, and  $a_B$  is the Bohr radius<sup>1</sup>. The Dzyaloshinskii-Moriya vector can only be non-zero if the system has a broken inversion symmetry [65, 66] at the point in the middle of the magnetic ions. The direction of the vector is connected to this broken symmetry. The Dzyaloshinskii-Moriya interaction can be controlled by an electric field [64]. The mechanism is illustrated in Figure 3.2. The electric field changes the one-electron potential  $V$  at the sites (Stark effect). Because ligands and metal ions have different dipole moments, the electric field  $E$  changes  $\nabla_i V$ . As can be inferred from equation (3.27), the effective Dzyaloshinskii-Moriya interaction changes, too. Due to oxygen's high polarisability, its  $p$ -orbitals are strongly affected in contrast to the  $d$ -orbitals in transition-metal oxides. Hence, a control of the Dzyaloshinskii-Moriya interaction seems possible in such materials, i.e. an electric field can affect the magnetic properties.

## 3.2. Magnetic order in the Heisenberg model

The Heisenberg Hamiltonian in equation (3.25) is symmetric under all rotations ( $SU(2)$  transformations). In my thesis, I look at excitations of magnetically ordered states, i.e. states that break this symmetry. Such states can still be a ground state of the corresponding Hamiltonian. Introducing an ordering field  $h$  to the Hamiltonian  $H_0$  in equation (3.25) [92]

$$H(h) = H_0 - h S_q^z \quad (3.31)$$

---

<sup>1</sup>For transition-metal oxides  $\lambda$  is of the order of electron volts

where  $H_0$  is the Hamiltonian from equation (3.25).  $S_q^z$  is a spin density wave in  $z$ -direction with ordering vector  $q$

$$S_q^z = \sum_i e^{iqr_i} S_i^z. \quad (3.32)$$

For  $q = 0$  this is the regular magnetisation, while e.g. for  $q = (\pi, \pi, \pi)$  it is the staggered magnetisation on a cubic lattice. The field  $h$  in equation (3.31) breaks the rotational symmetry. In this case, the state is said to spontaneously break the system's symmetry when the magnetisation  $m_q$  per site does not vanish in the thermodynamic limit and as the ordering field goes to zero<sup>2</sup> [92]:

$$\lim_{h \rightarrow 0^+} \lim_{N \rightarrow \infty} m_q = \lim_{h \rightarrow 0^+} \lim_{N \rightarrow \infty} \frac{1}{NZ} \text{Tr} \left( e^{-\beta H(h)} \right) \neq 0. \quad (3.33)$$

In general, the ordered state does only persist up to a certain temperature due to thermal fluctuations, i.e. there is a phase transition at a specific temperature  $T_C$ . For the Heisenberg model with nearest-neighbour interaction, which I consider in this thesis, the transition temperature  $T_C = 0$  for one- and two-dimensional lattices, i.e. there is no magnetic long-range order, because

$$m_q \propto \frac{h^{1/3}}{T^{2/3}} \quad (3.34)$$

in one dimension and

$$m_q \propto \frac{1}{T^{1/2} \sqrt{|\log h|}} \quad (3.35)$$

in two dimensions [92]. Both expressions go to zero for  $h \rightarrow 0$ . This is known as the Mermin-Wagner theorem [103]. There is, however, always a small interaction between two-dimensional layers. This usually leads to at least long correlation lengths [104], which justify the assumption of magnetic order over reasonably large distances.

There is another phenomenon that can prevent the occurrence of magnetic order for Heisenberg models with antiferromagnetic nearest-neighbour interaction or additional conflicting spin-spin interactions over longer distances. It can be best understood by looking at the example of three Ising spins on a triangle. Because only two of the three spins can be mutually anti-parallel, one of the three spins has to point in an energetically unfavourable direction. The spin is geometrically frustrated [105]. In my thesis, I consider a square lattice antiferromagnetic Heisenberg model with nearest neighbour interaction. This lattice is not frustrated.

---

<sup>2</sup>The order of the limits is important.

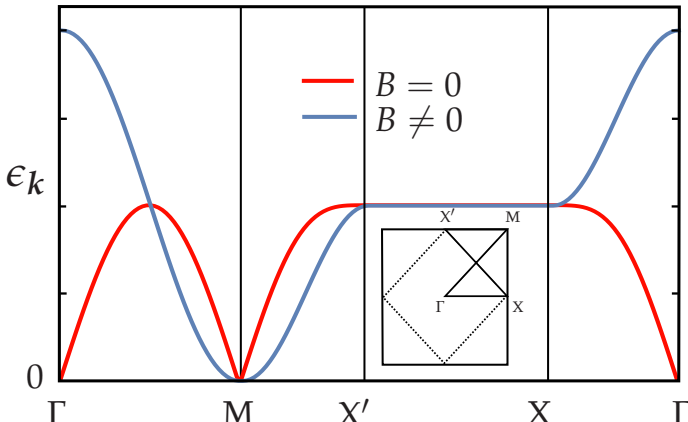


**Figure 3.3:** Magnon dispersion  $\epsilon_k$  on the path shown in the inset for vanishing ( $B = 0$ ) and finite ( $B \neq 0$ ) magnetic field. A finite magnetic field lifts the system's  $SU(2)$ -symmetry and the Goldstone mode around the  $\Gamma$ -point vanishes. The Goldstone mode around the  $M$ -point remains as spins can be still flipped by  $\pi$  without changing the system's energy.

Spontaneously broken symmetries are relevant for another reason. In systems that possess a ground state that spontaneously breaks a symmetry of the Hamiltonian, one finds so-called Goldstone modes [106–108], which appear around a high-symmetry point of the Brillouin zone where the dispersion vanishes [92]. In the Heisenberg model with its inherent  $SU(2)$ -symmetry in the absence of any fields, these modes occur naturally. They are of utmost importance in the thermal conductivity's low-temperature behaviour. By breaking the  $SU(2)$ -symmetry with the external fields in equation (3.26) and (3.29) these Goldstone modes disappear at certain high-symmetry points and a gap develops in the dispersion. This allows the control of the thermal transport by magnetic excitations which is the topic of this work's main part. In Figure 3.3 one can see an example of such a dispersion without an external magnetic field ( $B = 0$ ) and in the presence of a finite magnetic field ( $B \neq 0$ ). One can see that at the  $\Gamma$ -point the dispersion develops a gap at finite magnetic field. This is due to the broken  $SU(2)$  symmetry as the magnetic field singles out one specific direction. In contrast to this, the dispersion stays gapless around the  $M$ -point as spins can still be rotated by  $\pi$  without changing the system's energy.

The properties of magnetically ordered materials and transport within them can be described using linear response theory. Here the system is assumed to be only slightly off equilibrium due to an external field. Hence, the current that flows to reestablish the equilibrium depends linearly on the field's strength. The coefficients of proportionality are called transport coefficients. I calculate the thermal

conductivity and determine how it is affected by the external fields in my thesis. In the next chapter, I exemplify the linear response theory by looking at the possible currents that can be induced in a magnetic system.



## 4. Linear response theory and transport coefficients

Chapter 3 introduces the Heisenberg model (see section 3.1) for the interaction of the electrons' spin degree of freedom in an insulating crystal. Currents in such materials are used to build several kinds of devices that allow for a more efficient exchange of information and energy, as well as manipulating this process by external fields. I discuss what kinds of currents can be induced by which fields in this chapter. The currents and the fields are related by transport coefficients. In my thesis, I calculate the thermal conductivity, which is an example for such a transport coefficient. I investigate how a magnetic and an electric field affect the thermal conductivity. This chapter introduces the theory needed to calculate the transport coefficients.

Defining an energy density operator  $h_0(\mathbf{r})$

$$H_0 = \int h_0(\mathbf{r}) d^3\mathbf{r} \quad (4.1)$$

and assuming that the system is in equilibrium with an external inverse temperature  $\beta$  and magnetic field  $B$  which couples to the spin  $S(\mathbf{r})$

$$\beta(\mathbf{r}, t) = \frac{1}{T} + \alpha(\mathbf{r}, t), \quad (4.2)$$

$$B(\mathbf{r}, t) = B_0 + b(\mathbf{r}, t), \quad (4.3)$$

the canonical statistical operator  $\varrho$  [109] can be written as

$$\begin{aligned} \varrho &= \frac{1}{Z} \exp \left( - \int \left[ \left( \frac{1}{T} + \alpha(\mathbf{r}, t) \right) \left( h(\mathbf{r}) - b(\mathbf{r}, t) S(\mathbf{r}) \right) \right] d^3\mathbf{r} \right) \\ &= \frac{1}{Z} \exp \left( - \frac{1}{T} \left[ H + \int h(\mathbf{r}) T \alpha(\mathbf{r}, t) d^3\mathbf{r} - \int S(\mathbf{r}) b(\mathbf{r}, t) d^3\mathbf{r} \right] + \mathcal{O}(b\alpha) \right) \end{aligned} \quad (4.4)$$

where I absorb the homogeneous part of the magnetic field into  $h(\mathbf{r})$ . When the inhomogeneous parts of the temperature and magnetic field are small compared

to the homogeneous parts, they can be assumed as perturbations to the expectation value of a generic quantity. This is called the linear response regime.

For my thesis, the energy current  $j_e$  is of particular interest and in the field of magnonics, the spin current  $j_s$  occurs frequently. Both are defined by the time-derivative of a density polarisation operator  $P_d$  [110]

$$P_d = \int \mathbf{r} \rho(\mathbf{r}) d^3 r. \quad (4.5)$$

For the energy-current, the density  $d = h(\mathbf{r})$ , and for the spin-current  $d = S(\mathbf{r})$ . In the linear response regime [109],

$$\langle j_\mu^l(\mathbf{r}, t) \rangle = i \int_{-\infty}^t \int \left\langle \left[ j_\mu^l(\mathbf{r}, t), d_\nu(\mathbf{r}', t') \right] \right\rangle V_\nu(\mathbf{r}', t') dt' d^3 r'. \quad (4.6)$$

Here  $V_\nu$  is a potential that couples to the density  $d$ . For the energy current  $V_e = -T\alpha$  and for the spin current  $V_s = b$ . The Greek subscripts refer to the kinds of the associated densities and the Latin superscripts to spatial components. Einstein sum convention is used as well. This equation can be further manipulated by using [111]:

$$\begin{aligned} \langle [A, B] \rangle &= \text{Tr} (\varrho AB) - \text{Tr} (B\varrho A) = \text{Tr} (B\varrho A) - \text{Tr} (\varrho BA) \\ &= \text{Tr} \left( e^{-\beta H} e^{\beta H} B \frac{e^{-\beta H}}{Z} A \right) - \text{Tr} (\varrho BA) = \langle B(-i\beta) A \rangle - \langle B(0) A \rangle \\ &= -i \int_0^\beta \frac{d}{d\lambda} \langle B(-i\lambda) A \rangle d\lambda = -i \langle \langle \dot{B} A \rangle \rangle \end{aligned} \quad (4.7)$$

and the continuity equation

$$\frac{\partial d_\mu}{\partial t} = -\nabla_m j_\mu^m. \quad (4.8)$$

equation 4.6 becomes

$$\begin{aligned} \langle j_\mu^l \rangle(\mathbf{r}, t) &= -\frac{1}{\hbar} \int_{-\infty}^t \int \langle \langle \nabla_m j_\nu^m(\mathbf{r}', t') j_\mu^m(\mathbf{r}, t) \rangle \rangle V_\nu(\mathbf{r}', t') d^3 r' dt' \\ &= \frac{1}{\hbar} \int_{-\infty}^t \int \langle \langle j_\nu^l(\mathbf{r}', t') j_\mu^m(\mathbf{r}, t) \rangle \rangle X_{m,\nu}(\mathbf{r}', t') d^3 r' dt'. \end{aligned} \quad (4.9)$$

where I integrate by parts and introduce the forces  $X_\nu = \nabla V_\nu$  to obtain the last line. From this, one identifies the form of the transport coefficient  $L_{\mu\nu}$  in frequency- and momentum-space

$$L_{\mu\nu}^{lm}(\mathbf{q}, \omega) = \int_{-\infty}^t e^{i(\omega+i0^+)(t-t')} \langle\langle j_\mu^l(-\mathbf{q}, t') j_\nu^m(\mathbf{q}, t) \rangle\rangle dt'. \quad (4.10)$$

Hence, the response matrix for a Heisenberg quantum magnet is

$$\begin{pmatrix} j_s \\ j_h \end{pmatrix} = \begin{pmatrix} \sigma & S \\ ST & T\kappa \end{pmatrix} \begin{pmatrix} \nabla b \\ -T\nabla\alpha \end{pmatrix} \quad (4.11)$$

with the spin-conductivity  $\sigma$ , the Seebeck coefficient  $S$ , and the thermal conductivity  $\kappa$ .

I evaluate the thermal conductivity diagrammatically in the main part of my thesis. It is advantageous to bring the equation for the transport coefficients into a form that allows to read off its spectral function [109] for this purpose. Inserting complete sets of energy eigenstates  $|n\rangle$  and  $|m\rangle$ , one obtains

$$L_{\mu\nu}(\mathbf{q}, \omega) = \frac{1}{\hbar Z} \sum_{n,m} \int_{-\infty}^t \int_0^\beta \langle n | e^{\frac{i}{\hbar} H(t' - i\lambda)} j_\nu(\mathbf{q}) e^{-\frac{i}{\hbar} H(t' - i\lambda)} | m \rangle \langle m | e^{\frac{i}{\hbar} Ht} j_\mu(-\mathbf{q}) e^{-\frac{i}{\hbar} Ht} | n \rangle \times e^{i(\omega+i0^+)(t-t')} d\lambda dt'. \quad (4.12)$$

Using the fact that  $H|n\rangle = E_n|n\rangle$  and evaluating the real- and imaginary-time integrals (shifting the real-time integral by  $t$ ), the transport coefficient is

$$L_{\mu\nu}(\mathbf{q}, \omega) = \frac{i}{Z} \sum_{n,m} \frac{e^{-\beta E_n}}{\hbar(\omega + E_n - E_m + i0^+)} \frac{e^{\beta(E_n - E_m)} - 1}{E_n - E_m} \langle n | j_\nu(\mathbf{q}) | m \rangle \langle m | j_\mu(-\mathbf{q}) | n \rangle. \quad (4.13)$$

The spectral function of the transport coefficients is  $S_{\mu\nu} = -\frac{1}{\pi} \text{Im}(L_{\mu\nu})$  and, therefore,

$$S_{\mu\nu} = \frac{1}{2\omega\hbar} \left( 1 - e^{-\beta\omega} \right) \langle j_\mu(\mathbf{q}) j(-\mathbf{q}) \rangle(\omega) \quad (4.14)$$

with the Dirac  $\delta$ -function  $\delta(\omega) = \frac{1}{2\pi} \int_{-\infty}^\infty e^{-i\omega t} dt$ . As the imaginary- and the real-part of an analytic function are related via the Kramers-Kronig relations [112, 113], one only has to calculate one of the two. The real-part can be calculated from the imaginary-part and vice versa.

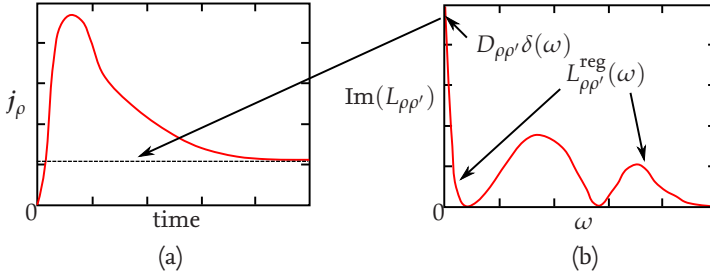


**Figure 4.1.:** The relaxation of a current  $j_\mu$  (a) is determined by the spectral function of the transport coefficient  $L_{\mu\nu}$  (b). If there is a finite Drude weight  $D_{\mu\nu} \neq 0$ , the current in (a) does not relax back to zero. The time-scale for which the current relaxes is determined by the regular part  $L_{\mu\nu}^{\text{reg}}$ .

The equation for the spectral function is often additionally decomposed at  $\omega = 0$  into the Drude-part  $D_{\mu\nu}$ , where  $E_n = E_m$ , and the regular part  $L_{\mu\nu}^{\text{reg}}$ , where  $E_n \neq E_m$

$$\text{Re}(L_{\mu\nu})(\mathbf{q}, \omega) = D_{\mu\nu}(\mathbf{q})\delta(\omega) + L_{\mu\nu}^{\text{reg}}(\mathbf{q}, \omega). \quad (4.15)$$

$L_{\mu\nu}^{\text{reg}}$  describes how fast the current decays in time and  $D_{\mu\nu}$  describes what part of the current persists to infinite time. This is illustrated in Figure 4.1. The delay of the response to the perturbation is determined by the real-part of the transport coefficient.

If the Drude-weight is finite, the system is a perfect conductor. At finite temperature, the  $\delta$ -peak broadens and the transport coefficient has a finite zero-frequency limit  $\omega \rightarrow 0$ . Usually, this limit vanishes due to interactions, characterising the system as a dissipative conductor. If both the Drude weight and the regular part are zero, it is an insulator<sup>1</sup>. The variable  $\omega$  can be identified as the frequency with which the system is driven by the perturbation. Therefore, one refers to the limit  $\omega \rightarrow 0$  and regular part also as the DC and AC response. For the calculation of the Drude-part, one only considers the  $\mathbf{q} \rightarrow 0$  limit as there should be no conserved quantities at finite momentum and then the number of the current's matrix elements with  $E_n = E_m$  is expected to be a set of zero measure.

Correlation functions like the one in equation (4.15) can be evaluated using Feynman diagrams and finite-temperature Matsubara-Green's functions  $G$  [114, 115]. These are discussed in the appendix A. The transport coefficients are

$$L_{\mu\nu} = \lim_{i\omega_n \rightarrow \omega + i0^+} \frac{1}{\omega_n} \int_0^\beta e^{i\omega_n \tau} \left\langle T_\tau \left( j_\mu(\tau) j_\nu(0) \right) \right\rangle d\tau. \quad (4.16)$$

<sup>1</sup>This should be read in respect of the density  $d$ . For example a material might be an electrical insulator, but a heat conductor.

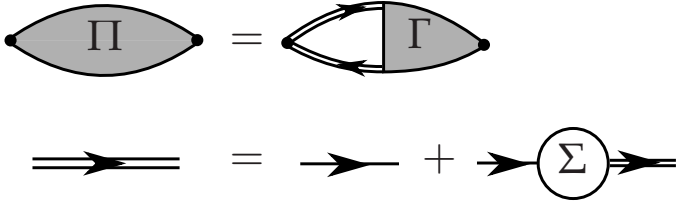


**Figure 4.2.:** Diagrammatic representation of the transport bubble  $\Pi$  with renormalised particle and hole lines (with self-energy  $\Sigma$ ) and vertex corrections  $\Gamma$

The symbol  $T_\tau$  indicates that the operators are time-ordered, i.e. operators at earlier times  $\tau$  have to be put to the right of operators at later times. This relation follows from comparison of its Källén-Lehmann representation [116, 117] to the same representation of  $\langle jj \rangle$  in equation (4.14). Diagrammatically, the calculation of the current-current correlators  $\Pi$  is equivalent to the evaluation of a legless bubble diagram like in Figure 4.2. In terms of the free Green's function  $G_0$  and renormalised Green's functions  $G$  and vertex  $\Gamma$  this reads

$$\Pi(\omega, k) = G(\omega + \omega', k + q)G(\omega, k)\Gamma(\omega + \omega', k + q; \omega, k), \quad (4.17)$$

$$G(\omega, k) = G_0(\omega, k + G_0(\omega, k)\Sigma(\omega, k)G(\omega, k)). \quad (4.18)$$

The self-energy  $\Sigma$  consists of all possible diagrams with one ingoing and one outgoing line conserving momentum, while the vertex correction includes all diagrams having a momentum difference of  $q$  between the one ingoing and the outgoing line. In this work, we will neglect vertex corrections ( $\Gamma=1$ ).



**Part II.**

**Field control of  
magnonic heat flow**



# 5. Control of magnonic heat flow by a magnetic field

In this chapter I discuss the influence of a magnetic field on the thermal transport due to excitations of the magnetic degrees of freedom (magnons) in an insulating, magnetically ordered material. I describe how the magnon spectrum is determined by linear spin-wave theory and the magnetic thermal conductivity is calculated from linear response theory in section 5.1. The magnon spectrum in finite magnetic field has a branch with linear dispersion (acoustic) and a flat, gapped branch (optical). The thermal conductivity depends on the magnons' velocity, heat capacity and lifetime. I start with calculations utilising effective expressions for the magnon lifetime in section 5.2. To gain a better understanding of the influence of the magnetic field on the first two of these three quantities, I look at how the magnons' velocity and their heat capacity evolve for an ideal acoustic and optic branch in section 5.2.1. From this I am able to take away valuable information for the discussion of the more complicated, complete magnon spectrum. As discussed in chapter 2, at low temperature, momentum-independent grain-boundary and impurity scattering are the dominant scattering mechanisms. These are the first scattering mechanisms I consider and show results for. At higher temperature, scattering of magnons among themselves and with other quasiparticles become more important. To qualitatively describe the high-temperature behaviour, such a momentum-dependent scattering mechanism has to be included. Hence, I add magnon-phonon scattering to the calculations in section 5.2.3.

In section 5.3 I calculate a magnon-magnon scattering rate from higher order terms in the  $1/S$ -expansion. This leads to one temperature-independent and one temperature-dependent scattering rate. For the former I repeat some of the calculations of[61] and discuss the results considering the consequences for the thermal conductivity in section 5.3.2. The temperature-dependent magnon-magnon scattering process I discuss in section 5.3.3 has not been considered before. The application of all the microscopic magnon-magnon scattering processes, temperature-dependent or -independent, and their dependence on the magnetic field's strength is new as well. In section 5.3.4 I add these processes to the grain-boundary scat-

tering and present the thermal conductivity as a function of magnetic field and temperature. I summarise the results of the chapter in section 5.4. Here I also include an examination of how the results might contribute to spin caloritronic applications. This might be the control of the thermal transport, but it can also be an overall effect that needs to be considered for spin caloritronic devices in a magnetic field. Furthermore, I discuss the possibility of using the thermal conductivity to demonstrate spontaneous magnon decay.

## 5.1. General theory of magnonic thermal conductivity

### 5.1.1. Linear spin-wave theory

The Hamiltonian of the Heisenberg model is introduced at the end of section 3.1. In this section I use linear spin-wave theory to calculate the excitation spectrum of that model on the square lattice in the presence of a magnetic field. These calculations have been performed already before [61, 118, 119]. Because of the importance of the results for the magnon spectrum for my thesis, I repeat the calculations in detail. When the term in equation (3.26) is added, the total Hamiltonian of the system is

$$H = J \sum_{\langle i,j \rangle} \mathbf{S}_i \cdot \mathbf{S}_j - B \sum_i S_i^z = J \sum_{\langle i,j \rangle} S_i^z S_j^z + \frac{1}{2} (S_i^+ S_j^- + S_i^- S_j^+) - B \sum_i S_i^z. \quad (5.1)$$

Here  $J$  is the (positive) superexchange parameter and  $B$  the strength of the magnetic field. Without loss of generality I choose the  $z$ -axis along the magnetic field. The summation in the first sum only goes over nearest neighbours i.e. spins for which  $|R_i - R_j| = a$  where  $R_i$  and  $R_j$  are their position vectors and  $a$  is the magnetic lattice constant.

The starting point for the linear spin theory is the system's classical magnetic ground state. It is common practice [45, 110] to change the frame of reference to one where the spins are ordered ferromagnetically. One can use the following site-dependent rotation

$$\mathbf{S}_i = \begin{pmatrix} \cos \theta_i & \sin \theta_i \sin \phi_i & \sin \theta_i \cos \phi_i \\ 0 & \cos \phi_i & -\sin \phi_i \\ -\sin \theta_i & \cos \theta_i \sin \phi_i & \cos \theta_i \cos \phi_i \end{pmatrix} \tilde{\mathbf{S}}_i, \quad (5.2)$$

with  $\theta_i$  being the angle of the spin at position  $R_i$  out of the  $x$ - $y$ -plane and  $\phi_i$  being the polar angle in it.

The excitations in the Heisenberg model can be obtained by using the following representation of the spin operators[98]

$$\begin{aligned} S_i^+ &= \left(2S - b_i^\dagger b_i\right)^\alpha b_i, \\ S_i^- &= b_i^\dagger \left(2S - b_i^\dagger b_i\right)^{1-\alpha}, \\ S_i^z &= S - b_i^\dagger b_i. \end{aligned} \quad (5.3)$$

For this transformation being canonic, i.e. preserving the commutation relation

$$\left[S_i^\lambda, S_j^\mu\right] = \epsilon_{\lambda\mu\nu} \delta_{ij} S_i^\nu \quad (5.4)$$

between the spin operator's components  $\lambda, \mu, \nu$ , two conditions have to be met: Firstly, the parameter  $\alpha$  has to be between zero and one. Secondly, the operators  $b_i^\dagger$  and  $b_i$  need to be bosonic creation and annihilation operators. The latter describe a spin excitation (magnon) at site  $i$ . Dyson and Maleev [120–122] considered the  $\alpha = 1$  case which is the most convenient parameter for calculations. Unfortunately,  $(S^+)^{\dagger} \neq S^-$  which is unphysical and the transformation is not unitary. This property is only fulfilled for  $\alpha = 1/2$ , which is the transformation proposed by Holstein and Primakoff [123]:

$$\begin{aligned} S_i^+ &= \sqrt{2S - b_i^\dagger b_i} b_i, \\ S_i^- &= b_i^\dagger \sqrt{2S - b_i^\dagger b_i}, \\ S_i^z &= S - b_i^\dagger b_i. \end{aligned} \quad (5.5)$$

In order to perform calculations, the square roots need to be expanded in powers of  $1/S$ . Terms up to quadratic order in the Hamiltonian describe non-interacting spin-waves and higher order terms interactions among these. The truncation of the expansion can lead to states with an eigenvalue to  $S^2$  larger than  $S(S + 1)$  which are not physical. Nevertheless, this spin-wave theory has turned out to give good approximations of the excitation spectrum of Heisenberg ferro- and antiferromagnets even for  $S = 1/2$  [17, 55].

I use equation (5.5) to map the spin operators canonically onto Bose-type creation and annihilation operators. The angles  $\phi_i$  and  $\theta_i$  are chosen in a way so that the classical energy is minimal. The latter is the part  $H^{(0)}$  of the Hamiltonian that

contains no spin-wave operators:

$$H^{(0)} = JS^2 \sum_{\langle i,j \rangle} \left[ \cos(\theta_i - \theta_j) \cos \phi_i \cos \phi_j + \sin \phi_i \sin \phi_j \right] - BS \sum_i \cos \theta_i \cos \phi_i. \quad (5.6)$$

Looking at the field-free system first, one finds that the classical energy only depends on the difference  $\psi := \theta_i - \theta_j$ , as well as  $\phi_i$  and  $\phi_j$  of neighbouring spins' angles. If the classical energy is minimal for this smaller subunit of the lattice, the overall energy is, too. Hence, one can assume that the ground state forms a lattice with a diatomic unit cell. Minimisation with respect to  $\psi$  leads to the condition  $\sin \psi = 0$ . That leaves

$$H^{(0)} = \frac{S^2 J N z}{2} \cos(\phi_i - \phi_j) \quad (5.7)$$

for the classical energy which is minimal for  $\phi_i - \phi_j = \pi$ , i.e. the Néel order of periodic pairs of antiparallel spins. Here  $N$  refers to the number of sites and  $z$  to the number of nearest neighbours on the lattice. For the square lattice  $z = 4$ . Because only the difference of the angles  $\phi_i$  and  $\phi_j$  has to be equal to  $\pi$ , one of the two can be chosen freely. I arbitrarily choose  $\phi_i = 0$  and  $\phi_j = \pi$ . Because the spins lie in the  $x$ - $y$ -plane and the magnetic field does not change the rotational invariance with respect to the  $z$ -axis, it seems natural to assume that the angles  $\phi_i$  and  $\phi_j$  are not changed by a finite field. The classical energy then is

$$H^{(0)} = -\frac{S^2 N J z}{2} \cos(\psi) + S B N \sin \frac{\psi}{2} \sin \frac{\delta}{2}, \quad (5.8)$$

where I introduce the sum  $\delta = \theta_i + \theta_j$ . I use the relation  $\cos \alpha - \cos \beta = -2 \sin \frac{\alpha}{2} \sin \frac{\beta}{2}$ , too. Minimising this expression with respect to  $\psi$ , I obtain

$$\sin \frac{\psi}{2} = -\frac{B}{2JSz} \sin \frac{\delta}{2} \quad (5.9)$$

which, when put into the classical energy, the latter becomes

$$H^{(0)} = -\frac{JS^2 Nz}{2} - \frac{B^2 N}{4Jz} \sin^2 \frac{\delta}{2}. \quad (5.10)$$

For  $\delta = \pi$ , this expression is minimal. If one chooses  $\theta_i = \frac{\pi+\psi}{2}$  on the one magnetic sublattice and  $\theta_j = \frac{\pi-\psi}{2}$  at the other magnetic sublattice the relations for  $\delta$  and  $\psi$  are both satisfied. These relations mean that at vanishing magnetic

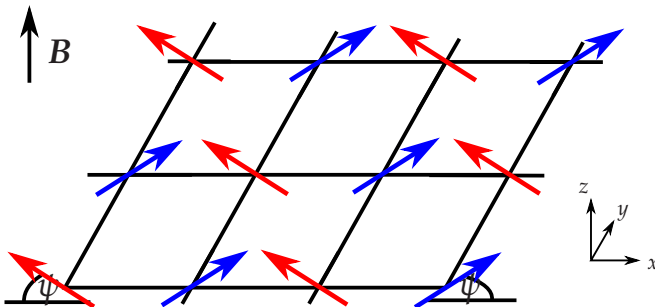


**Figure 5.1.:** The spin configuration of a Heisenberg AFM in the presence of a magnetic field  $B$  with minimal classical energy. The spins are canted from the Néel order by an angle  $\psi$  in the direction of the magnetic field.

field the spins lie pairwise antiparallel in the  $x$ - $y$ -plane and start to cant in the direction of the magnetic field ( $z$ -direction) with the angle

$$\sin \frac{\psi}{2} = \frac{B}{8JS}. \quad (5.11)$$

I show this in Figure 5.1. When the field exceeds  $B_S = 8JS$ , the spins are saturated and are all aligned with the magnetic field. According to equation (5.11), the saturation field is determined by the strength of the exchange interaction  $J$  between the spins. The exchange constant differs greatly. In materials such as CuPzN it is of the order of  $J \sim -0.5\text{ meV}$  [124], while it is of the order of  $J \sim 100\text{ meV}$  for cuprates [125]. Therefore, the saturation field  $B_S$  is of moderate order ( $\sim 10\text{T}$ ) for materials like the former [57, 126–128], but can also be experimentally unattainable ( $B_S \sim 3000\text{ T}$ ) as for the cuprates.

The site-dependent rotation of the spin-reference frame in equation (5.2) can now be simplified

$$\mathbf{S}_i = \begin{pmatrix} \cos \theta_i & 0 & e^{i\mathbf{Q} \cdot \mathbf{R}_i} \sin \theta_i \\ 0 & e^{i\mathbf{Q} \cdot \mathbf{R}_i} & 0 \\ -\sin \theta_i & 0 & e^{i\mathbf{Q} \cdot \mathbf{R}_i} \cos \theta_i \end{pmatrix} \tilde{\mathbf{S}}_i, \quad (5.12)$$

with the Néel ordering vector  $\mathbf{Q} = \pi\mathbf{e}_x + \pi\mathbf{e}_y$  of the square lattice and its basic vectors  $\mathbf{e}_i$ . The full Hamiltonian after applying the rotation and using trigonometric identities becomes

$$\begin{aligned} H = & -J \sum_{\langle i,j \rangle} \left( \tilde{S}_i^x \tilde{S}_j^x + \tilde{S}_i^z \tilde{S}_j^z \right) \cos \psi - \tilde{S}_i^y \tilde{S}_j^y + e^{i\mathbf{R}_i \cdot \mathbf{Q}} \left( \tilde{S}_i^z \tilde{S}_j^x - \tilde{S}_i^x \tilde{S}_j^z \right) \sin \psi \\ & - B \sum_i e^{i\mathbf{R}_i \cdot \mathbf{Q}} \tilde{S}_i^x \cos \frac{\psi}{2} + \tilde{S}_i^z \sin \frac{\psi}{2}. \end{aligned} \quad (5.13)$$

It is easily checked that the term linear in the spin-wave operators vanishes<sup>1</sup>. The first correction to the classical energy is the harmonic, quadratic part. I find using  $B = B_S \sin \frac{\psi}{2}$ , utilising the symmetry of the sum, and using equation (5.5)

$$\begin{aligned} H^{(2)} = & -\frac{JS}{2} \sum_{\langle i,j \rangle} (a_i^\dagger a_j + \text{h.c.}) (\cos \psi + 1) + 2a_i^\dagger a_j (\cos \psi - 1) - 4a_i^\dagger a_i \cos \psi \\ & + 2JSz \sum_i a_i^\dagger a_i \sin^2 \frac{\psi}{2}. \end{aligned} \quad (5.14)$$

The Fourier-transformations of the individual terms are

$$\begin{aligned} \sum_{\langle i,j \rangle} a_i^\dagger a_i &= \frac{z}{2} \sum_k a_k^\dagger a_k, \quad , \quad \sum_{\langle i,j \rangle} a_i^\dagger a_j = \sum_k \gamma_k a_k^\dagger a_k, \\ \sum_{\langle i,j \rangle} a_i^{(\dagger)} a_j^{(\dagger)} &= \sum_k \gamma_k a_k^{(\dagger)} a_{-k}^{(\dagger)}, \quad , \quad \sum_i a_i^\dagger a_i = \sum_k a_k^\dagger a_k, \end{aligned} \quad (5.15)$$

$$\text{with } \gamma = \cos k_x + \cos k_y$$

where I set the lattice constant to unity. With this the harmonic part becomes

$$\begin{aligned} H^{(2)} = & 4JS \sum_k A_k a_k^\dagger a_k - \frac{B_k}{2} (a_k a_{-k} + \text{h.c.}), \\ \text{with } A_k &= 1 + \gamma_k \sin^2 \frac{\psi}{2}, \\ \text{and } B_k &= \gamma_k \cos^2 \frac{\psi}{2}. \end{aligned} \quad (5.16)$$

The terms with the coefficient  $A_k$  are diagonal in the magnon basis and the ones with  $B_k$  are pair-breaking ones. Such a Hamiltonian is known from BCS-theory [129] and can be diagonalised by a Bogoliubov transformation [130, 131] which for bosons is

$$a_k = \alpha_k \cosh \vartheta_k + \alpha_{-k}^\dagger \sinh \vartheta_k := u_k \alpha_k + o_k \alpha_{-k}^\dagger \quad (5.17)$$

with the condition

$$\tanh 2\vartheta_k = \frac{B_k}{A_k}. \quad (5.18)$$

---

<sup>1</sup>In  $\sum_{\langle i,j \rangle} e^{iR_i \cdot Q} (a_i - a_j + \text{h.c.})$  the index  $j$  can be shifted by one (changing its sign) and the sum over nearest neighbours can be carried out leaving the sum over all sites  $i$  times  $z/2$ . Hence, the term  $JS \sum_{\langle i,j \rangle} e^{iR_i \cdot Q} (S_i^x S_j^x - S_i^z S_j^z) \sin \psi$  is equal to  $2JSz \sum_i e^{iR_i \cdot Q} \frac{S^{3/2}}{\sqrt{2}} (a_i + a_i^\dagger) \sin(\psi/2) \cos(\psi/2)$  in the order of  $S^{3/2}$ . By using  $B = -B_S \sin \frac{\psi}{2}$  in the term  $\sum_i e^{iR_i \cdot Q} B S_i^x \cos(\psi/2)$  in the term of order  $S^{3/2}$ , it becomes  $-\sum_i e^{iR_i \cdot Q} \frac{S^{3/2}}{\sqrt{2}} B_S \sin(\psi/2) \cos(\psi/2)$ . Because  $B_S = 2JSz$ , both terms cancel.

The result is

$$H^{(2)} = \sum_k \epsilon_k \left( \alpha_k^\dagger \alpha_k + \frac{1}{2} \right) - 2JS A_k \quad (5.19)$$

with the constant terms being  $1/S$  corrections to the classical energy and

$$\epsilon_k = 4JS \sqrt{A_k^2 - B_k^2} := 4JS\omega_k$$

the spin-wave or magnon dispersion. The latter is illustrated in Figure 5.2. Important features are the Goldstone mode at  $k = Q$ , which is a characteristic of the remaining symmetry under flipping every spin, and the field-induced gap at the origin of the Brillouin-zone. The asymptotics of the dispersion close to those two points below the saturation field  $B_S$  are

$$\epsilon_{k \approx 0} = JS \left( 8b - \frac{3b^2 - 1}{2b} k_r^2 \right) \quad (5.20)$$

$$\epsilon_{k \approx Q} = v k_r + d k_r^3 \quad (5.21)$$

$$\text{with } v = 2\sqrt{2}JS\sqrt{1-b^2} \text{ and } d = \frac{v}{16} \left( \frac{b^2}{1-b^2} - \frac{9 + \cos 4\varphi_k}{6} \right)$$

with  $k_r$  and  $\varphi_k$  being the polar coordinates in  $k$ -space and  $b = B/B_S$ . The gap  $\Delta = \epsilon_{k=0}$  at the  $\Gamma$ -point, as well as the velocity  $v$  at  $k = Q$  depend on the magnetic field's strength. I show that much of the thermal conductivity's behaviour can be understood with the help of both quantities, later in the text.

### 5.1.2. Linear response theory

In section 4 I show that, without vertex corrections, the thermal conductivity can be calculated by a transport bubble with two renormalised Green's functions. Here I present the detailed calculation for magnons. Before I start with the evaluation of the thermal conductivity, the vertex function of the current-current correlator needs to be calculated, i.e. the prefactor of the current operator in the magnon basis. To do so, I use the definition of the current operator in equation (4.5) via a local energy density  $h_l$  and the energy polarisation operator  $P_l = r_l h_l$ . Looking at the Hamiltonian with real-space operators in equation (5.14), one possible choice

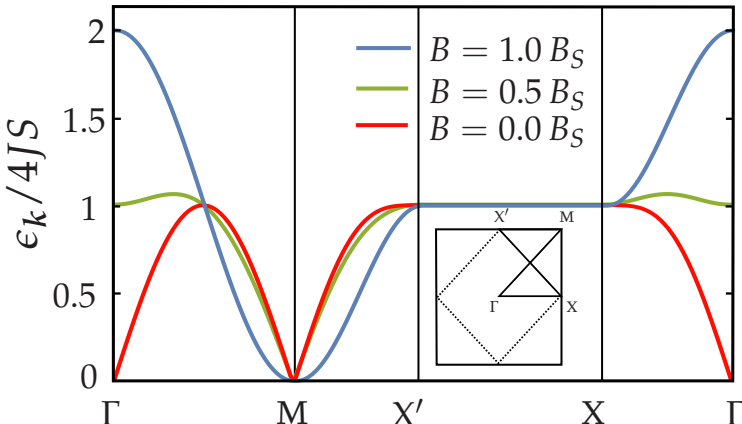


**Figure 5.2.:** Magnon dispersion  $\epsilon_k$  on the path shown in the inset for two magnetic fields  $B$  in units of the saturation field  $B_S = 8JS$ . A finite magnetic field induces a gap  $\Delta$  at the  $\Gamma$ -point which monotonically increases with the magnetic field's strength. At the point  $M = Q$  the magnon velocity  $c$  monotonically decreases with  $B$ .

for  $h_l$  is<sup>2</sup>

$$h_l = SJ \sum_{\Delta=\{\pm e_x, \pm e_y\}} a_l^\dagger a_l + a_l^\dagger a_{l+\Delta} \sin^2 \frac{\psi}{2} - \frac{1}{2} \left( a_l a_{l+\Delta} + \text{h.c.} \right) \cos^2 \frac{\psi}{2}. \quad (5.22)$$

Using the Fourier representation  $P_q$  of the polarisation operator, the energy current operator is in the long-wavelength transport limit

$$j_Q = \lim_{q \rightarrow 0} i [H, P_q]. \quad (5.23)$$

Because of

$$P_q = \sum_l e^{iq \cdot r_l} r_l h_l = -i \nabla_q \sum_l e^{iq \cdot r_l} h_l, \quad (5.24)$$

I determine the Fourier-transform of the energy density

$$\sum_l e^{iq \cdot r_l} h_l = 4SJ \sum_k A_{k-q} b_k^\dagger b_{k-q} - \frac{B_{k-q}}{2} \left( b_{-k} b_{k-q} + \text{h.c.} \right). \quad (5.25)$$

Here  $A_k$  and  $B_k$  are the same as in equation (5.16). Next, I insert the Bogoliubov transformation to be able to evaluate the commutator with the Hamiltonian more

<sup>2</sup>As for any density on a finite lattice, this choice is not unique. On the other hand, such a density is not experimentally accessible, too. Any other quantity that has physical meaning is, however, not expected to be affected by particular the choice of the density.

easily. The result is

$$\begin{aligned} h_q = \sum_l e^{iq \cdot r_l} h_l &= 4S J \sum_k \alpha_k^\dagger \alpha_{k-q} \left[ A_{k-q} u_k u_{k-q} - \frac{B_{k-q}}{2} (o_k u_{k-q} + u_k o_{k-q}) \right] \\ &\quad + \alpha_{-k}^\dagger \alpha_{-k} \left[ A_{k-q} o_k o_{k-q} - \frac{B_{k-q}}{2} (u_k o_{k-q} + o_k u_{k-q}) \right] \\ &\quad + \alpha_{-k} \alpha_{k-q} \left[ A_{k-q} o_k u_{k-q} - \frac{B_{k-q}}{2} (u_k u_{k-q} + o_k o_{k-q}) \right] \\ &\quad + \alpha_k^\dagger \alpha_{q-k}^\dagger \left[ A_{k-q} u_k o_{k-q} - \frac{B_{k-q}}{2} (o_k o_{k-q} + u_k u_{k-q}) \right]. \end{aligned} \quad (5.26)$$

Although the calculation of the commutator  $[H, \nabla_q h_q]$  is lengthy, it is still straightforward. Using the following relations

$$\nabla_q u_q = \frac{1}{2} o_q \left( \frac{A_q \nabla_q B_q - B_q \nabla_q A_q}{\omega_q^2} \right), \quad 2u_q o_q = \frac{B_q}{\omega_q} \quad (5.27)$$

$$\nabla_q o_q = \frac{1}{2} u_q \left( \frac{A_q \nabla_q B_q - B_q \nabla_q A_q}{\omega_q^2} \right), \quad u_q^2 + o_q^2 = \frac{A_q}{\omega_q} \quad (5.28)$$

$$\nabla_q \omega_q = \frac{A_q \nabla_q A_q - B_q \nabla_q B_q}{\omega_q}, \quad \omega_q = \sqrt{A_q^2 - B_q^2} \quad (5.29)$$

I arrive at the final result

$$j_Q = \sum_k \frac{1}{2} \begin{pmatrix} \alpha_k^\dagger & \alpha_{-k} \end{pmatrix} \begin{pmatrix} \epsilon_k \nabla_k \epsilon_k & 0 \\ 0 & \epsilon_k \nabla_k \epsilon_k \end{pmatrix} \begin{pmatrix} \alpha_k \\ \alpha_{-k}^\dagger \end{pmatrix}. \quad (5.30)$$

The energy current operator is the product of a mode's energy  $\epsilon_k$  and its velocity  $\nabla_k \epsilon_k$  which might have been the naive assumption.

Assuming that all interactions that can affect a free magnon are already taken into account, the renormalised (Matsubara-)Green's function is

$$\mathcal{G}(i\omega_n, k) = \frac{1}{i\omega_n - \epsilon(k) - \Sigma(k, i\omega_n)} \quad (5.31)$$

with the free magnon dispersion  $\epsilon$  and the self-energy  $\Sigma$ . According to equation

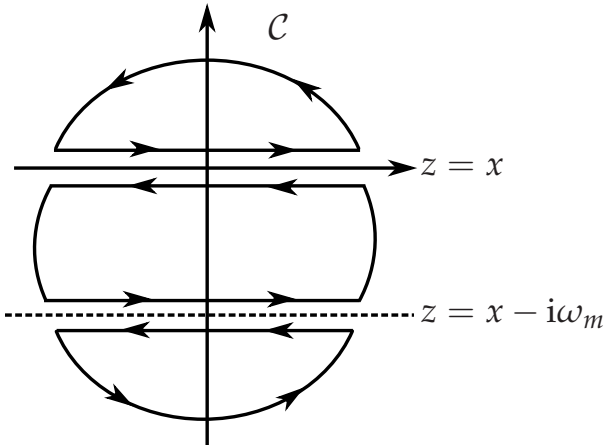


**Figure 5.3:** Contour  $\mathcal{C}$  for the evaluation of the Matsubara sum in equation (5.32) with branch cuts along the real axis and at  $\text{Im } z = -i\omega_m$ .

(4.16) and (4.11) the Drude-part of the thermal conductivity is [132]

$$\begin{aligned} \kappa' &= \lim_{\omega \rightarrow 0} \frac{\beta}{N\omega} \lim_{i\omega_n \rightarrow \omega + i0^+} \text{Im} \left( \int_0^\beta e^{i\omega_m \tau} \langle j_Q(\mathbf{k}, \tau) j_Q(-\mathbf{k}, 0) \rangle d\tau \right) \\ &= \lim_{\omega \rightarrow 0} \frac{1}{N\omega} \lim_{i\omega_n \rightarrow \omega + i0^+} \text{Im} \left[ \sum_{\mathbf{k}} \epsilon_{\mathbf{k}}^2 (\nabla_{\mathbf{k}} \epsilon_{\mathbf{k}}) (\nabla_{\mathbf{k}} \epsilon_{\mathbf{k}}) \sum_{i\omega_m} \mathcal{G}(\mathbf{k}, i\omega_m) \mathcal{G}(\mathbf{k} + \mathbf{q}, i(\omega_n + \omega_m)) \right]. \end{aligned} \quad (5.32)$$

Here the product of the two velocities is dyadic. One can treat the Matsubara-sum in the same manner as in A.2. Here the contour integration has to be carried out along the contour  $\mathcal{C}$  which I illustrate in Figure 5.3. As before, the contribution of the arcs vanishes in the limit  $R \rightarrow \infty$  and only the paths along the branch cuts at  $\text{Im}(z) = 0$  and  $\text{Im}(z) = -\omega_m$  remain. The result is

$$\begin{aligned} \sum_{i\omega_m} \mathcal{G}(\mathbf{k}, i\omega_m) \mathcal{G}(\mathbf{k} + \mathbf{q}, i(\omega_n + \omega_m)) &= \frac{\beta}{2\pi i} \int_{-\infty}^{\infty} n(z) \left[ \mathcal{G}(\mathbf{k}, z + i0^+) \mathcal{G}(\mathbf{k} + \mathbf{q}, z + i\omega_n + i0^+) \right. \\ &\quad - \mathcal{G}(\mathbf{k}, z - i0^+) \mathcal{G}(\mathbf{k} + \mathbf{q}, z + i\omega_n - i0^+) + \mathcal{G}(\mathbf{k}, z - i\omega_n + i0^+) \mathcal{G}(\mathbf{k} + \mathbf{q}, z + i0^+) \\ &\quad \left. - \mathcal{G}(\mathbf{k}, z - i\omega_n - i0^+) \mathcal{G}(\mathbf{k} + \mathbf{q}, z - i0^+) \right] dz = *. \end{aligned} \quad (5.33)$$

Because of  $\mathcal{G}(k, z - i\omega_n \pm i0^+) = \mathcal{G}(k, z - i\omega_n)$  this can further be simplified

$$\begin{aligned} * &= \frac{\beta}{2\pi i} \int_{-\infty}^{\infty} n(z) [\mathcal{G}(k + q, z + i\omega_n) (\mathcal{G}(k, z + 0^+) - \mathcal{G}(k, z - 0^+)) \\ &\quad + \mathcal{G}(k, z - i\omega_n) (\mathcal{G}(k + q, z + 0^+) - \mathcal{G}(k + q, z - 0^+))] dz. \end{aligned} \quad (5.34)$$

The differences of advanced and retarded Green's functions is the spectral function

$$S(k, z) = -\frac{1}{2\pi i} ((\mathcal{G}(k, z + i0^+) - \mathcal{G}(k, z - i0^+)). \quad (5.35)$$

After the analytic continuation  $i\omega_n \rightarrow \omega + i0^+$  the Matsubara sum is

$$* = -\beta \int_{-\infty}^{\infty} n(z) (S(k, z)\mathcal{G}(k + q, z + \omega + i0^+) + S(k + q, z)\mathcal{G}(k, z - \omega - i0^+)) dz. \quad (5.36)$$

The remaining complex quantities in equation 5.32 are the Green's functions and because of

$$S(k, z) = \mp \frac{1}{\pi} \text{Im} (\mathcal{G}(k, z \pm i0^+)), \quad (5.37)$$

I find

$$\begin{aligned} \kappa' &= \lim_{\substack{\omega \rightarrow 0 \\ q \rightarrow 0}} \frac{\beta}{N\omega} \sum_k \pi \int_{-\infty}^{\infty} (n(z) - n(z + \omega)) S(k, z) S(k + q, z + \omega) dz \\ &= -\lim_{\omega \rightarrow 0} \frac{\beta}{N} \sum_k (\epsilon_k \nabla_k \epsilon_k)^2 \frac{n(\epsilon_k + \omega) - n(\epsilon_k)}{\omega} \frac{2\Sigma''_k}{4(\Sigma''_k)^2 + \omega^2}. \end{aligned} \quad (5.38)$$

To obtain the result, I assume that the spectral functions are narrow Lorenzians around the magnon energies  $\epsilon(k)$ , so that  $n(z)$  is more or less constant at those energies. Hence, the  $z$  integration yields the Lorentzian times the Bose-distribution function at the magnon energies. Taking the frequency limit, the thermal conductivity is

$$\kappa' = -\frac{\beta}{N} \sum_k (\epsilon_k v_k)^2 \frac{\partial n(\epsilon_k)}{\partial \epsilon_k} \frac{1}{2\Sigma''_k} = \frac{1}{N} \sum_k v_k^2 \frac{\partial (\epsilon_k n(\epsilon_k))}{\partial T} \tau_k \quad (5.39)$$

where I abbreviate  $\nabla \epsilon(k)$  by  $v_k$ , replace the energy derivative by one with respect to temperature and use the fact that the self-energy's imaginary part is the rate

of decay of the two involved magnon modes  $2\Sigma''_k = \tau_k^{-1}$ . Because the quantity  $\epsilon_k n$  is the energy of a mode, its temperature derivative is its heat capacity (at constant volume). Hence, this relation is in accordance with the Drude-like form in equation (2.8). The velocity  $v_k = \nabla \epsilon_k$  is proportional to  $(\sin k_x, \sin k_y)$ . Hence, the integral/sum vanishes for  $\kappa_{xy} = \kappa_{yx}$  if the lifetime  $\tau_k$  does not break time-reversal symmetry, i.e.  $\tau_k = \tau_{-k}$ . For this reason, I only discuss the components  $\kappa_{xx} = \kappa_{yy} := \kappa$ . In the next section I use this expression to calculate the thermal conductivity for various scattering rates as a function of temperature and the external magnetic field.

## 5.2. Thermal conductivity using empiric lifetimes

### 5.2.1. Contribution of acoustic and optic modes as a function of the magnetic field

In equation 5.39 one can see that the magnon velocity  $v_k$  and lifetime  $\tau_k$  as well as the heat capacity per mode  $c_k := \frac{\partial \epsilon_k n_B}{\partial T}$  are the three quantities the thermal conductivity depends on. For now, I only focus on the contribution of the magnon velocity and heat capacity. As an additional temporary simplification, I restrict this discussion to two limits: the limit of acoustic and optical magnons by restricting the sum in equation (5.39)

$$\kappa'_\Omega = \frac{1}{N} \sum_{\Gamma} c_k v_k^2 \tau_k \quad (5.40)$$

to the region  $\Omega$  in  $k$ -space where these approximations are valid and by assuming a constant, momentum independent magnon lifetime  $\tau_k$ . For the acoustic approximation the region  $\Omega$  is a square of side length  $\pi/10$  in momentum space and center at the  $M$ -point for all magnetic fields below the saturation field  $B_S$  and at the  $\Gamma$ -point for  $B = 0$ . The optic approximation is only valid for  $B \neq 0$ . The square has its center at the  $\Gamma$ -point then. I describe the influence of the magnetic field on the magnon velocity and heat capacity in particular. In this way, some insights can already be had which are helpful for the understanding of the thermal conductivity's behaviour as a function of temperature and external magnetic field. In the next subsections, I include effective expressions of increasing complexity and consider the full magnon spectrum without approximations.

As can be inferred from equations (5.20) and (5.21), there is the opening of a gap at the  $\Gamma$ -point of the Brillouin zone and the change in the magnon velocity of the remaining Goldstone mode at the  $M$ -point. I consider the optical limit where the dispersion is assumed to be constant. In this approximation the velocity vanishes for  $B \neq 0$ . This implies according to equation (5.40) that the reduced thermal conductivity  $\kappa_T$  vanishes. The magnon dispersion at the  $\Gamma$ -point (see equation (5.21)) still has curvature and there is a small contribution to the thermal conductivity by magnons from the  $\Gamma$ -point's vicinity. Hence, the optical approximation can be seen as the maximal reduction that can be expected from applying the magnetic field: No magnon modes contributing to the thermal transport from the region around the  $\Gamma$ -point. For a more accurate estimation of the magnetic field's effect on these magnon modes, I look at the heat capacity in the following. The heat capacity is

$$c_k = \frac{\Delta^2}{T^2} \frac{\exp(\Delta/T)}{(\exp(\Delta/T) - 1)^2}. \quad (5.41)$$

Here  $\Delta = 8JS_b$  is the gap due to the external magnetic field (relative to the saturation field  $b = B/B_S$ ). I show the heat capacity as a function of the gap's size in Figure 5.4(a). Its behaviour is easily explained: because of the gap, the excitation energy of those magnon modes increases and fewer modes are excited as temperature increases. This implies a lower heat capacity. The effect is less pronounced for a larger temperature, as magnons above the gap are excited more easily. But even at a temperature of  $T = 0.3J$  the heat conductivity is reduced by about 30% with a magnetic field of less than 20% of the saturation field. With a field of half the saturation field, the heat capacity is reduced to 5% of its value at a vanishing magnetic field, as can be seen in Figure 5.4(b). In this consideration I do not include the contribution of the velocity. As it drops to zero at the  $\Gamma$ -point for non-zero fields and grows quadratically with momentum, I expect an even greater reduction. The optical magnon branch and the acoustic one are degenerate at zero magnetic field. Both are contributing the strongest to the thermal conductivity at in the low-temperature limit. Therefore, as I show later in this text, the opening of the gap is the primary cause for the reduction of the thermal conductivity for low magnetic fields. The heat capacity of the optical modes is almost reduced to zero at higher fields, since the these modes can not be excited and do not contribute to the thermal transport.

I consider the acoustic modes next. These modes are found in the region  $\Omega$  with short-wavelength modes in the corners of the Brillouin-zone. Here, the velocity monotonically decreases with an increasing magnetic field which can be inferred from looking at equation (5.21). The influence of the magnon velocity  $v$  is not as easy to identify as the one of the gap's size. On the one hand, the velocity directly

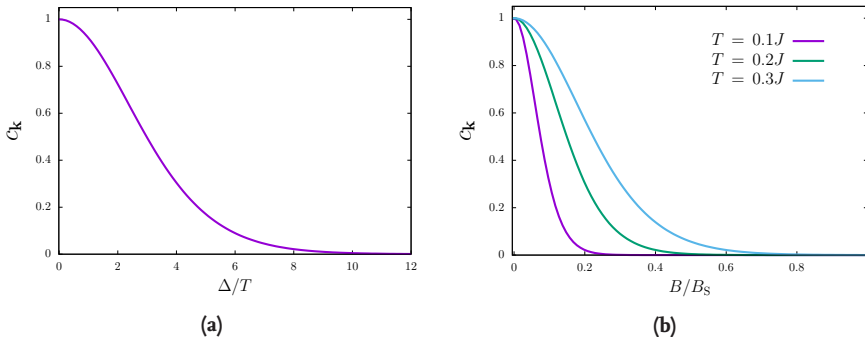


**Figure 5.4.:** Heat capacity  $c_k$  of a single magnon mode in the optical approximation  $\epsilon_k = \Delta$   
 (a) depending on the size of the gap  $\Delta$  and (b) on the external magnetic field. One  
 sees that the heat capacity is reduced by a gap and so is the contribution of that  
 mode to the overall thermal conductivity.

appears in the integrand in equation (5.40) as  $v^2$ . A smaller velocity means the mode does transport less energy per time. On the other hand, a lower velocity also means that exciting modes with momentum close to  $k = 0$  costs less energy. This means a higher heat capacity. As the dependence of the heat capacity of the acoustic modes on the product  $vk/T$  is the same as for the optical modes on  $\Delta/T$ , I do not illustrate this dependence again. I instead refer to Figure 5.4(a).

I infer from this that mainly modes close to the  $\Gamma$ -point need to be considered as the heat capacity drops quite sharply with momentum. For lower velocities and higher temperatures the number of modes that need to be considered increases, though. The heat capacity of the zero mode is

$$c_{k=0} = \lim_{k \rightarrow 0} \left( \frac{vk}{T} \right) \frac{\exp(vk/T)}{\left( \exp(vk/T) - 1 \right)^2} = 1 \quad (5.42)$$

independent of the velocity. Therefore, the contribution of this mode to the thermal transport is proportional to  $v^2$ . To get a first impression of the implications for a mode with finite momentum, I look at the dimensionless quantity  $v^2 c_k k^2 / T^2$  as a function of  $vk/T$ . I illustrate it in Figure 5.5(a). One can see that there are values of  $vk/T$  where the contribution of a mode decreases when the velocity increases. In the light of the fact that the contribution of a mode is smaller the higher its momentum, one can have a look at Figure 5.5(b). Here I show how the contribution of modes of different momenta and temperature evolves as a function of the velocity. One can see that the contribution of modes with finite momentum can have a maximum at a certain velocity. Generally, those modes are not important for the transport. Either they are not excited at the temperatures I am interested in ( $k$  is too high) and their contribution is small irrespective of the velocity, or the velocity can not be realised by any magnetic field. For systems with a higher attainable

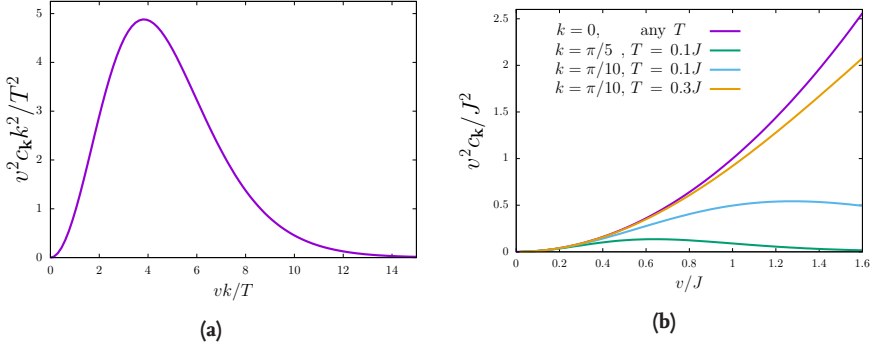


**Figure 5.5:** (a) Dimensionless quantity  $v^2 c_k k^2 / T^2$  where  $v$  is the velocity of an acoustic mode of momentum  $k$  as a function of  $vk/T$ . Here it can be seen that the contribution of a mode with momentum  $k$  at a temperature  $T$  can either increase or decrease with variation of its velocity. (b) Contribution of an acoustic mode to the thermal transport as a function of its velocity. It is apparent that for modes close to the  $\Gamma$ -point the contribution of those magnon modes monotonically increases as a function of the magnon velocity. Modes with higher momentum show more complicated behaviour. Their contribution can either grow or shrink depending on the temperature.

velocity, however, those modes might be important.

This can be seen more clearly in Figure 5.6 where I show the contribution of various modes of different momentum and at a different temperature as a function of the external magnetic field. One sees that the contribution to the thermal conductivity does not vary much for small fields. This is plausible as the velocity is not changing much, either. As the temperature increases, I observe a change in the contribution for smaller fields. The reason for this is the shallow behaviour of those modes that can be seen e.g. in the blue curve in Figure 5.5(b) at velocities close to  $v = \sqrt{2}J$ . For the mode with  $k = \pi/5$  I observe an increase in its contribution for moderate fields. Its overall contribution is, however, very small compared to the modes with smaller momentum. I also see that the contribution of modes with higher momenta increases at higher temperatures. For magnetic fields close to the saturation field the contribution of acoustic modes goes to zero. From this discussion, I expect the overall thermal conductivity to vanish at  $B = B_S$  as both the contribution of purely optic ( $\epsilon_k = \Delta$ ) and acoustic modes ( $\epsilon_k = vk$ ) go to zero at that point. Up to this point, I neglect the change in curvature of the acoustic modes which diverges at the saturation field. Therefore, the magnon velocity is not constant around the  $\Gamma$ -point and does not vanish everywhere at  $B = B_S$ . Clearly, the true behaviour of the thermal conductivity is more complicated because of the magnon dispersion. The aim of this discussion is just to get a first impres-

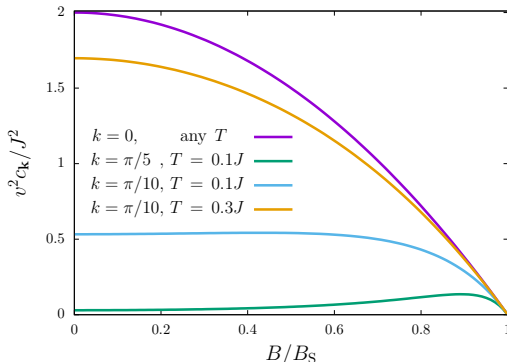


**Figure 5.6.**: Contribution of acoustic magnons to the thermal transport as a function of the external magnetic field  $B/B_S$  where  $B_S$  is the saturation field. I observe a quite constant behaviour for moderate magnetic fields and a drastic reduction for fields close to  $B_S$ . Modes whose contribution increases with the field are of less importance compared to others.

sion of what to expect from the two magnon branches. Deviations are expected and give indication of a contribution from other types of magnon modes. In the following sections, I consider the full dispersion  $\epsilon_k$  from equation (5.19) first, for a momentum-independent scattering rate and second, for a momentum-dependent rate.

### 5.2.2. Thermal conductivity with temperature-independent scattering

In section 5.1.2 I derive the magnetic thermal conductivity as a function of the magnons' energy, velocity, heat capacity and their lifetime. Neglecting the contribution of the lifetime, in section 5.2.1 I look at the contribution of two kinds of modes that can be found in the magnon's spectrum: the optical and the acoustic mode. Now I include scattering processes which are most important at a temperature low compared to the exchange interaction and consider the full magnon dispersion, i.e. without the acoustic or optic approximation. At such a low temperature, only few low-energy modes are excited. These are the modes around the  $\Gamma$ -point and the corners of the Brillouin-zone. For the long-wavelength modes, grain-boundary scattering and for the short-wavelength modes scattering on impurities is the dominant mechanism for the reduction of the magnetic thermal transport at low temperature [19]. The former scattering processes can arise either due to a finite sample size, a boundary between two magnetic domains or because of the correlation length of the magnetic order parameter. They lead to the modes not

being able to pass the boundary unhindered, therefore complicating the propagation. The larger a grain's average size  $l_{\text{gb}}$  is and the slower the mode travels, i.e. the lower  $v_k$ , the higher is the mode's lifetime [83] or inverse lifetime

$$\tau_{\text{gb}} = \frac{l_{\text{gb}}}{|v_k|}. \quad (5.43)$$

For impurity scattering there is a similar formula with  $l_{\text{gb}}$  being replaced by the mean distance of two impurities. In this section I use  $\tau_{\text{gb}}$  synonymously for both processes. The relaxation time of the magnon is just the average time it takes the magnon to go from one grain or impurity to another. As I show in the previous section, at these temperatures the main contribution is due to the acoustic modes. Their velocity has hardly any momentum-dependence. Hence, both scattering rates are not a function of momentum or temperature and a lot can be learned about the full spectrum for different magnetic fields.

The whole temperature dependence of the conductivity (see equation (5.39)) is contained in the heat capacity

$$c_k = \frac{\partial \epsilon_k n(\epsilon_k)}{\partial T} = \frac{\epsilon_k^2}{T^2} \frac{e^{\epsilon_k/T}}{(e^{\epsilon_k/T} - 1)^2} \quad (5.44)$$

of a mode with momentum  $k$ . In the high-temperature limit  $T \rightarrow \infty$  the expression is one and temperature-independent. Every mode therefore contributes  $v_k^2 \tau_{\text{gb}}$ . Hence, information about the average velocity of all the modes can be extracted from this limit. If the spectrum becomes flat in certain regions of the Brillouin-zone, the thermal conductivity indicates this fact for large  $T$ . The modes from these regions do not contribute to the thermal transport in that case.

At low temperature it can be assumed that all contributing modes are isotropic and acoustic, i.e.  $\epsilon_k = k_r v_k$  with  $k_r$  being the distance to the origin of the acoustic branch. After changing variables  $x = \epsilon_k/T$  and replacing the sum by an integral, equation (5.39) becomes<sup>3</sup>

$$\kappa \approx \frac{T^2 \tau_{\text{gb}}}{2\pi} \int_0^\infty \frac{x^3 e^x}{(e^x - 1)^2} dx = \frac{3T^2 \tau_{\text{gb}}}{\pi} \zeta(3) \quad (5.45)$$

with the Riemann zeta function  $\zeta$ . This means that for small  $T$  the thermal conductivity of magnons on a square lattice is proportional to  $T^2$  according to equation (5.45) and for large temperature a non-zero constant according to equation (5.44).

---

<sup>3</sup>The range of integration was extended to infinity because the contribution of high-energy modes is small at low  $T$ .

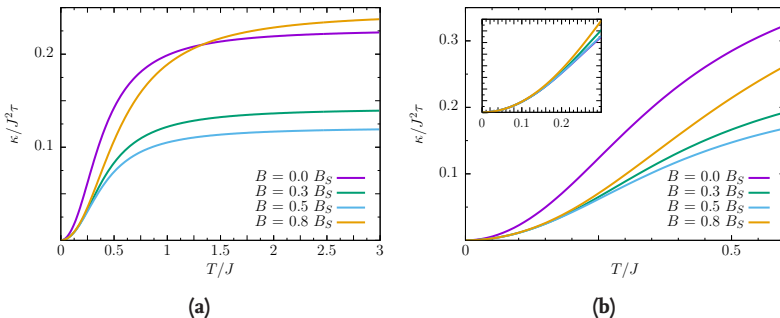


**Figure 5.7:** Thermal conductivity  $\kappa$  as a function of temperature for different values of the external magnetic field in (a) for a larger temperature range and in (b) for lower temperature (the line of the thermal conductivity at zero magnetic field is divided by two in the inset)

Both the low- $T$  as well as the high- $T$  behaviour can be observed in Figure 5.7a for several magnetic fields. I also observe that the curve of  $B = 0.8B_S$  intersects with the curve of zero field at  $T \approx 1.3J$ . For reasons that will become clear later in this section, the spectrum allows for better thermal transport of modes with higher energy for magnetic fields above  $B = 0.5B_S$ . In Figure 5.7b the temperature dependence is shown for a smaller temperature range. Here all curves, except for the curve at vanishing magnetic field, lie more or less on top of each other. This has to do with the fact that the magnon spectrum has two acoustic branches at  $B = 0$ : one at the  $\Gamma$ - and one at the  $M$ -point. For a finite magnetic field, the spectrum has only one acoustic branch. Hence at small temperature, the thermal conductivity increases twice as fast in zero field compared to that in a finite field. By dividing the zero-field curve by two (see the inset in Figure 5.7b), all curves lie on top of each other for small  $T$ .

To get a better impression of which parts of the spectrum are most important at a certain temperature, I look at a reduced conductivity similar to the expression in equation (5.40) of the previous section 5.2.1, but without any approximations of the magnon spectrum

$$\kappa_X = \int_{\Omega} v_k^2 c_k \tau_{gb}, \quad (5.46)$$

where the integration is, again, only over a small region  $\Omega$  of the Brillouin zone. In particular these are the ones around the  $\Gamma$ - and the  $M$ -point. The area of integration is a square with side lengths  $\delta = \pi/10$  and center at the respective points.

I illustrate the behaviour for small fields in Figure 5.8a and 5.8b. I find that, as expected, the main contribution at low temperatures is solely due to the acoustic

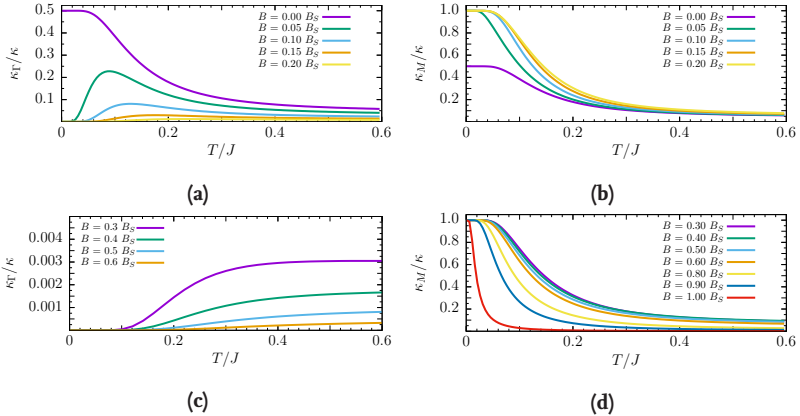


**Figure 5.8.:** Reduced thermal conductivity (a) and (c)  $\kappa_M$  around the  $M$ -point and (b) and (d)  $\kappa_T$  around the  $\Gamma$ -point for low ((a) and (b)) as well as high ((c) and (d)) magnetic field  $B$  (normalised to the total thermal conductivity  $\kappa$ ).  $B_S$  is the saturation field  $8SJ$ .

magnons and that at finite field the optical magnons do not contribute at all<sup>4</sup>. As the temperature increases and those optical modes can be excited, their contribution  $\kappa_T$  increases. Because the gap increases with the magnetic field, the temperature interval where the acoustic modes are dominant is larger the higher the magnetic field is. At higher temperatures, modes from other regions can be excited and the relative contribution diminishes.

For high magnetic fields the gap is so large that there is hardly any contribution from the optical modes. At the same time the velocity of the acoustic modes decreases and the dispersion becomes more quadratic than linear, i.e. the velocity decreases while the curvature increases. The contribution of modes close to the  $M$ -point is reduced by their lower velocity. At the same time the lower slope allows modes further away to still be excited at low temperature. Because of the higher curvature, their velocity is high enough so that these mode can have a noteworthy contribution. This means that modes closer to the  $M$ -point contribute less than those further away from it. Therefore with increasing temperature, the temperature range where only modes close to the  $M$ -point are important becomes smaller for higher magnetic fields.

One can see in Figure 5.2 that for all fields the magnon spectra intersect at  $Q/2$ <sup>5</sup>. Although the magnon energy is the same at this point, the velocity is not. For  $B = 0$  the dispersion has a maximum at that point, i.e. the velocity is zero there. With

<sup>4</sup>As I mention before, the spectrum has two acoustic modes at  $B = 0$  and because of that both contribute 50% at low temperature

<sup>5</sup>The vector  $Q$  is the Néel ordering vector  $Q = \pi e_x + \pi e_y$  of the square lattice.

increasing magnetic field, this maximum shifts in the direction of the  $M$ -point. At  $B \approx 0.5B_S$  the dispersion is almost flat between  $Q/2$  and the  $M$ -point. This means that all these modes in this interval have almost no contribution. For these fields, the conductivity in the high-temperature limit is also the lowest of all fields. For higher magnetic fields the velocity increases again and the contribution of these modes surpasses the one at zero magnetic field at temperatures where they are excitable.

Next, I consider the thermal conductivity as a function of the external magnetic field. In Figure 5.9a the absolute value is shown for different temperatures and in Figure 5.9b it is normalised by the thermal conductivity  $\kappa(B = 0)$  at zero field. One can see in the left figure that the overall conductivity increases with temperature. This is pretty clear as the number of contributing modes grows with temperature and there is no temperature-dependent scattering which would prevent any mode from contributing. For magnetic fields small compared to the saturation field  $B_S$  the conductivity is decreasing quite rapidly. The reduction in conductivity is due to the opening of the gap and is seen most clearly in the normalised curves. The lower the temperature the steeper the decline. As I discuss in section 5.2.1 the reason for this is the gap that opens at the  $\Gamma$ -point, depopulating the magnon modes in this region. Afterwards an increase in the magnitude of the field has no effect. For higher temperature it takes a larger magnetic field to reduce the number of excited modes and hence the curves decrease over a larger field interval.

All curves have their minimum around  $B = 0.48B_S$ . At these fields the spectrum is flat between  $Q/2$  and the  $M$ -point and there is hardly a contribution from these modes. For larger fields the spectrum becomes less flat around  $Q/2$  and the conductivity increases if the temperature is high enough to excite these modes. This is why the conductivity increases for the higher-temperature curves and does not for the low-temperature ones. For magnetic fields close to the saturation field the magnon dispersion starts to become more quadratic close to the  $M$ -point. As seen before, the contribution of modes in the vicinity of the  $M$ -point diminishes, while the contribution of modes further away increases. The higher the temperature, the more of these modes can be excited and the earlier the curves begin to rise again. Those modes can still be excited at low temperature. At higher temperature, modes further apart from the  $M$ -point can be excited and the thermal conductivity increases even beyond the value at zero field.

To summarise this section, I show that at temperatures small compared to the exchange interaction  $J$  almost the sole contribution comes from acoustic modes. Acoustic modes are present at the  $\Gamma$ - and the  $M$ -point for a vanishing magnetic field and for a finite field at the  $M$ -point alone. A gap opens at the  $\Gamma$ -point reducing the contribution of modes in the vicinity to almost zero. This behaviour might

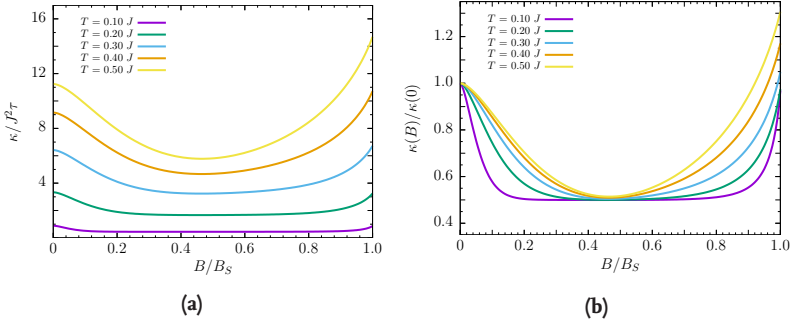


**Figure 5.9.:** Thermal conductivity as a function of the external magnetic field (a) non-normalised value and (b) normalised to the conductivity at zero field.

have already been expected from the results of section 5.2.1. However, I find that at higher temperatures of the order of  $T = 0.4J$  modes close to  $Q/2$  are important, too. At fields of the order of  $B = 0.4B_S$  the spectrum becomes flat all the way from this point to the  $M$ -point. The contribution of these modes goes to zero and the thermal conductivity decreases. For magnetic fields comparable to the saturation field  $B_S$ , the modes' velocities in that region and as a result their overall contribution grows again.

The discussion of this section should not be regarded as very realistic for high temperatures. For one, different scattering processes besides grain-boundary scattering become important, for another the magnon lifetime in equation (5.43) can not be considered as momentum-independent when the magnon mode's velocity is not. In a sense, the purpose of this section is to get a better understanding of the effect of the magnetic field on the thermal conductivity just due to changes in the spectrum. The upcoming section includes a scattering mechanism which is important at higher temperature.

### 5.2.3. Thermal conductivity with magnon-phonon scattering

In the previous section, I consider momentum-independent grain-boundary scattering. In this subsection, I consider the effect of a momentum-dependent scattering mechanism. There are many of such processes like, e.g. magnon-magnon and magnon-phonon scattering. I have a more thorough look at the former scattering process in section 5.3. Here, I consider scattering of magnons with optical phonons. While grain-boundary scattering is the dominant scattering process of the magnons in the low-temperature limit, scattering with optical phonons is most relevant in the high-temperature limit, i.e. at a temperature above the Debye-

temperature [83]. This section concludes the elementary overview over the effect of different scattering processes and the magnetic field on the magnetic thermal conductivity's behaviour.

Interactions between magnons and phonons arise from the change in the exchange interaction  $J$  between spins, when their distance changes due to lattice vibrations. The corresponding interaction Hamiltonian reads

$$H_{\text{s-p}} = \sum_{i,j} \left( \left[ \nabla_r J_{ij} \right]_{r=r_i} \cdot \Delta \mathbf{U}_{ij} \right) (\mathbf{S}_i \cdot \mathbf{S}_j) \quad (5.47)$$

with the relative displacement operator  $\Delta \mathbf{U}_{ij}$  of the atoms from their equilibrium at position  $r_i$  and  $r_j$ , respectively. After bosonising the spin operators according to equation (5.5), Fourier transforming, and replacing the displacement operators with phonon operators via [82]

$$\mathbf{U}_q = \sum_s \frac{\delta_{q,s}}{\sqrt{2m\omega_{q,s}}} (b_{q,s}^\dagger + b_{-q,s}) , \quad (5.48)$$

where  $\delta_{q,s}$  is the unit vector of the phonon with polarisation  $s$  and energy  $\omega_{q,s}$ , to leading order the magnon-phonon interaction is

$$H_{\text{s-p}} = \sum_{k,k'} \sum_s \left\{ V_{k,k',q}^s \alpha_k^\dagger \alpha_{k'} + V_{k,k',q}^{\text{an},s} (\alpha_k^\dagger \alpha_{-k'}^\dagger + \text{h.c.}) \right\} (b_{q,s}^\dagger + b_{-q,s}) . \quad (5.49)$$

Here the superscripts  $s$  refer to the possible phonon-branches and the superscript an indicates that the interaction is anomalous because the magnon number is not conserved. The detailed calculation of the magnon relaxation rate  $1/\tau_{\text{m-p}}$  involves the dispersion relation of both particles, as well as the magnon-phonon coupling constants  $V_{k,k',q}^s$  and  $V_{k,k',q}^{\text{an},s}$ . Such an elaborate calculation is quite involved and goes beyond the scope of this coarse overview on the effects of different scattering mechanisms on the magnetic thermal conductivity. Luckily, the behaviour of experimentally determined thermal conductivities can be described quite well with an expression that is obtained by a solution of the Boltzmann equation and the memory function formalism[83]. This effective magnon-relaxation rate due to magneto-elastic interactions is

$$\tau_{\text{m-p}}^{-1} = g \frac{T^2 k^2}{\omega_{\text{opt}}} \theta(k_B T - \omega_{\text{opt}}/2) , \quad (5.50)$$

where  $k$  is the magnon's momentum (with respect to the acoustic magnon point<sup>6</sup>),  $\omega_{\text{opt}}$  is the optical phonon mode's energy, and  $g$  is the spin-phonon coupling con-

---

<sup>6</sup>By this point I mean the origin of the acoustic branch, i.e. where the energy is zero and grows linear with momentum.

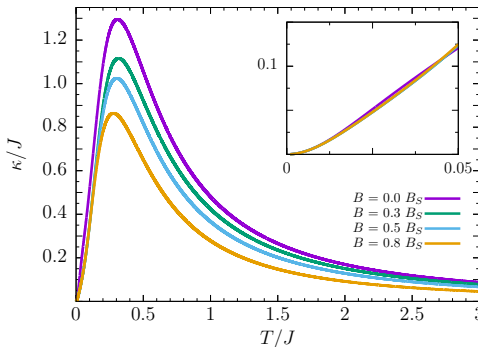


**Figure 5.10.**: Thermal conductivity  $\kappa$  over temperature  $T$  with empiric expressions for grain-boundary and magnon-phonon scattering for different external magnetic fields  $B$  in units of the saturation field  $B_S$  (inset:  $\kappa$  for small  $T$  and the curve for  $B = 0$  divided by two).

stant. The latter is of the order of  $(0.05 \dots 0.3)$  [83]. It has to be mentioned that this expression is derived assuming a linear magnon dispersion. The expression in equation (5.21) shows that the curvature of the acoustic magnon branch increases with the magnetic field's magnitude. The approximation and, as a result, the magnon-phonon scattering rate is valid for fewer magnons the larger the magnetic field is, i.e. for the modes close to the  $M$ -point at  $B \simeq B_S$ .

For  $\text{La}_2\text{CuO}_4$   $\omega_{\text{opt}}$  is of the order of  $J/4$ . The Heaviside function  $\theta$  mimics the observation that scattering of magnons with optical phonons is most important for temperatures  $k_B T$  above half the energy of the optical phonon mode's energy  $\omega_{\text{opt}}$ . As I mainly concentrate on the high-temperature behaviour of the thermal conductivity in this section, I drop the  $\theta$ -function for convenience in the following. I assume a ratio  $g/\omega_{\text{opt}}$  of  $0.3J^{-1}$  in the relaxation time due to the scattering with phonons and a ratio of  $l_{\text{gb}}/v$  of  $150J^{-1}$  for the grain-boundary scattering in equation (5.43). The overall relaxation rate  $1/\tau$  is obtained by adding the rates of both scattering mechanisms according to Matthiessen's rule [27]

$$\frac{1}{\tau} = \frac{1}{\tau_{\text{gb}}} + \frac{1}{\tau_{\text{m-p}}}. \quad (5.51)$$

At temperatures below  $J/4$  mainly acoustic magnons on the thermal shell  $\epsilon_k = T = vk \simeq Jk$  are excited which results in a much smaller magnon-phonon scattering rate of  $\tau_{\text{m-p}}^{-1} = \frac{3k^4 J}{2560}$  when all previously introduced constants are put in. At this temperature the excitation of additional magnon modes compensates the higher scattering rate for modes of higher momentum  $k$ . However, the high-temperature behaviour is strongly changed by the inclusion of magnon-phonon scattering. All curves go to zero as  $T \rightarrow \infty$ . Because of the momentum-dependence in equation

(5.50), modes further away from the  $M$ -point are affected more strongly. At temperatures which are small compared to the exchange interaction  $J$ , though, scattering of magnons with phonons is dominated by grain-boundary scattering. This fact can be seen from equation (5.50). As the temperature increases, modes with higher momentum and energy decay and their contribution to the thermal transport declines. When the magnon modes' heat capacity does not increase as much as the magnon-phonon scattering rate does with temperature, the thermal conductivity assumes a maximum.

The resulting temperature dependence for different magnetic fields of the thermal conductivity can be seen in Figure 5.10. The low-temperature behaviour is hardly affected by the inclusion of the magnon-phonon scattering rates. I still observe that all the curves lie on top of each other (again the curve for  $B = 0$  has to be divided by two because of the additional acoustic mode), which is best seen in the inset of the figure. One can see that the thermal conductivity decreases with the magnetic field. For the results, that only take grain-boundary scattering into account, modes further away from the  $M$ -point contribute at higher temperature. Because of the momentum- and temperature-dependence of  $\tau_{m-p}$  modes further away from the  $M$ -point are affected at a higher temperature than modes closer to the  $M$ -point are. At the same time, modes near the  $\Gamma$ -point are still removed from the thermal transport by the opening of the gap. Hence, it is plausible that the overall thermal conductivity is reduced by increasing the magnetic field.

In Figure 5.11 one can see the behaviour of the maximum in the thermal conductivity as a function of the magnetic field in more detail. In the left Figure 5.11a I illustrate the evolution of the non-normalised value of the maximum  $\kappa_{\max}$  and in the right Figure 5.11b the evolution of the temperature  $T(\kappa_{\max})$  at which this maximum occurs. One can see that the thermal conductivity decreases monotonically up to  $B = 0.9B_S$ . Beyond that the thermal conductivity increases. The reason for this is the change in curvature of the acoustic branch at these fields. Because it decreases with the magnetic field, modes further away from the  $M$ -point can be excited at lower temperature. Therefore, their number grows faster than the scattering rate with phonons at  $T(\kappa_{\max})$ . Their contribution is not reduced as dramatically as it is at lower magnetic fields.

This behaviour can also be observed in Figure 5.11b. There I see that the temperature at which the conductivity is largest increases for small magnetic fields. The gap at these fields is small enough so that the magnons in the region around the  $\Gamma$ -point can still be excited at a temperature before magnon-phonon scattering becomes relevant, i.e.  $\Delta \ll \omega_{\text{opt}}$ . As a result,  $T(\kappa_{\max})$  increases. When the gap is too large, magnons above the gap are excited at a temperature when magnon-phonon scattering is important. The contribution of these modes decreases. As

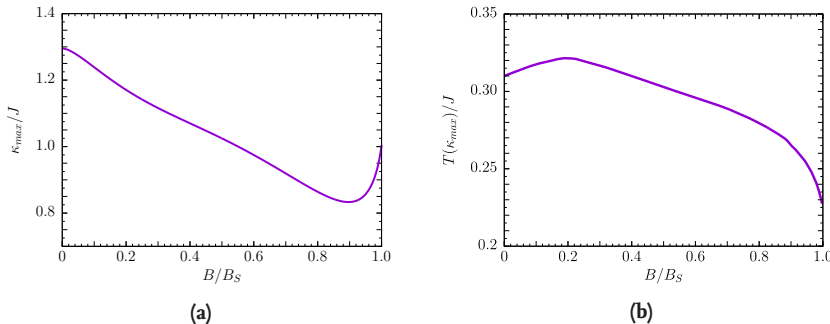


**Figure 5.11:** The maximum of the thermal conductivity  $\kappa_{\max}$  with effective expressions for grain-boundary and magnon-phonon scattering in (a) and the temperature  $T(\kappa_{\max})$  at which it is reached in (b) as a function of the external magnetic field  $B$  in units of the saturation field  $B_S$ .

acoustic magnons have a much higher momentum than the optic magnons with the same energy, their scattering rate is much higher, too. As a result,  $T(\kappa_{\max})$  decreases. For increasing magnetic field, the acoustic branch becomes more shallow, i.e. the magnon's velocity decreases. Hence, modes with higher momentum are excited at a lower temperature. At first, the acoustic branch's curvature is nearly zero. Therefore, due to the smaller velocity of the excited modes their contribution diminishes. As a result, the maximum shifts to smaller temperature as these modes are excited earlier and the absolute value of that maximum diminishes as their contribution is lower, too. When the curvature close to the  $M$ -point increases, the modes in the vicinity have large enough velocity to contribute more to the thermal transport. The thermal conductivity increases and reaches its maximum at a lower temperature.

In the derivation of the relaxation rate in equation (5.50) it is assumed that the magnons that scatter with the phonons have a linear dispersion, i.e. they are acoustic. Because the dispersion is more quadratic than linear, it can be debated whether the results for high magnetic field should be taken too seriously. For this qualitative investigation, however, I do not want to get into more detail and leave the discussion as it is.

In this section I give an overview of the magnetic thermal conductivity's general behaviour, taking into account effective expressions for the magnon relaxation rate. I show that the behaviour at temperatures small compared to the exchange interaction  $J$  is dominated by the grain-boundary scattering. Considering this kind of scattering alone in section 5.2.2, I determine which parts of the spectrum would, in principle, contribute most to the thermal transport at a given temperature if the scattering is momentum- and temperature-independent. In the low-temperature limit the acoustic modes are the most relevant. The thermal conductivity is re-

duced by a magnetic field due to the creation of a gapped optical magnon branch. Considering a momentum- and temperature-independent scattering rate is unrealistic for the high-temperature behaviour, because in reality the persistence of high thermal conductivity at large temperature is not observed.

When considering the magnon-phonon scattering, I show that the scattering of the magnons with other quasi-particles prohibits such a behaviour. At a certain temperature, the scattering magnons with optical phonons is more important than grain-boundary scattering. The contribution of the magnons to the thermal transport reduces with increasing temperature. In the next section, I consider the scattering of magnons on magnons. These processes arise from higher order terms in the  $1/S$  expansion. For the non-collinear ordered Heisenberg antiferromagnet in an external magnetic field, these processes and their effect on the magnon spectrum are well studied [45]. I take an interest in the consequences on the thermal conductivity.

The insights I gain in section 5.2.2 and this one are useful for the discussion of the magnon-magnon interaction in the next section. From section 5.2.2 I know which magnon modes are most relevant for the thermal transport at higher temperature, too. In the next section I determine which regions in the Brillouin-zone are mostly affected by magnon-magnon scattering at different magnetic fields and combine this with the knowledge I gain in section 5.2.2. The consideration of magnon-phonon scattering in this gives us a rough estimation of the temperature scale (up to  $T = \omega_{\text{opt}}$ ) to consider before magnon-phonon scattering becomes dominant. I compare this temperature scale to the one I find for magnon-magnon scattering to become most relevant.

## 5.3. Thermal conductivity considering magnon-magnon scattering rates

In section 5.1.1 I demonstrate that the classical spin ground state is the Néel state, when there is no magnetic field. For a finite magnetic field, spins cant from this state in the direction of the applied magnetic field. This leads to an interesting contribution in the magnon-magnon scattering process: in the linear spin-wave approximation of section 5.1.1 I omit terms beyond the harmonic order. Those neglected terms represent scattering among the magnons. In collinear systems, i.e. spin configurations with  $\theta_i$  and  $\phi_i$  being either zero or  $\pi$  for all  $i$  of spins at site  $i$ , the sublattice-rotation in equation (5.12) does not mix different components of the spin operators and only longitudinal terms  $(S_i^\mu S_j^\mu)$  remain. There is an even number

of magnon operators for this reason and magnon-magnon scattering occurs first due to terms of order  $(1/S)^0$  in the  $1/S$  expansion. In systems where the spins are coplanar, i.e. they all lie in a plane but not on one line like the ferromagnetic or Néel order, transversal terms can occur ( $S_i^\mu S_j^\nu$  with  $\mu \neq \nu$ ). Such terms contribute to the order of  $S$ . Processes like this are best known from anharmonic crystals [46], but are certainly not limited to it. The rich variety of magnetic materials allows one to study the phenomenon for a number of different dispersion laws, lattice geometries, and most importantly manipulate the interaction with external fields. I investigate the consequences for the current-current correlation function and for the thermal conductivity when these interactions are included.

I begin by rederiving the explicit form of the cubic terms and its effect as a correction of the previous harmonic results like in [61, 118]. The renormalisation of the canting angle and, following from this, of the magnon spectrum, are discussed in section 5.3.1. After that I look at the scattering of the magnon modes among themselves leading to a finite lifetime. I begin with the so-called spontaneous magnon decay in section 5.3.2. These are scattering processes that are independent of the number of excited magnons. Next, I include temperature-dependent scattering from three magnon interactions in section 5.3.3. Such a process has not been discussed before. Combining these two scattering mechanisms, I discuss their impact on the thermal transport<sup>7</sup> in section 5.3.4. In particular, I look at the influence of the magnetic field for the control of the magnonic contribution. This is my thesis' contribution to the extension of the existing results of field-dependent magnon-magnon scattering in the square-lattice Heisenberg antiferromagnet[61]. The importance of these scattering processes is discussed in the low- and the high-temperature limit.

### 5.3.1. Leading $1/S$ corrections

In the process of calculating the magnon spectrum in section 5.1.1, a sublattice rotation is introduced. Because of it, different components of the spin operators are mixed in the Heisenberg interaction and components other than the  $z$ -component (to which the magnetic field is aligned) occur in the term representing the Zeeman interaction. As a result, cubic magnon-magnon interaction terms arise from these transversal terms like  $S_i^x S_j^z$  and from the  $S_i^x$  term in equation (5.13). After inserting the Holstein-Primakoff transformation up to order  $(1/S)^{1/2}$  and using

---

<sup>7</sup>I assume that the one-particle lifetimes are a decent approximation for the two-particle scattering rates. This assumption can not be verified without the calculation of the vertex corrections, though.

$B = 8JS \sin \psi / 2$ , the cubic part of the Hamiltonian reads [61]

$$H^{(3)} = J\sqrt{2S} \sum_{\langle i,j \rangle} (-1)^i (a_i + a_i^\dagger) n_j \sin \psi. \quad (5.52)$$

Corrections to the linear order  $H^{(1)}$  arise due to these terms. As adding a magnon to the system should not reduce the classical energy, this part still has to vanish. Specifically, this means a renormalisation of the canting angle firstly, and inserting it to the quadratic terms  $H^{(2)}$  a renormalisation of the magnon dispersion secondly. The easiest way to obtain these corrections is to use a Wick decomposition of equation (5.52) [118]. One of the terms remains uncontracted<sup>8</sup> and is multiplied by a ground state expectation value of the other two. As an example, one obtains for the expectation value  $n$  of the operator  $a_i^\dagger a_i$

$$\begin{aligned} n := \langle a_i^\dagger a_i \rangle_0 &= \frac{1}{N} \sum_i a_i^\dagger a_i = \frac{1}{N} \sum_k a_k^\dagger a_k = \langle a_k^\dagger a_k \rangle_0 \\ &= \langle u_k^2 \alpha_k^\dagger \alpha_k + o_k^2 \alpha_k^\dagger \alpha_k^\dagger + u_k o_k (\alpha_k \alpha_k + \alpha_k^\dagger \alpha_k^\dagger) \rangle_0 = \frac{1}{N} \sum_k o_k^2. \end{aligned} \quad (5.53)$$

Here I introduce the Bogoliubov transformation from equation (5.17) in the second line and use that no magnons are excited in the ground state. The other two ground state averages that occur are obtained in a similar fashion:

$$m := \langle a_i a_j \rangle_0 = \frac{1}{N} \sum_k \gamma_k o_k^2, \quad (5.54)$$

$$\Delta := \langle a_i^{(\dagger)} a_j^{(\dagger)} \rangle_0 = \frac{1}{N} \sum_k \gamma_k u_k o_k. \quad (5.55)$$

Using identities for the hyperbolic functions  $u_k$  and  $o_k$ ,  $\sum_k \gamma_k = 0$ , and the result from equation (5.18), all three coefficients can be evaluated via

$$n = \frac{1}{N} \sum_k \frac{1}{2} \left( \frac{1 + \gamma_k \sin^2 \phi / 2}{\omega_k} - 1 \right), \quad (5.56)$$

$$m = \frac{1}{N} \sum_k \frac{1 + \gamma_k + \gamma_k^2 \sin^2 \phi / 2}{2\omega_k}, \quad (5.57)$$

$$\Delta = \frac{1}{N} \sum_k \frac{\gamma_k^2 \cos^2 \phi / 2}{2\omega_k}. \quad (5.58)$$

---

<sup>8</sup>See appendix A for the definition of a contraction and Wick's theorem for the decomposition of products of creation and annihilation operators

In the thermodynamic limit, the sums can be replaced by integrals over the first Brillouin zone and calculated numerically for all values of the external field  $B = B_S \sin \phi / 2$ .

The result for the quantum correction of the linear term from the cubic terms  $H_1^{(3)}$  is

$$H_1^{(3)} = \sqrt{2S} J \sum_{\langle i,j \rangle} (-1)^i (n - m - \Delta) \sin \psi (a_i + a_i^\dagger). \quad (5.59)$$

Writing out the linear term without inserting the canting angle that minimises the classical energy, and adding the above correction of it, its expression becomes

$$H^{(1)} + H_3^{(1)} = \sqrt{\frac{S^3}{2}} J \sum_i (-1)^i \left( 1 + \frac{1}{S} (n - m - \Delta) - \frac{B}{2S J \sin \psi / 2} \right) (a_i + a_i^\dagger) \sin \psi. \quad (5.60)$$

As mentioned before, this term has to vanish for all  $i$  so that no energy is gained by adding a magnon to the ground state configuration. The canting angle is renormalised from the one  $\psi_0$  in equation (5.11) to  $\psi_r$

$$\sin \frac{\psi_r}{2} = \sin \frac{\psi_0}{2} \left( 1 + \frac{1}{S} (n - m - \Delta) \right). \quad (5.61)$$

This angle  $\psi_r$  has to be reinserted into the harmonic part  $H^{(2)}$  of the Hamiltonian to obtain the  $1/S$  correction to the free magnon dispersion

$$\begin{aligned} H^{(2)} &= 4JS \sum_k \frac{(1 + \gamma_k)(1 - \gamma_k \cos \psi_r)}{\omega_k} \alpha_k^\dagger \alpha_k^\dagger \\ &= \sum_k \epsilon_k^{(0)} + \frac{16J(1 + \gamma_k)^2(n - m - \Delta) \sin \psi_0 / 2}{\omega_k} \alpha_k^\dagger \alpha_k^\dagger. \end{aligned} \quad (5.62)$$

The result can be seen in Figure 5.12a. Because the renormalised angle is always smaller than the non-renormalised one, effectively a higher magnetic field is needed to obtain the same canting angle. For the resulting thermal conductivity, this means that the reduction due to the magnetic field related opening of the gap is smaller than what is expected from the harmonic approximation. The corrections are most prominent for small  $S$  and small magnetic fields. At fields above  $B = 0.4B_S$  the correction is less than 1% of the absolute value. For  $B = B_S$  the term  $(n - m - \Delta)$  is zero. Therefore, the transition from the canted Néel state to the complete ferromagnetic order occurs at the same field with or without quantum corrections. Because at  $B = 0$  the canting angle vanishes, the system

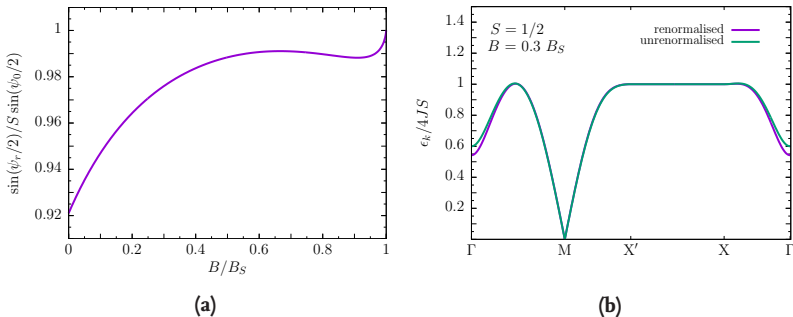


**Figure 5.12.:** Frequency-independent renormalisation of (a) the canting angle  $\psi_0$  to  $\psi_r$  and (b) the magnon dispersion  $\epsilon_k$  at  $B = 0.3B_S$  due to the cubic terms for  $S = 1/2$

still assumes the Néel state-order. As expected, the  $1/S$  terms do not change the harmonic magnon spectra of the collinear states.

In Figure 5.12b the spectrum is shown when the renormalised angle is taken into account for a spin  $1/2$  and a field of  $B = 0.3B_S$ . One can see that the most drastic change is the reduction of the gap at the  $\Gamma$ -point. The acoustic modes are unaffected. As long as  $T \ll B$ , even with the quantum corrections, the number of excited magnons around the  $\Gamma$ -point is small and they hardly contribute to the thermal transport. As I am mainly interested in the effect of the cubic terms on the thermal conductivity on a qualitative level, these quantum corrections are not considered in the following. I assume that the decline of the thermal conductivity as a function of the magnetic field is slightly more shallow compared to the harmonic results due to the size of the gap increasing slower as a function of the magnetic field.

Next, I consider the direct influence of magnon-magnon scattering by the cubic terms. After a successive Fourier- and Bogoliubov-transformation of equation (5.52) the cubic Hamiltonian becomes [61]

$$H^{(3)} = -\sqrt{\frac{B_S^2 - B^2}{2SNB_S}} B \sum_{k,q} \Phi_1(k, q) \left( \alpha_{k-q+Q}^\dagger \alpha_q^\dagger \alpha_k + \text{h.c.} \right) \\ + \Phi_2(k, q) \left( \alpha_k^\dagger \alpha_q^\dagger \alpha_{-k-q+Q}^\dagger + \text{h.c.} \right). \quad (5.63)$$

It is apparent that momentum is not conserved, but that there is a residual of  $Q = (\pi, \pi)$ . The latter arises from the sublattice rotation that introduces an additional factor of  $\exp(iR_i \cdot Q)$  in the Fourier transformation of the cubic magnon-magnon interaction, i.e. in the original reference frame momentum is conserved explicitly. In equation (5.63), I symmetrise the vertex functions  $\Phi_1$  and  $\Phi_2$  with respect to a change of momenta  $q \rightarrow k - q + Q, k - q + Q \rightarrow q$  in the first term and introduce

all possible permutations of the momenta in the last term. They are

$$\begin{aligned}\Phi_1(k, q) = \frac{1}{2!} & \left[ \gamma_k(u_k + o_k)(u_q o_{k-q+Q} + o_q u_{k-q+Q}) \right. \\ & + \gamma_q(u_q + o_q)(u_k u_{k-q+Q} + o_k o_{k-q+Q}) \\ & \left. + \gamma_{k-q+Q}(u_{k-q+Q} + o_{k-q+Q})(u_k u_q + o_k o_q) \right] \quad (5.64)\end{aligned}$$

$$\begin{aligned}\Phi_2(k, q) = \frac{1}{3!} & \left[ \gamma_k(u_k + o_k)(u_q o_{k+q-Q} + o_q u_{k+q-Q}) \right. \\ & + \gamma_q(u_q + o_q)(u_k o_{k+q-Q} + o_k u_{k+q-Q}) \\ & \left. + \gamma_{k+q-Q}(u_{k+q-Q} + o_{k+q-Q})(u_k o_q + o_k u_q) \right] \quad (5.65)\end{aligned}$$

as has already been found in [61]. In equation (5.63) one can see that the interaction involving three magnons vanishes when there is no external magnetic field or when the saturation field is reached. This is to be expected as such an interaction does not occur in a collinear spin order. From this term one can identify three different kinds of magnon interactions: a magnon decay, source, and polarisation process. The first two of these are temperature-independent. They are responsible for an effect called spontaneous magnon decay. In the following section, I investigate the influence of it on the magnon spectrum, the decay of magnon modes in particular. Afterwards, I look at the temperature dependent scattering process. In the end, I discuss the consequences for the magnetic thermal transport.

### 5.3.2. Spontaneous magnon decay

As can be seen from equation (5.63) there are two different vertices for three-magnon scattering processes. The first process involves either the annihilation of one and the creation of two magnons or the creation of one and the annihilation of two magnons. In the second process, either three magnons are annihilated or they are created in the vertex. I consider the diagrams that are shown in Figure 5.13 in this section. The left one 5.13(a) describes a regular decay of one magnon into two normal magnons and the right one 5.13(b) describes the decay into two anti-magnons or magnon-holes. The latter are a result of the Bogoliubov transformation mixing particles and holes, blurring the distinction between them. According to the discussion in the appendix A in particular equation (A.24) the self-energy for the left diagram is

$$\Sigma_{\text{smd},1} = -\frac{B^2 \cos^2 \theta}{4SN} \sum_q \frac{|\Phi_1|^2}{\omega - \epsilon_q - \epsilon_{k-q+Q} + i0^+}, \quad (5.66)$$

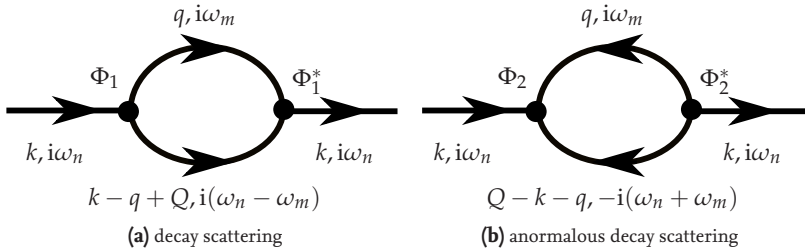


**Figure 5.13.:** Spontaneous magnon decay processes

and for the right one it is

$$\Sigma_{\text{smd},2} = -\frac{B^2 \cos^2 \theta}{4SN} \sum_q \frac{|\Phi_2|^2}{\omega + \epsilon_q + \epsilon_{Q-k-q} - i0^+}. \quad (5.67)$$

For both terms I use the invariance of the vertex functions  $\Phi_1$  and  $\Phi_2$  under  $q \rightarrow k - q$  and  $q \rightarrow k + q$ , respectively. Because of this the Bose functions in equation (A.24) cancel. The expressions are therefore temperature-independent, i.e. they occur with the same intensity at zero temperature as they are at finite temperature.

In the following, I assume that the incoming magnon's energy and momentum obeys the dispersion relation from linear spin-wave theory ( $\omega = \epsilon_k$ ). This is referred to as the on-shell approximation. Furthermore, I only consider the imaginary part of the self-energy, i.e. the magnon decay rate  $1/\tau_i$ . Accordingly, the corresponding expressions are

$$\tau_1^{-1}(k) = -\frac{B^2 \pi \cos^2 \theta}{4SN} \sum_q |\Phi_1|^2 \delta(\epsilon_k - \epsilon_q - \epsilon_{k-q+Q}) \quad (5.68)$$

$$\tau_2^{-1}(k) = \frac{B^2 \pi \cos^2 \theta}{4SN} \sum_q |\Phi_2|^2 \delta(\epsilon_k + \epsilon_q + \epsilon_{Q-k-q}) \quad (5.69)$$

where I used the definition of the Dirac  $\delta$ -distribution via a Lorenzian

$$\delta(\omega) = \lim_{\eta \rightarrow 0} \frac{1}{\pi} \frac{\eta}{\omega^2 + \eta^2}. \quad (5.70)$$

The results in equations (5.68) and (5.69) are Fermi's golden rule for the decay of a magnon into two and the spontaneous absorption of two magnons by a single one.

Only the decay process in Figure 5.13a can have a finite contribution to the lifetime reduction in the on-shell approximation. Within the context of the discussion below equation (5.63), momentum is conserved as well<sup>9</sup>. Such an N-process

<sup>9</sup>This qualitative discussion follows [61] and gives a more detailed guide to the derivation of the results.

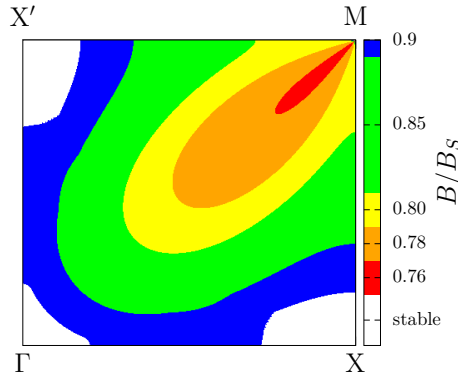


**Figure 5.14:** Region of unstable magnon modes for different magnetic fields

does not lead to a current-relaxation and as a result to a finite conductivity. Assuming that the one-particle lifetimes describe the two-particle scattering rates is only an approximation. To be fully certain that this is true, one would need to calculate the neglected vertex-functions, as well as the Umklapp-scattering rates, and compare those to the one-particle lifetimes. I do not do this in this thesis. Being fully aware of this approximation, I assume that the dissipation of momentum in the system is well described by the one-particle-lifetimes and that the current relaxes as a result.

It is informative to look at the set  $(k, B)$  of the initial mode's momentum  $k$  that can undergo such a decay at a certain strength of the magnetic field  $B$ . Although the matrix elements are an essential part of the affected modes' lifetime reduction, much can already be learned from the area and the position of unstable magnon modes for different magnetic fields. Because I am interested in the low-temperature regime where phonon scattering is negligible, mainly the decay of magnon modes with  $k \approx Q$  is of interest. I follow the argumentation of [61] for this limit. Due to this constraint, the momenta of the two outgoing modes need to be close to the ordering vector  $Q$ , too. The asymptotic behaviour of the modes' dispersion is [61]

$$\epsilon_k \simeq ck + dk^3 \quad (5.71)$$

$$\text{with } c = \sqrt{8JS} \cos \theta, \quad d = \frac{c}{16} \left( \tan^2 \theta - \frac{9 + \cos 4\varphi}{6} \right)$$

and  $k, \varphi$  being the polar coordinates in momentum space and  $\theta$  is the canting angle which depends on the magnetic field's magnitude.

The argument of the  $\delta$ -distribution is

$$\epsilon_k - \epsilon_q - \epsilon_{k-q+Q} \simeq c(k - q - |k - q|) + d(k^3 - q^3 - |k - q|^3) \quad (5.72)$$

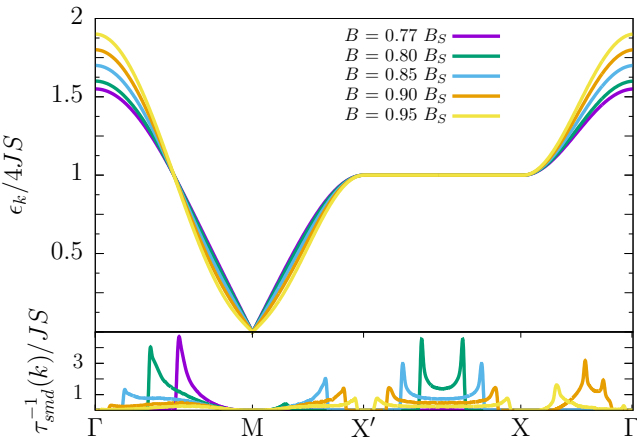


**Figure 5.15.**: The free magnon dispersion  $\epsilon_k$  and the scattering rate  $1/\tau_{\text{smd}}$  from spontaneous magnon decay

which can be simplified further by using  $|k - q| \simeq k - q + \frac{kq\varphi^2}{2(k-q)}$ :

$$\epsilon_k - \epsilon_q - \epsilon_{k-q+Q} \simeq -\frac{ckq}{2(k-q)} \left( \varphi^2 - \frac{6d}{c} (k-q)^2 \right). \quad (5.73)$$

A magnon with momentum  $k$  can only decay when the above expression has roots. As  $d \propto c$  this implies  $d/c \geq 0$  and especially [61]

$$\left( \frac{B}{B_S} \right)^2 \geq \frac{9 + \cos 4\theta}{15 + \cos 4\theta}. \quad (5.74)$$

This means that there is a critical magnetic field  $B_c$ . For fields smaller than this threshold field all magnon modes are stable. Above this field there are single magnon modes that decay into the two-magnon continuum. As a result of this process, those single magnon modes have a finite lifetime. Energy is no longer solely transported in the direction of the initial decayed magnons, because its momentum is only conserved in the two-magnon continuum. As a result, the contribution of such modes to the thermal transport decreases.

From this simple calculation, one determines the critical field to be  $B \geq 0.756 B_S$  [61]. This fact is corroborated by Figure 5.14 where I highlight the location of (possibly) unstable magnons in a quarter of the first Brillouin zone for different magnetic fields. Because the dispersion is invariant under  $k \rightarrow -k$  and  $(k_x \rightarrow k_y, k_y \rightarrow k_x)$ , I consider only one quadrant of the first Brillouin zone. To obtain these illustrations, I loop over all possible combinations for the  $\delta$ -distribution's argument that conserves energy and momentum. One can see that with increasing magnetic field, more and more of the low-energy modes in the vicinity of the

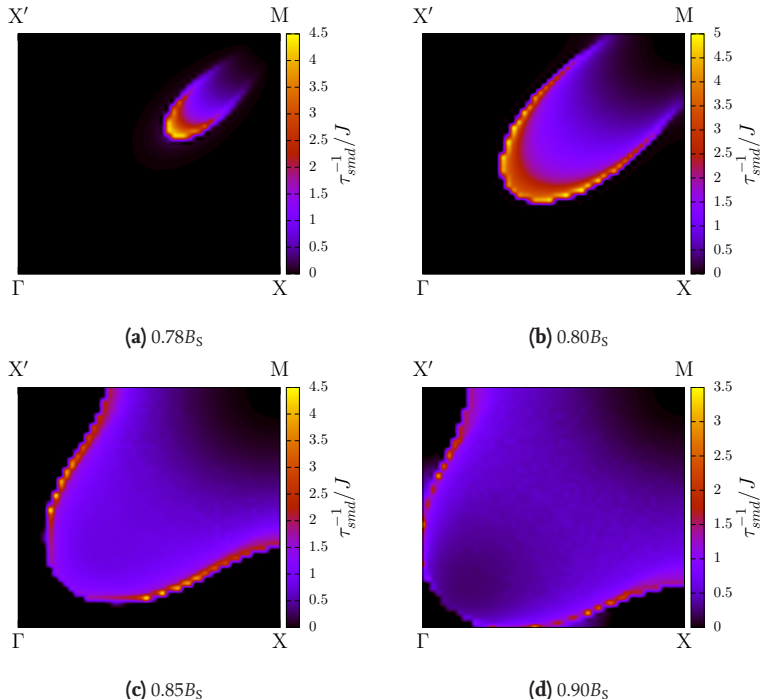


**Figure 5.16.:** Rates of spontaneous magnon decay  $\tau_{\text{smd}}^{-1}$  at different magnetic fields

$M$ -point become unstable. Considering the importance of these modes for the thermal transport as discussed in the previous sections, this is quite encouraging for the purpose of controlling the former process. When the lifetime of low-energy magnon modes diminishes, so does the thermal conductivity as is clear from the simple Drude-like relation in equation (5.39).

To be able to assess the relevance of spontaneous magnon decay though, the absolute value of the magnon decay rate needs to be known. By evaluating the sum in equation (5.68) one obtains the latter as a function of the initial magnon's momentum  $k$ . One can see in Figure 5.15 the decay rate beneath the free magnon spectrum along a specific path in the first Brillouin zone. The maximum of the magnon scattering rate on the path from the  $\Gamma$ - to the  $M$ -point shifts closer to the  $\Gamma$ -point for higher magnetic fields. The height of said peak decreases while its width increases. Between other high-symmetry points the same behaviour can be observed, although the peaks first appear at slightly higher magnetic fields. This means that magnons with a lower energy have a shorter lifetime at a magnetic field slightly above the threshold value than at a higher magnetic field. At the same time more magnon modes are unstable.

The increase in the area of magnon-instability in the first Brillouin zone can be seen more clearly in the density plots of Figure 5.16. While the area of affected magnons is rather small for  $B = 0.78B_S$ , above  $B = 0.9B_S$  the majority of magnon modes in the first Brillouin zone is affected. The results match quite well with the previously determined contours in Figure 5.14. As I already stressed when discussing these contours, the increase in the area of unstable magnons does not necessarily mean that the ability of the magnetic system to transport heat diminishes. It depends on whether the contribution of magnon modes which are essential for the thermal transport decreases. I see that with an increasing magnetic field, the van Hove singularities shift to modes with higher energies. This means that while more magnon modes become unstable, low-energy modes regain stability, i.e. their lifetime increases again. There is a trade-off between suppressing few magnon modes which are essential for the thermal transport and suppressing more magnon modes which are, however, less important for the heat transport. As I mentioned before, when the saturation field is reached, there is no magnon-magnon interaction up to this order in the  $1/S$  expansion. Clearly, there is a magnetic field for which the thermal conductivity increases again due to the increase in the lifetime of certain magnon modes. I gave an extensive discussion of the influence of the temperature on the contribution of the magnon modes before. These insights strongly suggest that the field at which this turnaround happens depends on temperature. It is apparent that modes close to the  $M$ -point are rather stable for all magnetic fields. Mostly modes between the  $\Gamma$ - and the  $M$ -point are affected by spontaneous magnon decay. Because those modes are rather unimportant for the thermal transport at low temperature, it can be already suspected that this process is more relevant at higher temperature.

Spontaneous magnon decay has been observed to renormalise the linear spin-wave magnon spectrum in inelastic neutron scattering [55, 133]. Because the spontaneous scattering rates are temperature-independent, i.e. the number of magnons that are excited overall does not matter, a very strong effect on the thermal transport can be expected if the scattered magnons are important to it. In that way, thermal transport measurements might be an alternative way to observe spontaneous magnon decay experimentally. There is, however, another magnon-magnon interaction that is temperature-dependent. Hence, such a process might be as large or larger than the spontaneous magnon decay at all relevant temperatures. Therefore I consider this process in the next section.

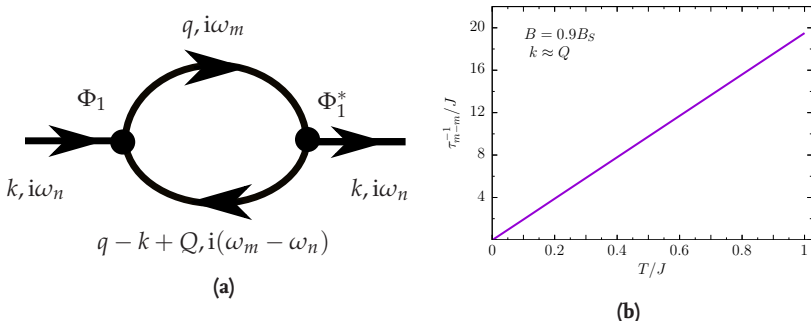


**Figure 5.17.**: Temperature-dependent magnon scattering process: (a) the associated diagram and (b) the temperature-dependence of a magnon mode's scattering rate  $\tau_{m-m}^{-1}$  with a momentum  $k$  close to the  $M$ -point at a magnetic field of  $0.9B_S$ .

### 5.3.3. Finite temperature decay

The last of the three possible magnon decay processes can be seen in Figure 5.17a. According to equation (A.25) the contribution to the magnon-self-energy is

$$\Sigma_3 = \frac{B^2 \cos^2 \theta}{4SN} \sum_q |\Phi_1|^2 \left( \frac{n(\epsilon_q) - n(\epsilon_{q-k+Q})}{\omega - \epsilon_q + \epsilon_{q-k+Q} + i0^+} \right). \quad (5.75)$$

Here there is no symmetry that averts the Bose-functions to cancel and the associated scattering rate in the on-shell approximation is

$$\tau_3^{-1}(k) = \frac{B^2 \pi \cos^2 \theta}{4SN} \sum_q |\Phi_1|^2 (n(\epsilon_q) - n(\epsilon_{q-k+Q})) \delta(\epsilon_k - \epsilon_q + \epsilon_{k-q+Q}). \quad (5.76)$$

The scattering rate of this process is, in contrast to the spontaneous magnon decay of the last section, depending on temperature. The argument of the  $\delta$ -distribution in the equation above does not necessitate all momenta involved to be from the region around the  $M$ -point at low temperature. Because of this, it is not so easy to determine from a kinematic condition whether there is a critical field such as for the spontaneous decay.

In Figure 5.17b the temperature-dependence of the scattering rate is shown for a momentum close to  $Q$ . Modes close to this point are most relevant for the thermal conductivity. It can be seen that the temperature-dependent scattering rate exceeds the maximum of the spontaneous decay rates ( $\tau_{smd}^{-1} = 3.5J$ ) at temperatures above  $T \simeq 0.25J$  for the momentum shown in the figure. For the thermal transport, the location of unstable magnon modes is essential. I argue that the magnon modes which are most strongly affected by spontaneous magnon decay are not the ones with a high contribution to the heat transport at low temperature. The scattering

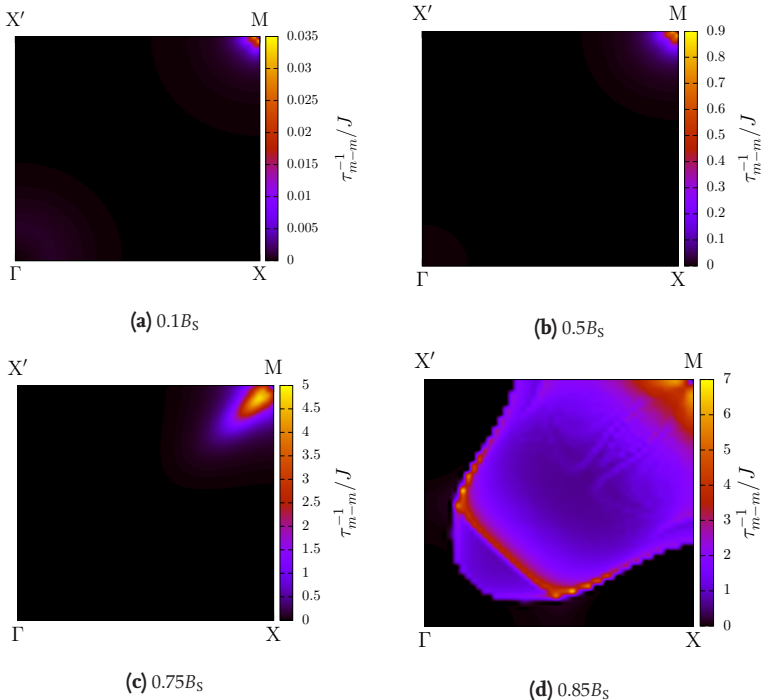


**Figure 5.18:** Magnon scattering rates  $\tau_{m-m}$  at different magnetic fields for  $T = 0.3J$

rates considered so far, however, are close to magnon modes which contribute much to the heat transport at this temperature. Hence, although the scattering rates  $\tau_{m-m}^{-1}$  are not as high as those of the spontaneous decay at low temperature, the former can still be more important than the latter.

Figure 5.18 shows the momentum-dependence of the combined scattering rate of all previously considered magnon-magnon interaction processes for different magnetic fields at a temperature of  $T = 0.3J$ . In the pictures (a)-(c) no spontaneous magnon decay occurs. One can see that temperature-dependent magnon-magnon scattering is confined to modes close to the  $M$ -point. At small magnetic fields, few magnon modes are unstable and the scattering rates for these are comparable to the orders of magnitude considered for grain-boundary and impurity scattering. The latter depend on the material's defect density or the size of a typical grain-boundary, respectively. At a magnetic field that is of the order of half the saturation field  $B_S$  like in Figure 5.18(b), the magnitude of the scattering rate  $\tau_{m-m}^{-1}$  dramatically increases. At such fields, there is no spontaneous magnon decay and the contribution is solely due to the temperature-dependent decay process. One can see by comparing Figures 5.18(a) and (b) that not many additional

magnon modes become unstable. For magnon-magnon scattering to be more important than grain-boundary scattering at a small temperature and magnetic field, the material needs to be very clean.

For fields slightly smaller than the threshold field like in Figure 5.18(c), the scattering rates of the modes affected by the temperature-dependent scattering process are of the same order of magnitude as the scattering rates for the magnon modes affected by the spontaneous decay process above the critical field. The spontaneous decay processes involve magnons further away from the  $M$ -point than the temperature-dependent decay process does. For fields above the threshold field of the spontaneous decay process, the area of unstable magnon modes is increasing. This is mostly due to the occurrence of the spontaneous decay, but also due to the temperature-dependent decay process. By comparing Figure 5.16(c) and 5.18(d) one can see that certain modes are affected by both kinds of scattering processes. The instability of magnon modes close to the  $M$ -point as well as the diagonal line in the middle of the unstable region is due to the temperature-dependent scattering. The unstable region between the  $\Gamma$ - and the  $M$ -point is a result of the spontaneous decay. There are, however, modes that remain stable for all magnetic fields considered.

Now that all magnon-magnon scattering processes are finally discussed, I am able to discuss their influence on the thermal transport in the following section. This includes the thermal conductivity's temperature as well as its dependence on the external magnetic field. The main objective is determining to what extent the thermal transport can be controlled by the field. To do so all the previous insights about the influence of the field on the magnon spectrum and on the magnon-magnon scattering prove helpful. Furthermore, I consider the possibility of using thermal transport measurements for the indirect observation of spontaneous magnon decay. It is interesting as well to see in which temperature range the leading order terms for the magnon-magnon interaction are more important for the magnetic thermal transport than the effective magnon-phonon interaction. This of course depends on whether the magnon modes affected by either one of these processes are relevant for the heat transport or not.

### 5.3.4. Resulting magnonic thermal conductivity

To determine the thermal conductivity  $\kappa$  I use the Drude-like expression from equation (5.39). Apart from the magnons' heat capacity and dispersion  $\epsilon_k$ , their lifetime  $\tau_k$  are relevant for  $\kappa$ , too. All quantities depend on the magnetic field's strength. I discuss the influence of the magnon dispersion in previous sections in detail. For the magnon lifetime I use effective expressions taking into account

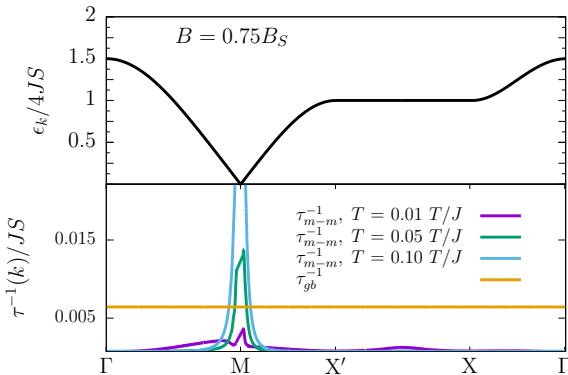


**Figure 5.19:** Full magnon-magnon scattering rate  $\tau_{m-m}^{-1}$  for different temperatures  $T$ , the temperature-independent grain-boundary scattering rate  $\tau_{gb}$ , and the magnon dispersion  $\epsilon_k$  along a specific path through the first Brillouin zone, for  $B = 0.75B_S$

momentum-independent scattering with grain-boundaries/impurities and momentum-dependent magnon-phonon scattering, there. In this section I discuss the influence of the previously determined expressions for magnon-magnon-scattering. Because no sample is free from defects and the correlation length of the order parameters is always finite, I keep the impurity and grain-boundary scattering rate from the previous sections of  $\tau_{gb}^{-1} = 1/150 J^{-1}$ . Although the degree of cleanliness might vary, the results are similar when the magnitude of this type of interaction is one order higher or lower. For those two reasons, this assumption is not too unrealistic.

Figure 5.19 shows the full magnon-magnon scattering rate  $\tau_{m-m}^{-1}$  and the dispersion  $\epsilon_k$  at a magnetic field of  $B = 0.75 B_S$  along a path connecting different high-symmetry points of the Brillouin zone. At this magnetic field, no spontaneous magnon decay occurs and only the temperature-dependent scattering of the last section contributes to this total magnon-magnon scattering time. In the figure I compare the magnon-scattering rates with the chosen (temperature-independent) grain-boundary scattering rate  $\tau_{gb}^{-1}$  at different temperatures. One can see that the magnon-magnon scattering rate is only higher than the grain-boundary scattering rate in the close proximity of the M-point at a temperature above  $T = 0.05J$ , i.e. the low-energy acoustic magnons' lifetime reduction is dominantly due to  $\tau_{m-m}$ . The largest contribution to the thermal transport comes from magnons with an energy of  $\epsilon_k = 4T$  (see the discussion below equation (2.8) for details). At a temperature of  $T = 0.1J$ , the magnon-magnon scattering rate is larger than the assumed grain-boundary scattering rate for magnons of energy below an energy of about  $\epsilon_k \approx 1/JS$ . For  $S = 1/2$ , therefore, the magnon-magnon-scattering reduces the

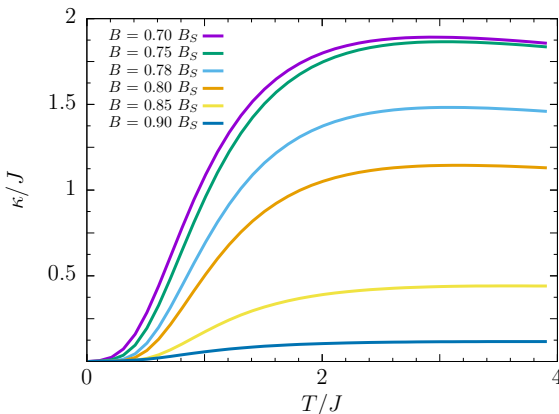


**Figure 5.20.:** Thermal conductivity  $\kappa$  taking into account magnon-magnon scattering as a function of temperature  $T$  for different external magnetic fields  $B$

contribution of the most important magnon modes more than grain-boundary scattering does at such temperatures. At lower temperature, grain-boundary scattering is the dominant scattering process. At lower magnetic field, the magnon-magnon scattering rates are lower than the scattering rates shown in the figure. I do not expect a change in the thermal conductivity's behaviour due to the inclusion of the magnon-magnon scattering with respect to the results presented in section 5.2.2 at magnetic fields below  $B = 0.7B_S$ . For this reason, I limit the consideration to fields above this value.

In the following, I do not include the effects of phonon-magnon scattering because determining a microscopic expression for these processes increases the number of parameters. This certainly goes beyond a general investigation of the possibility to control thermal transport by an external field. Actually, the contribution of magnon-phonon interaction to magnetic thermal conductivity can only be neglected if magnon-magnon interaction is the dominant process. I try to answer the question for which temperatures and magnetic fields this is the case. I evaluate the momentum-sum in equation (5.39) for a square mesh with  $2000 \times 2000$  points in the Brillouin-zone. I obtain the lifetime of each of those magnon modes from the evaluation of the self-energy at  $100 \times 100$  points and then use a bicubic interpolation for the points in between [134].

In Figure 5.20 one can see the results for the thermal conductivity's temperature-dependence for a variety of magnetic fields. The low-temperature behaviour is hardly affected by the magnon-magnon scattering. In the discussion of Figure 5.19, I argue that for magnetic fields much smaller than the threshold field for spontaneous magnon decay, the temperature-dependent magnon scattering is too small to cause observable effects in the thermal conductivity. For magnetic fields of

the order of  $B = 0.7B_S$ , the magnon-magnon scattering rates become larger than grain-boundary scattering rates for acoustic magnons at temperatures where their contribution to the thermal transport is high. When there is no magnon-magnon scattering, the thermal conductivity increases with the magnetic field beyond  $B = 0.7B_S$  (see Figure 5.9b). I do not observe this behaviour when I include magnon-magnon scattering. One can see that the thermal conductivity at  $B = 0.75B_S$  is smaller than the thermal conductivity at  $B = 0.7B_S$  at all temperatures shown. For higher temperatures the difference decreases, though. At both fields, no spontaneous magnon decay and only the temperature-dependent magnon-magnon scattering process occurs. Because the latter is only non-negligible for magnon modes in the vicinity of the  $M$ -point and the effect of these modes' lifetime-reduction diminishes at higher temperature, this behaviour is observed.

Spontaneous magnon decay occurs at fields above  $B_{tr} = 0.76B_S$ . For the modes that are prone to this type of decay, the scattering rates are large compared to grain-boundary scattering at any temperature. However, mostly magnon modes which get excited at higher temperature and are of lesser importance for the low-temperature behaviour are affected. In the high-temperature behaviour the influence of magnon-magnon scattering can be seen clearly. The thermal conductivity is drastically reduced as the magnetic field increases. The observed trend can only be induced by the additional magnon-magnon interaction. For fields above the threshold field  $B_{thr} \approx 0.76B_S$  of spontaneous magnon decay, there is a greater variety of the magnon modes' momenta affected by magnon-magnon scattering. As a result, there is a large reduction of the thermal conductivity when this field is exceeded.

It can also be seen that the curves do not asymptotically approach zero. The thermal conductivity does go to zero when magnon-phonon scattering is included. The difference between both scattering mechanisms is that not all of the magnons are affected by magnon-magnon interaction. Their contribution to the thermal transport never vanishes and therefore  $\kappa$  does not go to zero in the high-temperature limit. Another interesting detail is that none of the curves has a clear maximum. For the two curves with a magnetic field below  $B_{tr}$ , the affected magnon modes are only important at low and not at high temperature. Therefore, the thermal conductivity is not drastically reduced when more magnons are excited and the scattering rates increase. For magnetic fields above the critical field scattering rates due to spontaneous decay are already high for modes that are excited at higher temperature. Hence, the modes that are affected by temperature-dependent scattering are already suppressed by the spontaneous decay. There is no drastic reduction in the thermal conductivity at higher temperature as relevant magnon modes are already removed from the transport process.

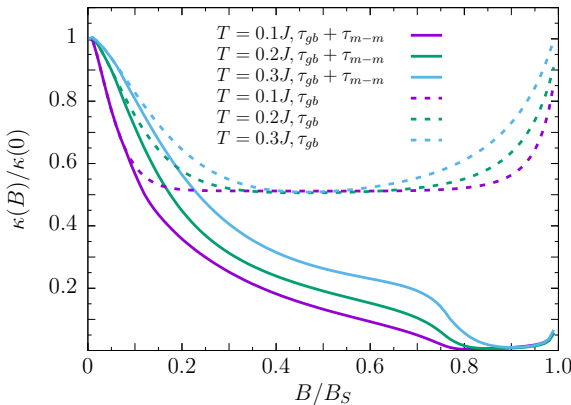


**Figure 5.21.:** Thermal conductivity  $\kappa$  (normalised by the value at vanishing magnetic field  $\kappa(0)$ ) as a function of the external magnetic field  $B$  with and without magnon-magnon scattering rates  $\tau_{m-m}$  at different temperatures  $T$

These results show that the magnon-magnon scattering processes considered so far are not more important in the high-temperature limit than magnon-phonon scattering processes. From the two types of magnon interaction, one depending on temperature and the other not, the latter one is the most important when the magnetic field exceeds  $B = 0.76B_S$ . The number of magnon modes that can contribute to the thermal transport at any given temperature is drastically reduced when such processes are possible. The temperature-dependent scattering processes only affect a minority of the magnon modes and the scattering rates are not high enough at small temperature that the thermal transport is significantly reduced. To be absolutely certain that magnon-magnon scattering can be neglected at higher temperature, higher order terms in the  $1/S$  expansion should be considered. In conclusion, magnon-magnon scattering seems most important at intermediate temperatures. In this context, the dependence of the thermal conductivity on the magnitude of the external magnetic field is of particular interest.

In Figure 5.21 I show the thermal conductivity  $\kappa(B)$  as a function of the external magnetic field  $B$  for different temperatures  $T$  relative to the thermal conductivity  $\kappa(0)$  without a magnetic field. Because of this normalisation, although the thermal conductivity as seen in Figure 5.20 is finite and much larger than zero, the ratio  $\kappa(B)/\kappa(0)$  can go to zero when  $\kappa(0)$  is large compared to  $\kappa(B)$ . For the dashed curves, only grain-boundary scattering with scattering rate  $\tau_{gb}$  is considered while for full curves the previously discussed magnon-magnon scattering processes with a rate of  $\tau_{m-m}$  are added. All curves are normalised to the thermal conductivity at zero magnetic field  $\kappa(0)$ . The evolution of the dashed and full curves at

the same temperature and for small magnetic fields is similar. At these fields, spontaneous magnon decay is absent and the temperature dependent scattering rates are small as discussed in section 5.3.3. The thermal transport is, therefore, limited by grain-boundary scattering. At higher magnetic fields and temperatures, the magnon-magnon scattering rates increase and the dashed and full curves deviate from each other. The thermal conductivity is constant for intermediate magnetic fields when only grain-boundary scattering is considered. In contrast to this, when magnon-magnon interactions are included, the thermal conductivity diminishes. According to equation (5.76) the magnon-magnon scattering rate  $\tau_{m-m} \propto (B^2(1 - B^2/B_S^2))^{-1}$ . This means that the magnon lifetime decreases for fields  $B \leq B_S/\sqrt{2}$ . Because at those fields the contribution of the unstable magnons diminishes, there is no increase in the thermal conductivity. Above this magnitude of the magnetic field, the number of unstable magnons increases. Although some of the scattering rates are reduced by a higher magnetic field, a larger variety of magnon modes is affected by magnon-magnon scattering. It is this trade-off that keeps the thermal conductivity from increasing at higher magnetic fields. At smaller temperature, the contribution of modes that are affected by the magnon-magnon interactions is higher. The thermal conductivity increases with temperature as other magnon modes participate, too.

At  $B \geq B_{tr}$  magnons start to spontaneously decay. One can see this process most clearly at a higher temperature. Then, the number of excited magnon prone to this process is higher. In comparison to the system without an external magnetic field, the contribution of magnetic excitations is dramatically reduced at fields  $B \geq 0.85B_S$ . At these fields, most of the magnon modes scatter among each other, which explains this behaviour. For  $B \simeq B_S$  the thermal conductivity increases again. The reason for that is the reduction of the field dependent prefactor in the scattering rate in equation (5.63). Compared to the length of the interval in which the thermal conductivity is reduced by an increase in the magnitude of the external magnetic field, the length over which it increases is small. Additionally, the scattering processes considered so far only appear for a non-collinear spin-order. When scattering processes of a higher order in the  $1/S$  expansion are included that occur for both collinear and non-collinear order, it can be expected that this behaviour is no longer observed.

The results of this section suggest that the contribution of magnetic excitations to the thermal transport can be drastically reduced by an external magnetic field. When the field is strong enough to appreciably change the magnetic order, the thermal conductivity is reduced to a small fraction of the thermal conductivity at zero magnetic field. In the following section, I summarise the results of the chapter as a whole. In particular, I give a rough estimation of the involved magnetic

field's strength and the implication for the thermal transport not just by magnetic excitations, but also due to all other contributions.

## 5.4. Summary

In this chapter, I discuss the effect of an external magnetic field on the contribution of magnetic excitations to the thermal transport. Section 5.1 contains the derivation of the magnon excitation spectrum, the associated heat current and an expression for the thermal conductivity. The magnon dispersion explicitly depends on the magnitude of the magnetic field. Here, the most apparent effect is the opening of a gap at the  $\Gamma$ -point. Its size can be increased by the magnetic field, allowing for a direct external control. Using a continuity equation for the energy density, I derive an intuitive result for the heat current. It is the product of the number of excited magnons, their velocity and their energy. Furthermore, I evaluate the thermal conductivity via a diagrammatic analysis. There I neglect vertex corrections and find a Drude-like relation, i.e. the conductivity depends solely on the magnons' heat capacity, velocity and mean free path. The latter is determined by different scattering mechanisms.

On a very basic level, the influence of grain-boundary and magnon-phonon scattering processes on the heat transport is studied in section 5.2 by using effective expressions from the literature [135]. Especially momentum-independent scattering allows me to study acoustic and optical magnon modes in more detail. An acoustic magnon branch is always observed in the spectrum and an optical magnon branch appears at finite magnetic fields at the  $\Gamma$ -point of the Brillouin zone. I briefly discuss the importance of both kinds of branches for the thermal conductivity. A magnetic field increases the excitation energy of the optical modes, reducing their number at a given temperature. Additionally, their velocity is low. Optical magnons, therefore, hardly contribute at small temperatures due to their low mobility and heat capacity. In the low-temperature-regime, most of the heat is transported by acoustic magnons. Their energy grows linear with their momentum. There is a certain temperature where a mode's heat capacity does no longer increase and modes of higher excitation energy, i.e. momentum, become more important for the transport. The magnetic field decreases the velocity and increases the curvature of the acoustic mode close to the high-symmetry-point. When the magnetic system approaches ferromagnetic order, the acoustic branch's dispersion becomes quadratic. Although the velocity is zero at the high-symmetry-point, in its vicinity it is not. The approximation of a purely acoustic mode with a single magnon velocity is no longer a good one. Hence, I go beyond the approxim-

ation of acoustic and optic magnon branches and use the full spectrum to calculate the thermal conductivity.

When only momentum-independent scattering is included, I find that the low-temperature limit of the thermal conductivity is very similar for every finite magnetic field. It is only the curve for vanishing magnetic field that deviates, because here there are two acoustic branches instead of only one. This implies that once the optical gap is opened and one of the acoustic branches has become optic, the low-energy spectrum is hardly affected by the field. As long as the temperature is not sufficient to excite those optical modes, the thermal conductivity is determined by the acoustic magnons. Because the optical magnon modes are missing, the thermal conductivity is drastically reduced. For higher temperature, the acoustic contribution diminishes as modes from other parts of the Brillouin zone become more important. As the temperature increases and magnon modes of higher energy are excited, one sees whether or not their ability to conduct heat is improved by the magnetic field. I find that for small magnetic fields, the opening of the gap reduces the thermal conductivity in general. At moderate magnetic fields, certain magnon modes are more apt to transport energy than at lower magnetic field. The thermal conductivity increases and can even become higher than for a vanishing magnetic field at appropriate temperatures.

Of course, at such temperatures, other quasiparticles, in electrical insulators most likely phonons, are excited. Magnons scatter with these and their lifetime reduces. Because the rates depend on the energy and momentum of the involved particles, such scattering rates are momentum-dependent. When these processes are considered, the low-temperature limit is unaffected. However, the thermal conductivity asymptotically approaches zero in the high-temperature limit. For most of the magnetic fields the thermal conductivity is reduced by a higher magnetic field independent of the ambient temperature. The highest thermal conductivity is realised without an external magnetic field.

After the overview on the effect of different scattering mechanisms using effective results, I use expressions derived from a microscopical point of view for magnon-magnon scattering [61] from the leading order terms in the  $1/S$ -expansion. These terms are only non-zero when the magnetic order is non-collinear. Therefore, this kind of magnon-magnon scattering is induced by the magnetic field. I distinguish two kinds of magnon-decay processes: temperature-independent spontaneous decay and regular temperature-dependent magnon-magnon scattering. For both types I discuss the effect on the thermal conductivity. As the magnetic field grows, the scattering rates increases and more magnon modes are involved. This increase in the number of magnon modes prone to magnon-magnon scattering causes the thermal conductivity to decrease. Spontaneous decay only occurs

beyond a certain threshold field. Hence, a distinct drop in the thermal conductivity is visible when this value is exceeded. At this point, the contribution of magnetic excitations to the thermal transport is reduced to nearly zero compared to the initial value at vanishing magnetic field. Although it turns out that it might be necessary to include higher order terms in the  $1/S$  expansion, the results demonstrate that it is certainly possible to control the thermal conductivity by a magnetic field under the right circumstances.

There is a trade-off between materials that have a large magnetic thermal conductivity and materials where this contribution is easily controllable by a magnetic field. On the one hand a large exchange interaction also means a larger magnetic thermal conductivity, on the other hand it also means higher magnetic fields are necessary to make an impact. While for cuprates the fields necessary to attain observable results is of the order of hundreds of Tesla, for organic materials [136] fields of a magnitude of just a few Tesla are enough to induce spontaneous magnon decay. So far, there are no experiments that indicate a reasonable contribution of magnetic excitations to thermal transport in these organic materials. Therefore, the strong dip in magnetic thermal conductivity would simply be blurred or overshadowed by other contributions. Nevertheless, the results I obtain in this chapter suggest that with a field of about 20% of the field necessary to induce ferromagnetic order in an antiferromagnet, the magnetic thermal conductivity can be reduced by 50%. This fact might be interesting for magnonic applications.

The additional occurrence of field-controllable magnon-magnon scattering might also be useful in materials with negligible magnetic thermal transport. Although magnons do not affect the transport directly, they can do this indirectly by scattering with heat carrying quasiparticles, like e.g. phonons. When the lifetime of the magnons diminishes, the probability of them scattering with said quasiparticles decreases, too. In this sense, the mean-free-path of relevant heat carriers increases and so does their ability to transport energy. It is also conceivable that magnon-phonon scattering rates are affected due to changes in the magnon-spectrum. This, however, requires an explicit microscopic calculation, a more detailed look at the phonon spectrum, as well as magneto-vibrational properties of the specific material. This is beyond the scope of this work.



# 6. Electric field control of the magnetic thermal conductivity

I consider the control of the magnetic thermal conductivity by an electric field in this chapter. In contrast to a magnetic field, an electric field can be precisely applied to a spatially confined region. A magnetic material can be, e.g. partially brought between two plates of a small capacitor. As I briefly discuss in section 3.1, when the inversion symmetry of a system is broken, spin-orbit interaction leads to the occurrence of the Dzyaloshinskii-Moriya (DM) term in the effective Hamiltonian of spin-spin interaction [65, 66]. According to equation (3.29) and the discussion after it, an electric field can change the strength of this interaction [72]. In this sense, an electric field can be used to control the DM-interaction in the same sense as the magnetic field is used to control the Zeeman term. This allows one to control the spin transport as well [64, 74].

In this chapter, I look at the manipulation of the thermal conductivity by an electric field. The spins that do not lie in between the plates of the capacitor interact solely via the Heisenberg interaction, while the spins in between additionally interact via the DM-interaction. I refer to this configuration as a heterostructure, because the field is applied only in a finite spatial region and vanishes everywhere else. Such a setup can be found in many electronic, but also spintronic devices [137–139]. In the context of my thesis, it is of interest to determine how an electric field influences the magnetic thermal transport.

Although there are materials with a finite inherent DM-interaction, i.e. it is present at zero electric field too, I do not focus on such materials in the main part of this work. Including an external electric field leads to a superposition of the internal and the field-induced external DM-interaction. The discussion of the effect of the internal DM-interaction on the magnetic contribution to the thermal conductivity is included in appendix C. Here, I focus on the influence of the externally induced DM-interaction. When I feel that additional insights can be gained

by comparing the results of this chapter to the ones in the appendix C I indicate this in the main text. In principle, the general case of both internal and external DM-interactions being present at the same time can be treated by the methods I present in this chapter. I do not expect any insights that can not be gained already by the investigation of either one of the two simpler configurations.

I begin the discussion of the control of the thermal transport by an electric field with the situation where the field is homogeneously applied to the whole system. In section 6.1 I start with the analytic determination of the magnetic ground state. Interestingly, no spin-canting as for the system with an external magnetic field like in chapter 5<sup>1</sup> is observed. I show analytically that a spiral order in one of the crystallographic directions realises at least a local minimum of the classical energy. The spiral configuration breaks the systems inherent  $C_4$ -symmetry of the 2d-square-lattice, because the direction in which the spiral rotates around is distinguished from the perpendicular direction. I study the thermal transport in a spatially inhomogeneous system. In this system there is one direction where an electric field does not change spatially and one where it does. Hence, the  $C_4$ -symmetry is broken from the start. I present numerical results for the minimisation of the classical energy using several numerical algorithms to check that the spin-spiral-configuration is the system's ground state. Next, I present results for the magnon excitation spectrum and the results for the thermal conductivity in the presence of a homogeneously applied electric field at the end of the section.

In section 6.2, I describe the results for a system where an electric field is applied in a confined region. As a result of this, the DM-interaction is only non-zero there. Due to the broken translational invariance, the magnon spectrum can no longer be obtained from linear spin-wave theory in momentum-space. I present the numerical real-space spin-wave theory and show the results for the magnon spectrum and the thermal conductivity in detail. Afterwards I discuss the relevance of the length of the barrier, the strength of the electric field, and the ambient temperature the system is subjected to. At last, I summarise the insights of this chapter and give an outlook on possible applications in section 6.3.

---

<sup>1</sup>In a system with internal DM-interaction one can also observe this spin canting. I include the details in appendix C.1.1.

## 6.1. Homogeneous electric field in entire system

### 6.1.1. Magnetic ground state

When an external electric field is applied to a material, the gradient of the one electron potential  $\nabla_i V$  from equation (3.29) points in the same direction throughout the whole lattice. In a material with a two-dimensional magnetic lattice, the field can be applied in-plane, out-of-plane, and in a linear combination of the former two directions. Here I consider the case of an electric field perpendicular to the magnetic plane ( $z$ -direction). Such a configuration is realised e.g. by a capacitor with plates parallel to this plane. The DM-vector is according to equation (3.29)

$$\mathbf{D}_{ij} = -\frac{J}{\lambda} E_z \mathbf{e}_z \times \mathbf{e}_{ij} \quad (6.1)$$

with  $\mathbf{e}_{ij}$  being the vector from site  $i$  to site  $j$ . The DM-vector therefore points in negative  $y$ -direction for an  $x$ -bond and in positive  $x$ -direction for a  $y$ -bond. In Figure 6.1 I illustrate the configuration of DM-vectors on the square lattice<sup>2</sup>. The anisotropy of the DM-interaction complicates the determination of the system's classical ground state. For this reason, I begin with considering only the DM-interaction in  $x$ -direction before I include the interaction in the other direction as well.

The Hamiltonian for these circumstances reads

$$H = \sum_{\langle i,j \rangle_y} J \mathbf{S}_i \cdot \mathbf{S}_j + \sum_{\langle i,j \rangle_x} -E_z \mathbf{e}_y \cdot (\mathbf{S}_i \times \mathbf{S}_j) \quad (6.2)$$

with  $\langle i,j \rangle_x$  referring to a summation over neighbours in  $x$ -direction only. The classical energy of the system, using spherical coordinates is then

$$\begin{aligned} H^{(0)} = & S^2 \sum_{\langle i,j \rangle_y} \sum_{\langle i,j \rangle_x} -\frac{J}{2} \left[ \cos(\delta_{ij}) \left( 1 + \cos(\alpha_{ij}) \right) + \cos(\gamma_{ij}) \left( 1 - \cos(\alpha_{ij}) \right) \right] \\ & + E_z \left[ \sin(\gamma_{ij}) \sin \frac{\beta_{ij}}{2} \sin \frac{\alpha_{ij}}{2} - \sin(\delta_{ij}) \cos \frac{\beta_{ij}}{2} \cos \frac{\alpha_{ij}}{2} \right]. \end{aligned} \quad (6.3)$$

---

<sup>2</sup>The orientation of the DM-vector is unambiguously determined by the direction of the electric field. One has, however, to always state whether the DM-vector belongs to the DM-interaction between a spin and its neighbour in positive or negative direction, i.e. whether  $e_{ij}$  or  $e_{ji}$  is meant, when drawing a picture for the spatial orientation of the DM-vectors. Because both the DM-vector and the vector product of the two spins change their sign when  $e_{ji}$  is used instead of  $e_{ij}$ . Therefore, the choice has no physical consequences. Here, the DM-interaction is always between a spin and its neighbour in positive direction.

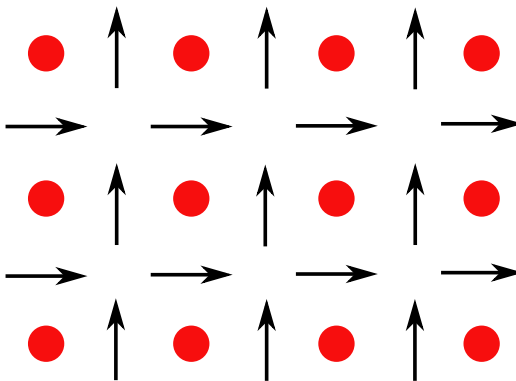


**Figure 6.1.:** When an electric field is applied in plane, the ligand atoms in the superexchange process are displaced in the same direction. This leads to the shown distribution of DM-vectors.

In the above expression I replaced the differences  $\delta_{ij} := \theta_i - \theta_j$  and  $\alpha_{ij} := \phi_i - \phi_j$ , as well as the sums  $\gamma_{ij} := \theta_i + \theta_j$  and  $\beta_{ij} := \phi_i + \phi_j$  of adjacent angles which are its only dependencies. I can additionally limit the minimisation to a single chain in the  $x$ -direction, because the energy is minimised when spins with the same  $x$ -coordinate are anti-parallel to each other. The Néel order can be assumed along the  $y$ -direction without any effect on the minimisation process in the  $x$ -direction.

The condition that all partial derivatives of the classical energy with respect to the four relative angles  $\gamma_{ij}$  and  $\delta_{ij}$  should vanish, leads to the following relations:

$$\frac{\partial H^{(0)}}{\partial \delta_{ij}} \stackrel{!}{=} 0 \Rightarrow \tan \delta_{ij} \cos \frac{\alpha_{ij}}{2} = \frac{E_z}{J} \cos \frac{\beta_{ij}}{2}, \quad (6.4)$$

$$\frac{\partial H^{(0)}}{\partial \gamma_{ij}} \stackrel{!}{=} 0 \Rightarrow \tan \gamma_{ij} \sin \frac{\alpha_{ij}}{2} = -\frac{E_z}{J} \sin \frac{\beta_{ij}}{2}. \quad (6.5)$$

I insert these into the equation arising for the partial derivative with respect to  $\beta_{ij}$  to obtain

$$\cos \gamma_{ij} = \cos \delta_{ij} \quad (6.6)$$

where I readily extract  $\gamma_{ij} = -\delta_{ij}$ . From the derivative with respect to  $\alpha_{ij}$  I conclude

$$\tan \frac{\beta_{ij}}{2} = \tan \frac{\alpha_{ij}}{2}, \quad (6.7)$$

which means  $\alpha_{ij} = \beta_{ij}$ . Putting all those relations back into the expression for the classical energy, it becomes

$$H^{(0)} = -J \cos \delta_{ij} + E_z \sin \delta_{ij} \quad (6.8)$$

which is minimal if

$$\tan \delta_{ij} = -\frac{E_z}{J}. \quad (6.9)$$

In addition, equation (6.4) and (6.5) yield  $\alpha_{ij} = \pi$ , i.e. the spins lie in the  $x$ - $z$ -plane. Because of  $\alpha_{ij} = \beta_{ij}$  the angle of the spin in the  $x$ - $y$ -plane alternates between zero and  $\pi$ . This fact can be absorbed into the the angle between the spin and the  $z$ -axis by adding  $\pi$  when going from one spin to its neighbour. The absolute angles are then<sup>3</sup>

$$\theta_{i+e_x} = \theta_i + \pi - \arctan \frac{E_z}{J} \quad (6.10)$$

$$\theta_{i+e_y} = \theta_i + \pi \quad (6.11)$$

$$\phi_i = 0 \quad \forall i \quad (6.12)$$

These conditions characterise a spiral around the  $y$ -axis along the  $x$ -direction with an underlying Néel order on top of it. The same calculation can be repeated neglecting the  $x$ -component of the DM-vector instead of the  $y$ -component. In the resulting ground state,  $x$ - and  $y$ -component are exchanged and the sense of the spiral is opposite.

Up to this point, the DM-interaction in one direction is neglected. The energy of the spiral state is unaffected by this. Another state might still be energetically more favourable than the spiral state because energy can be gained by the DM-vector's other component. In this case the spiral state is not the system's true ground state. The magnon spectrum derived from this state is misleading then. An analytic minimisation of the classical energy with the full DM-interaction is further complicated by the fact that the energy no longer solely depends on the relative angles between neighbouring spins, i.e. the absolute angle of every single spin is of importance, too. For this reason, I do not try to analytically find the spin texture that minimises the classical energy. Instead, I use different numerical routines for optimisation on a finite lattice. Because for every spin on the lattice there are two Euler-angles, the number of variables rapidly grows with the size of the lattice.

For a system of  $16 \times 16$  sites I am still able to use the SHGO (simplicial homology global optimization) algorithm for minimisation at one specific electric field. The routine optimises a function by brute force. In comparison to the energy of the spiral state, the energy of the state found by this algorithm is slightly smaller. Spins on the margin of the system can gain some energy by ordering differently than the spins in the bulk. The deviations most likely stem from this and are, therefore,

---

<sup>3</sup>Note that relation 6.6 is fulfilled because of  $\theta + \pi = -\theta$  as the angles  $\theta$  are limited to the interval  $[0, \pi]$

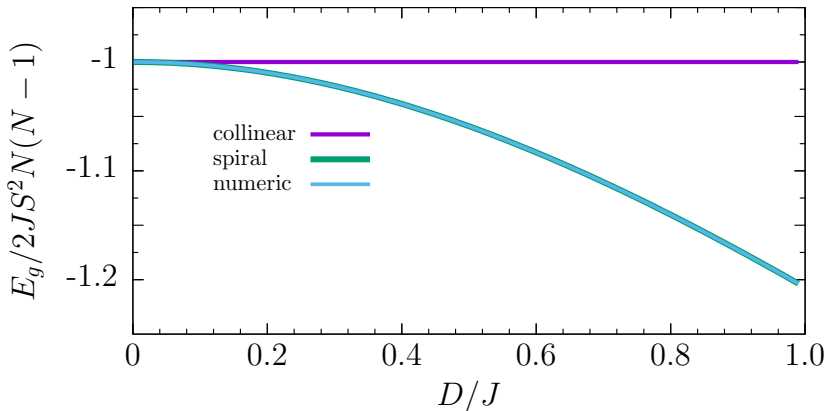


**Figure 6.2.:** Comparison of the ground state energy  $E_g$  of different spin textures as a function of the DM-interaction  $D$  (the dimension of the square lattice used for the numeric calculations is  $N \times N$  where  $N = 64$ ). The curves for the spiral and the numerically determined order lie on top of each other.

finite size effects. For larger fields I use a steepest decent algorithm (conjugate gradient method). Usually, such a routine does not yield the true global minimum if the starting point is not close to it or in the vicinity of local minima. Therefore, high-dimensional systems are problematic in most cases. For this problem, however, the fact can be used that the global minimum is known for the system without DM-interaction. If this interaction is very small, this Néel state is not too far away from the new global minimum in the parameter space of the Euler angles. The new global minimum is found by the algorithm. By successively increasing the DM-interaction, the ground state of the system at higher interaction strengths can be obtained.

In Figure 6.2 I show a comparison of different spin texture's energy  $E_g$  as a function of the DM-interaction. One is the Néel state, another the spiral state defined by equations 6.10 to 6.12, and the last is the state obtained from the numerical minimisation. For the collinear Néel-state, the DM-interaction does not change the energy. The latter, therefore, is the sum of all contributions from the Heisenberg interaction:

$$E_g = -JS^2 \sum_i \frac{z_i}{2}, \quad (6.13)$$

with  $z_i$  being the number of nearest neighbours of a spin on position  $r_i$  of the lattice. On a finite square lattice, a spin in the bulk has four and on the margin either three (on the margin but not on a corner) or two (on a corner) nearest neighbours.

Hence, the energy of the Néel state on an  $N \times N$  square lattice is

$$E_g = -JS^2 \left( 2(N-2)^2 + 6(N-2) + 8N \right) = -2JS^2 N(N-1). \quad (6.14)$$

I normalise the energy of the other two spin textures by this value. The results shown are for the largest system size that I considered ( $64 \times 64$ ).

The curves for the energies of the spirally ordered system and the numerically determined ground state lie on top of each other. By experimenting with the initial value of the in-plane Euler-angle, I am able to obtain different results for the numerical states, i.e. the final values of all Euler-angles. The energies of these states, however, are the same. This implies that no energy can be gained on a global scale when the vector product between two neighbouring spin vectors rotates out of the plane where one of the DM-vectors lies in.

### 6.1.2. Magnetic excitation spectrum

The results for the ground state energy suggest that the spiral state that I determine analytically by neglecting one of the DM-vector's components is also the (or one of many degenerate) ground state configuration(s) of the system with the full DM-interaction in both crystallographic directions. Therefore and to simplify the analysis, I use this state as the starting point for the calculation of the magnon excitation spectrum in this section.

The harmonic part of the Hamiltonian in the spin-spiral configuration is

$$\begin{aligned} H^{(2)} = & -\frac{JS}{2} \sum_{\langle i,j \rangle} \left( a_i^\dagger a_j + a_j^\dagger a_i + a_i a_j + a_i^\dagger a_j^\dagger - 2a_i^\dagger a_i - 2a_j^\dagger a_j \right) \cos \delta_{ij} \\ & - a_i^\dagger a_j - a_j^\dagger a_i + a_i a_j + a_i^\dagger a_j^\dagger \\ & - SE_z \sum_{\langle i,j \rangle_x} \left[ -a_i^\dagger a_i + \frac{1}{2} \left( a_i^\dagger a_j + a_j^\dagger a_i + a_i a_j + a_i^\dagger a_j^\dagger \right) \right] \sin \delta_{ij} \quad (6.15) \\ & + SE_z \sum_{\langle i,j \rangle_y} \frac{1}{i} \left[ a_i a_j - a_i^\dagger a_j^\dagger \right] \sin \theta_i. \end{aligned}$$

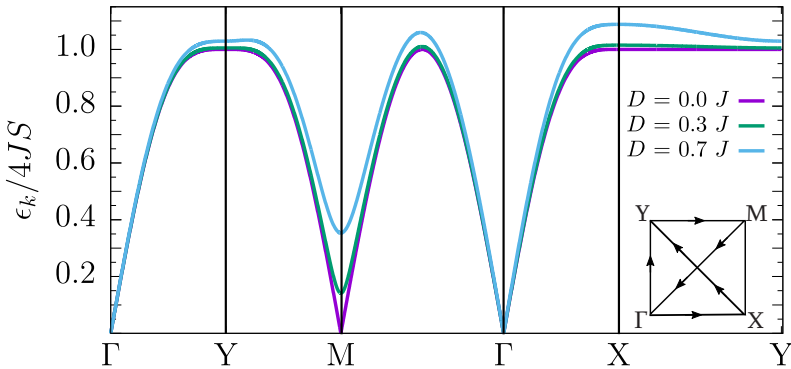


**Figure 6.3.:** Magnon dispersion  $\epsilon_k$  for different strengths  $D$  of the DM-interaction along a specific path through upper right part of the first Brillouin-zone

The term on the last line can be manipulated as follows

$$\begin{aligned} SE_z \sum_{\langle i,j \rangle_y} \frac{1}{i} [a_i a_j - a_i^\dagger a_j^\dagger] \sin \theta_i &= \frac{SE_z}{2i} \sum_{\langle i,j \rangle_y} [a_i a_j + a_j a_i - a_i^\dagger a_j^\dagger - a_j^\dagger a_i^\dagger] \sin \theta_i \\ &= \frac{SE_z}{2i} \sum_{\langle i,j \rangle_y} [a_i a_j - a_i^\dagger a_j^\dagger] (\sin \theta_i + \sin \theta_j). \end{aligned} \quad (6.16)$$

Because  $\theta_j = \theta_i + \pi$  along the  $y$ -direction, the term vanishes.

After a subsequent Fourier- and Bogoliubov-transformation in the same manner as in chapter 5 the magnon dispersion is

$$\begin{aligned} \epsilon_k &= 4JS \sqrt{A_k^2 - B_k^2} \\ A_k &= \frac{1}{2} (1 + \cos \delta_{ij}) - \frac{1}{4} \cos k_x \cos \delta_{ij} - \frac{1}{4} \cos k_y + \frac{1}{2} \gamma_k + \frac{E_z}{4J} (2 - \cos k_x) \sin \delta_{ij} \\ B_k &= \frac{1}{4} \cos k_x \cos \delta_{ij} + \frac{1}{4} \cos k_y + \frac{1}{2} \gamma_k + \frac{E_z}{4J} \cos k_x \sin \delta_{ij} \end{aligned} \quad (6.17)$$

where  $\gamma_k = \frac{1}{2}(\cos k_x + \cos k_y)$  as before.

In Figure 6.3 I illustrate the dispersion for different external electric fields. One can see that a gap opens again at the point  $M = Q$ . It grows linear with the absolute value of the field's strength due to the broken  $SU(2)$  invariance in transversal direction to the spiral. This is in contrast to spirals occurring in  $SU(2)$  invariant models, e.g. due to frustration [140] where the gap, if present, is located at the spiral's pitch vector. Furthermore, the dispersion is very asymmetric with respect

to the  $x$ - and  $y$ -direction which is to be expected because the spiral state breaks this symmetry, too.

Slightly turning every spin into the magnetic plane costs no energy. Flipping every spin changes the system's energy, though. As a result, there is an acoustic branch at the  $\Gamma$ -point and a gapped optic branch at the  $M$ -point for a finite electric field. For a vanishing electric field, there is an additional acoustic branch. From this and the insights of chapter 5, I infer that mainly the acoustic magnons are important for the thermal transport. By increasing the strength of the electric field, one can reduce the contribution of the optic magnons. The amount of how fast the contribution of such modes diminishes is determined by how rapidly the gap at the  $M$ -point increases with the field. There is an anisotropy of the dispersion due to the spiral distinguishing the  $x$ - from the  $y$ -direction. I suspect that this anisotropy transfers to the components  $\kappa_{xx}$  and  $\kappa_{yy}$  of the thermal conductivity tensor, too. I investigate whether an electric field leads to a higher conductivity along the direction of the spiral or perpendicular to it in the next section.

The anisotropy I observe is due to the structure of the ground state used as a basis for the linear spin-wave theory. For a pitch vector pointing along the perpendicular direction, the dispersion is rotated as well. Because other possible degenerate spin ground states are not considered, the results are only valid for this particular spin-spiral ground state. The same can be said about the thermal conductivities components which might be an average of the components  $\kappa_{xx}$  and  $\kappa_{yy}$  for different spin ground states. The spin state I consider in this section is distinguished from all others by the fact that it is the ground state of the inhomogeneous system I consider in section 6.2. I compare the dispersion of this chapter's system to the system with a staggered unidirectional DM-vector in Figure C.2 of appendix C.

### 6.1.3. Thermal conductivity

In section 5.2.1, I discuss the effects of a gap and the influence of the acoustic magnons' velocity on a general level. I do not repeat it here. Although the gap opens at another symmetry point for the electric field than for the magnetic field, at least for the translational invariant system the insights remain valid. I use some of the results from there in this section. If some of the terminology is unclear, a look at section 5.2.1 can be helpful.

Here, I briefly discuss the influence of the electric field on the magnons' ability to transport heat. In particular, I illustrate the anisotropy of the thermal conductivity tensor. As in section 5.2.2, I solely consider scattering of the magnons with grain-boundaries in the crystal. In the low-temperature limit when the number of excited quasi-particles is low, this is the dominant process. The resulting scatter-

ing rate is momentum-independent. Hence, in contrast to other scattering mechanisms, a minimal amount of knowledge about the system is required. Only considering grain-boundary scattering, therefore, allows one to identify which modes are essential for the thermal transport and which are not. When other scattering processes become more important, one can determine whether these affect those modes and change the ability of the magnetic system to conduct heat. All the steps taken in section 5.1.2 to obtain an expression for the thermal conductivity are still correct. Equation (5.39) can, therefore, be used.

As I do in chapter 5, I begin with an examination of the relevance of magnons from specific parts of the first Brillouin-zone. For this, I calculate the thermal conductivity by only extending the sum in  $k$ -space of equation (5.46) to a circle of radius  $\pi/10$  around the high-symmetry point. I compare this reduced thermal conductivity to the total thermal conductivity which includes all modes in the Brillouin zone. It is natural to consider the contribution of magnons in the vicinity of the  $\Gamma$ -point where low-energy acoustic magnons are situated and of the  $M$ -point where the electric field produces gapped optical magnons. These two types of magnons are the most important for the understanding of the thermal conductivity's field control at low-temperature.

The spiral wave vector is pointing in the  $x$ -direction, i.e. spins rotate around the  $y$ -direction when one traverses along the  $x$ -direction. As can be seen in the last section, for this reason the dispersion is anisotropic. Therefore, I show results both for the  $xx$ -and the  $yy$ -component of the thermal conductivity tensor in Figure 6.4. This helps to identify whether certain magnon modes are more relevant for the heat transport along the spiral than perpendicular to it.

For the magnon modes at the  $M$ -point a gap proportional to the DM-interaction opens. This means their heat capacity decreases, i.e. they are harder to excite. At low temperature, those modes hardly contribute to the thermal transport. This can be seen in Figures 6.4(c) and (d). The contribution of said modes to the thermal conductivity reduces as the DM-interaction increases. I observe that there is a maximum in both components of the reduced conductivity  $\kappa_M$  which shifts to higher temperature and reduces in height as  $D$  increases. The optic modes can still be excited if the temperature is high enough. At this temperature, modes from the vicinity of the  $\Gamma$ -point start to contribute too, though. The higher the temperature, the smaller is the contribution from the modes close to the  $M$ -point in comparison to the modes close to the  $\Gamma$ -point. In contrast, the magnon modes at the  $\Gamma$ -point remain gapless at a finite DM-interaction. As a result, the thermal conductivity is almost exclusively due to these modes. This can be seen in Figures 6.4(a) and (b). At  $D = 0$  the modes at the  $\Gamma$ - and the  $M$ -point are gapless acoustic modes and contribute to an equal extent to the thermal transport in the

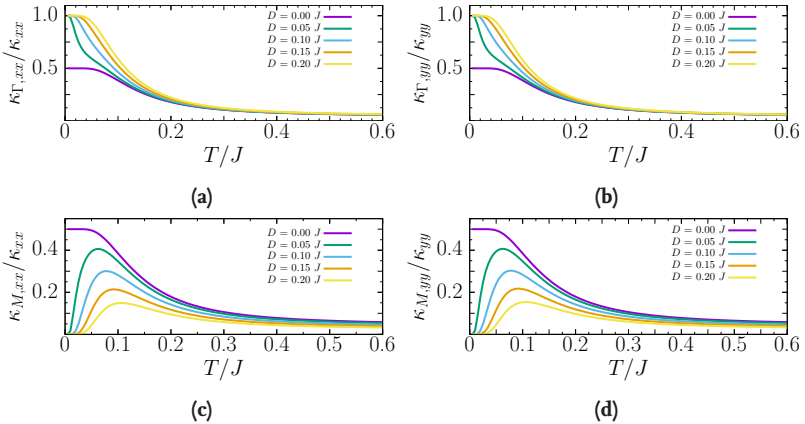


**Figure 6.4:** Reduced thermal conductivity (a)  $\kappa_{\Gamma,xx}$  and (b)  $\kappa_{\Gamma,yy}$  around the  $\Gamma$ -point as well as (c)  $\kappa_{M,xx}$  and (d)  $\kappa_{M,yy}$  around the  $M$ -point for different strengths of the DM-interaction  $D$  as a function of temperature  $T$  (normalised to the total thermal conductivity  $\kappa_{xx}/\kappa_{yy}$ )

low-temperature-limit. The relative contribution of both types of mode reduces as the temperature increases and modes further away of the symmetry points are excited. The low-temperature behaviour is determined by acoustic magnons and the opening of the gap. In this temperature-regime, the anisotropy of the magnon dispersion is not too great. At higher temperatures, magnons from all parts of the Brillouin-zone can transport heat. Hence, the results for the reduced thermal conductivities around the high-symmetry points look similar. This, however, does not imply that the total thermal conductivity can not be anisotropic. The anisotropy is best seen comparing the temperature-dependences of the thermal conductivity's components.

Figure 6.5 shows the temperature-dependence of the thermal conductivity: in (a) the  $xx$ - and in (b) the  $yy$ -component of the tensor. It is apparent that due to the finite gap in the presence of an electric field, in the low-temperature limit the conductivity is reduced with an increase in the electric field's strength for both components. At a higher temperature, one can see, however, that the behaviour of the  $xx$ -component is different to the  $yy$ -component. The explanation for this can be found in the anisotropy of the magnon spectrum again. It is best seen by comparing the dispersion between the  $\Gamma$ - and the  $X$ -point with the dispersion between the  $\Gamma$ - and the  $Y$ -point in Figure 6.3. The energy and mobility of magnon modes which can contribute to a current in  $x$ -direction is increased, while the mobility and energy of magnons which can contribute to a current in  $y$ -direction is not enhanced. Therefore, the thermal conductivity's  $xx$ -component can increase when such modes are excited in a sufficient number, while the  $yy$ -component can

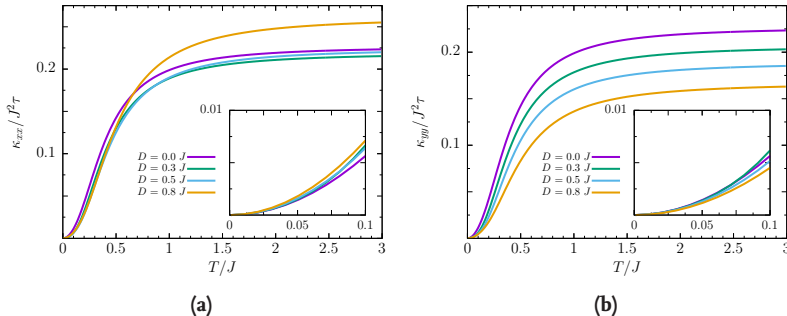


**Figure 6.5.:** Thermal conductivity (a)  $\kappa_{xx}$  and (b)  $\kappa_{yy}$  as a function of temperature  $T$  for different strengths of the DM-interaction. The insets show the low-temperature behaviour of the thermal conductivity. I divide the thermal conductivity of the  $D = 0$ -curve by two to account for the number of acoustic branches and to show that the thermal transport is dominated by these kinds of magnons in the low-temperature limit. Here  $\tau$  is the magnon lifetime due to grain-boundary scattering which I assume to be the same for every mode.

not. For the  $xx$ -component, the thermal conductivity at a field causing a DM-interaction of  $D = 0.8J$  exceeds the conductivity for zero electric field in the high-temperature limit. This fact should not be taken too seriously, because as mentioned before these results are only valid when scattering with other quasiparticles is rare. That is definitely not the case in the high-temperature limit.

The anisotropy of the thermal conductivity can be seen more clearly in Figure 6.6. Here, I plot both components as a function of the DM-interaction's strength normalised to the zero-field value  $\kappa_{xx/yy,0}$  and for different temperatures. Like for the magnetic field one can see an initial decline of the thermal conductivity as the electric field's strength is increased. Due to the opening of the gap, the heat capacity of magnons which this process pertains reduces. At higher temperature, the loss of these modes for the thermal transport is compensated by magnons with a higher energy. The reduction of the thermal conductivity is larger at lower temperatures for this reason. Interestingly, the velocity of the acoustic magnon branch increases in  $x$ -direction with the electric field. When the contribution of the optical magnon is negligible, i.e. the gap's size is large compared to the ambient temperature, the thermal conductivity increases as a function of the electric field's strength due to the higher magnon mobility. For a higher temperature the necessary field is higher too. The minimum therefore shifts to higher electric field for increasing ambient temperature.

Both components are affected by the opening of the gap and the associated decrease of the mobility of these magnon modes. However, the mobility of magnons is improved along the  $x$ -direction for some modes, but not in the  $y$ -direction.

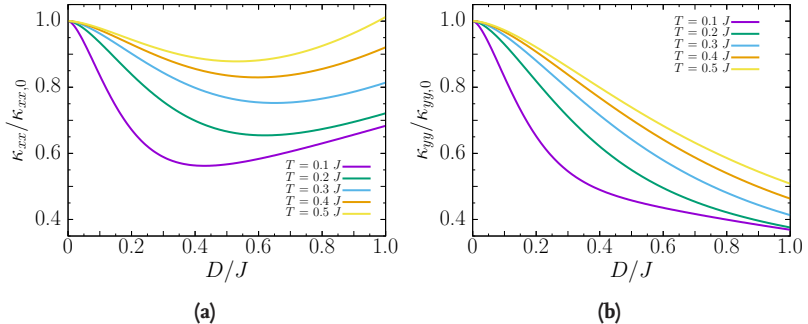


**Figure 6.6.:** Thermal conductivity (a)  $\kappa_{xx}$  and (b)  $\kappa_{yy}$  as a function of the DM-interaction's strength  $D$  for different temperatures  $T$  (normalised to the conductivity at zero field  $\kappa_{xx/yy}(0)$ )

At higher fields, because of this, the  $xx$ -component of the conductivity increases again, whereas the  $yy$ -component only decreases when the magnitude of the electric field's strength is increased. The ability of the magnetic system to transport heat is reduced more drastically in the perpendicular direction of the spiral.

One can compare these results to the thermal conductivity in the system with staggered collinear DM-vectors. I investigate the behaviour of such a system in appendix C. In the next section, I consider an inhomogeneous system where the field is only applied in a limited region.

## 6.2. Electric field in finite region

After discussing the effect of a homogeneously applied electric field on the magnetic thermal transport in the last section, I consider an inhomogeneous setup next. This geometry can be realised in a spintronic device. The plates of a capacitor can be used to supply an electric field whose strength can be controlled by the applied voltage in a spatially confined region. The corresponding field vector points out of the material-plane. This is schematically sketched in Figure 6.7. As I demonstrate in the last section, the field causes a finite DM-interaction which alters the system's magnetic order. When a temperature-gradient is present in the system, the ability of the magnetic system to restore thermal equilibrium is affected. An electric field's strength can be controlled by the voltage and is higher the closer the two plates are to each other, i.e. the thinner the system is. According to equation (3.29) the relation between the DM-interaction's strength  $D$ , the magnitude of the applied voltage  $U$ , and the thickness over which the latter drops  $w$ ,

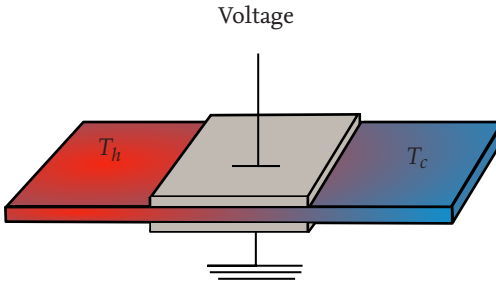


**Figure 6.7:** Schematic sketch of magnetic thermal field effect transistor

is

$$D = \frac{JUe}{\lambda} \frac{a}{w} \quad (6.18)$$

where  $\lambda$  is a spin-orbit dependent material constant and  $a$  is the magnetic lattice constant. For oxides, it is of the order of a few electronvolts [64]. When the system's thickness is only a few monolayers and the voltage is of the order of a few volts, this implies  $D \sim 0.1 \dots 0.3J$ .

In the direction which is both perpendicular to the material-plane and to the interface between the regions with and without an electric field ( $x$ -direction), translational invariance is broken. The analytical determination of the magnetic ground state, as well as the excitation spectrum is much more involved compared to the previous translational invariant system. I therefore use a numerical procedure which I describe in the beginning of this section. After calculating the classical spin ground state and the magnon spectrum, I discuss the results. Afterwards, I show how the current-current correlation functions can be calculated, using the previously determined magnon-eigenstates and -eigenenergies. At last, I present the results for the thermal conductivity as a function of all relevant parameters. These are the ambient temperature, the electric field's magnitude, and the length in  $x$ -direction over which the electric field is applied to.

### 6.2.1. Magnetic ground state and spectrum

As I discuss in section 6.1 of this chapter, the analytic determination of the classical ground state is complicated. There I find that a spiral in the direction of one of the crystallographic axes has the same energy as any of the configurations determined by numerical procedures with the purpose of minimising the energy. From this I conclude that the spiral state is at least one of many degenerate ground

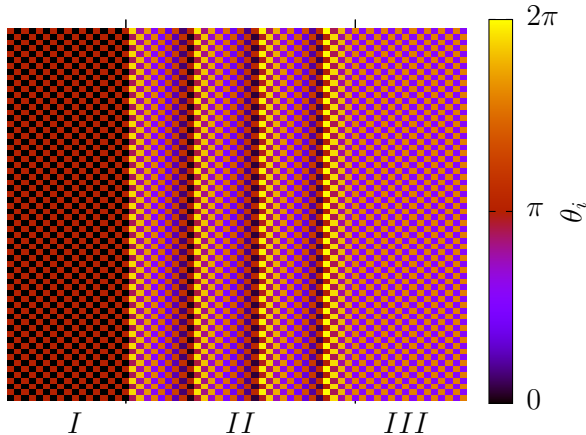


**Figure 6.8.:** Spin texture of magnetic ground state when no electric field is applied in region  $I$  and  $III$  and a finite field (leading to  $D = 0.35J$ ) is applied in region  $II$

states. In the system which I examine in this section, translational invariance in one direction is broken by the spatially limited electric field. The  $C_4$ -symmetry, which is inherent in the homogeneous system, also does no longer exist in the inhomogeneous system. Potentially, this lifts any ground state degeneracy.

The spin ground state configuration for the homogeneous system is calculated analytically. For the inhomogeneous system, I use a numerical procedure to determine the two Euler angles of every spin on the square lattice. I utilise the fact that at zero field, the classical magnetic ground state is already known from the discussion of the homogeneous system to be the Néel state. I successively increase the electric field in the region, obtaining the initial state for the higher field in the next numerical step of the conjugate gradient routine. Because the in-plane Euler-angle is not uniquely defined for the Néel state, I run the routine with different starting values that still fulfil the translational invariance of the geometry with a vanishing electric field. In contrast to the system where the field is applied to the whole system, I obtain one solution for all initial conditions. One of the results can be seen in Figure 6.8. Here the electric field is applied only in the region  $II$ . In region  $I$  and  $III$  one can observe the Néel order, while in region  $II$  the system has a spiral order again. In region  $III$  one can see that the Néel order is rotated with respect to the one in region  $I$ . The electric field is chosen so that  $D = 0.35J$  and region  $II$  extends over 32 sites in  $x$ -direction. According to equation (6.9) the spiral rotates by about  $3.43\pi$  from one end of region  $II$  to the other. Because of the superposed Néel order, one can see three complete revolutions. The relative rotation of the Néel orders left and right of  $II$  is a manifestation of the fourth revolution not being completed.

With the magnetic ground state at hand, I can determine the magnon excitation spectrum from the real-space Hamiltonian in equation (6.16) by diagonalisation. I describe the diagonalisation process in the next section.

### 6.2.2. Thermal conductivity

#### Calculation of the current-current correlation functions

As I mention in the last section, due to the broken translational invariance, all calculations have to be performed in real-space instead of in momentum-space. Although the numerical diagonalisation is more involved, there are methods [141] to obtain the correct eigenenergies and eigenstates. In this section, I show why the transformation diagonalising the Hamiltonian can not be unitary. Afterwards, I derive the formulas for the evaluation of the current-current correlation functions from the numerical results. To be able to do this is essential for the determination of the thermal conductivity.

I write the spinors  $A^{(\dagger)}$  of the Spin-Bose-operators from the Holstein-Primakoff-transformation (5.5) as

$$A = (a_1, a_2, \dots, a_N, a_1^\dagger, a_2^\dagger, \dots, a_N^\dagger) \quad (6.19)$$

$$A^\dagger = (a_1^\dagger, a_2^\dagger, \dots, a_N^\dagger, a_1, a_2, \dots, a_N) \quad (6.20)$$

where the components  $a_i^{(\dagger)}$  obey regular Bose-commutation relations. For the Spinors' commutators one readily finds

$$[A, A] = \begin{pmatrix} [a_\mu, a_\nu] & [a_\mu, a_\nu^\dagger] \\ [a_\mu^\dagger, a_\nu] & [a_\mu^\dagger, a_\nu^\dagger] \end{pmatrix} = \begin{pmatrix} 0 & 1 \\ -1 & 0 \end{pmatrix} = \underbrace{\begin{pmatrix} 1 & 0 \\ 0 & -1 \end{pmatrix}}_{I_p} \underbrace{\begin{pmatrix} 0 & 1 \\ 1 & 0 \end{pmatrix}}_{\underline{x}} = I_p \underline{x},$$

$$[A, A^\dagger] = \dots = I_p, \quad (6.21)$$

$$[A^\dagger, A] = \dots = -I_p,$$

$$[A^\dagger, A^\dagger] = \dots = -I_p \underline{x} = \underline{x} I_p.$$

Here I define the paraunitary matrix  $I_p$  ( $\mathbf{1}$  is the  $N \times N$  identity matrix) and the operator  $\underline{x}$  in the first line. The effect of the operator  $\underline{x}$  on a combination of a general one-particle operator  $MA$  is to transform it to  $MA^\dagger$ , i.e. turning creation into annihilation operators and vice versa.

The harmonic part of the Hamiltonian can then be expressed as

$$H = \frac{1}{2} A^\dagger h A = \frac{1}{2} A_\mu^\dagger h_{\mu\nu} A_\nu, \quad (6.22)$$

where I use the Einstein sum convention. Note the factor of  $1/2$  which results from double counting of terms due to hermitian conjugation. The equation of motion of the spinor operator  $A$  is

$$\begin{aligned} \dot{A}_\lambda(t) &= \frac{i}{2} [A_\mu^\dagger h_{\mu\nu} A_\nu, A_\lambda] = \frac{i}{2} \left( A_\mu^\dagger h_{\mu\nu} [A_\nu, A_\lambda] + [A_\mu^\dagger, A_\lambda] h_{\mu\nu} A_\nu \right) \\ &= \frac{i}{2} \left( (-x I_p)_{\lambda\nu} (h A^\dagger)_\nu + (-I_p)_{\mu\lambda} (h A)_\mu \right) \\ &= \frac{i}{2} \left( (-I_p)_{\lambda\nu} (h A)_\nu + (-I_p)_{\lambda\mu} (h A)_\mu \right) \\ &= i(-I_p h)_{\lambda\mu} A_\mu \end{aligned} \quad (6.23)$$

here I use the hermiticity of the Hamiltonian to exchange the positions of spinors and the Hamiltonian. The solution of the above equation is

$$A_\lambda(t) = (\exp[-iI_p h t])_{\lambda\mu} A_\mu \text{ or } A(t) = \exp[-iI_p h t] A. \quad (6.24)$$

Similarly for the  $A^\dagger$  operator I arrive at

$$A_\lambda^\dagger(t) = A_\mu^\dagger (\exp[ihI_p t])_{\mu\lambda} \text{ or } A^\dagger(t) = A^\dagger \exp[ihI_p t]. \quad (6.25)$$

The goal is to find a transformation  $B$  that diagonalises the Hamiltonian, i.e.

$$(U^\dagger)^{-1} h U^{-1} = \text{diag}(\epsilon_1, \dots, \epsilon_{2N}) := E. \quad (6.26)$$

This defines the Bogoliubov particle spinor  $B$  in which the Hamiltonian is diagonal  $H = B^\dagger E B$  to be

$$B = U A, \quad (6.27)$$

$$B^\dagger = A^\dagger U^\dagger, \quad (6.28)$$

with respect to the normal spinor  $A$ . Demanding that this spinor also fulfils the Bose-commutators (6.21) and solving the equations of motion, one finds

$$B(t) = \exp(-iI_p E t) B, \quad (6.29)$$

$$B^\dagger(t) = B^\dagger \exp(iE I_p t). \quad (6.30)$$

As  $B(t) = UA(t)$  and  $B^\dagger(t) = A^\dagger(t)U^\dagger$  one deduces, e.g. from the last equation by inserting  $h = U^\dagger EU$  in  $A^\dagger(t)$ ,

$$U^\dagger \exp(iEI_p t) \stackrel{!}{=} \exp(iU^\dagger EUI_p t)U^\dagger. \quad (6.31)$$

In the series of the exponential, one has to evaluate expressions containing  $(U^\dagger EUI_p)^n$  which by demanding  $UUI_p U^\dagger = I_p$  yields (6.31). By examining  $B(t) = UA(t)$  one readily finds the same. Furthermore, one can derive

$$A(t) = U^{-1} \exp(-iEI_p t)B, \quad (6.32)$$

$$A^\dagger(t) = B^\dagger \exp(-iEI_p t)(U^\dagger)^{-1}. \quad (6.33)$$

The takeaway from this is that the transformation  $U$  is not unitary, but paraunitary. The last property is defined by

$$UUI_p U^\dagger = I_p. \quad (6.34)$$

Therefore regular diagonalisation routines can not be used. Instead one needs to follow the one described<sup>4</sup> in [141].

I use this procedure to calculate the density of states  $\varrho$

$$\varrho(\omega) = \sum_i \text{Im} \left( \frac{1}{\omega - \epsilon_i + i0^+} \right), \quad (6.35)$$

where the sum runs over all numerically determined eigenenergies  $\epsilon_i$ . This function has structure at the energies  $\omega$  necessary to excite magnons. In a system with broken translational invariance, momentum is no longer a good quantum number. Hence, the magnon spectrum can not be illustrated on a specific path in the Brillouin-zone. The density of states, however, can be calculated for the translational invariant homogeneous and the inhomogeneous system where translational invariance is broken. Comparison of the density of states for different geometries and electric fields indicates how the magnon spectrum changes. In Figure 6.9 I show the density of states for the homogeneous system<sup>5</sup> with and without an electric field as well as for a system where the field is only applied to half of the system, i.e.  $l = L/2$ .

The density of states which I determine numerically for the system without an electric field coincides with the density of states I calculate with the analytic results of section 6.1.2. For the inhomogeneous system with a finite electric field such a

<sup>4</sup>I slightly changed the notation of [141]. All the  $U$ 's here need to be replaced by  $U^{-1}$  and vice versa to be consistent with the text.

<sup>5</sup>By this I mean a system where the whole system is subjected to the electric field, i.e.  $l = L$

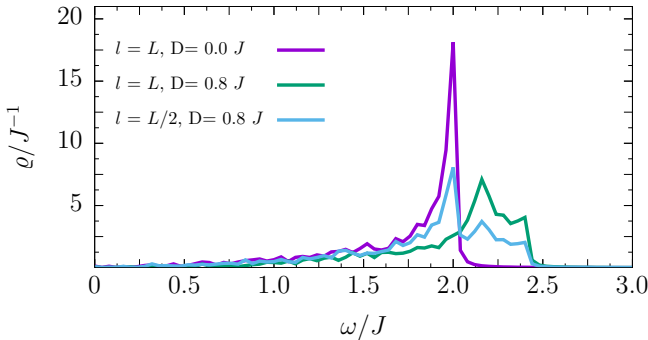


**Figure 6.9.:** Density of states  $\rho$  for different lengths  $l$  over which an electric field is applied, leading to a finite DM-interaction of strength  $D$  ( $L$  is the overall length of the numerical square lattice)

direct comparison of the numeric and the analytic results for the density of states is not possible: because the Néel order on the left side of the region where the electric field is applied is rotated relative to the Néel order on the right side, closed boundary conditions can not be used in the  $x$ -direction for the inhomogeneous system. As a result, the numeric results for the eigenenergies in a system where the whole system is subjected to the electric field, can not be completely identical to the analytical results obtained in the last section. Deviations become smaller for larger systems, suggesting that these are finite size effects. This implies that the diagonalisation routine from [141] is implemented correctly. A similar comparison of the results can be found in the appendix C where closed boundary conditions can be used.

In Figure 6.9 one can see that the peaks of the homogeneous systems can also be found in the inhomogeneous system with a reduced intensity. This implies that the magnon spectrum, like the ground state configuration, is a mixture of magnon energies from both the Néel ordered and the spiral ordered system. I suspect that the energy gap from the spiral persists. I use the results for the thermal conductivity  $\kappa$  to corroborate this.

In order to calculate the thermal conductivity tensor  $\kappa$ , the current operator  $j(t)$ <sup>6</sup> needs to be expressed in terms of the new Bogoliubov spinor  $B^{(\dagger)}$

$$\begin{aligned}
 j(t) &= A^\dagger(t)jA(t) = B^\dagger \exp(iEI_p t) \left( U^\dagger \right)^{-1} j U^{-1} \exp(-iEI_p t) B, \\
 &= e^{i(z_\alpha E_\alpha - z_\beta E_\beta)t} B_\alpha^\dagger (U^\dagger)^{-1}_{\alpha\gamma} j_{\gamma\delta} U^{-1}_{\delta\beta} B_\beta \\
 &:= e^{i(z_\alpha E_\alpha - z_\beta E_\beta)t} B_\alpha^\dagger L_{\alpha\beta} B_\beta.
 \end{aligned} \tag{6.36}$$

<sup>6</sup>The specific form is derived in B.

Here  $z_{\alpha/\beta}$  is 1 for  $\alpha \geq N$  and  $-1$  otherwise.  $L_{\alpha\beta}$  is defined in the equation's last line. With this the current-current correlation function reads

$$\langle j(t)j \rangle = e^{i(z_\alpha E_\alpha - z_\beta E_\beta)t} L_{\alpha\beta} L_{\gamma\delta} \langle B_\alpha^\dagger B_\beta B_\gamma^\dagger B_\delta \rangle \quad (6.37)$$

in the time-domain or

$$\langle jj \rangle(\omega) = \sqrt{2\pi}\delta(\omega - (z_\alpha E_\alpha - z_\beta E_\beta)) L_{\alpha\beta} L_{\gamma\delta} \langle B_\alpha^\dagger B_\beta B_\gamma^\dagger B_\delta \rangle \quad (6.38)$$

in the frequency-domain. I apply Wick's theorem to this expression decomposing it into three products of two two-spinor expectation values. In contrast to pure creation and annihilation operator's expectation values, terms like  $\langle B_\mu B_\nu \rangle$  and  $\langle B_\mu^\dagger B_\nu^\dagger \rangle$  do not necessarily vanish, as the spinors' components contain both creation and annihilation operators. The term  $\langle B_\alpha^\dagger L_{\alpha\beta} B_\beta \rangle \langle B_\gamma^\dagger L_{\gamma\delta} B_\delta \rangle$  in (6.38) is nothing but the expectation value of the current operator squared. Using the real-space definition of the current operator from equation (5.23) and utilising the cyclic property of the trace, it can be shown that this term vanishes<sup>7</sup>

$$\begin{aligned} \langle j \rangle &\propto \text{Tr}(e^{-\beta H} j) = \text{Tr}(e^{-\beta H} i[H, P]) = i(\text{Tr}(He^{-\beta H} P) - \text{Tr}(e^{-\beta H} PH)) \\ &= i(\text{Tr}(He^{-\beta H} P) - \text{Tr}(He^{-\beta H} P)) = 0 \end{aligned} \quad (6.39)$$

This result means that there is no net current flowing in the system. This corroborates the exclusion of the one disconnected diagram representing a term of the same nature when using the diagrammatic approach.

In order to write the result for equation (6.38) more compactly, I define the following two functions

$$f_{\alpha\beta} = \delta_{\alpha\beta} \begin{cases} n_\alpha, & \alpha \leq N \\ (n_\alpha + 1), & \alpha > N \end{cases} \quad (6.40)$$

$$g_{\alpha\bar{\beta}} = \delta_{\alpha\bar{\beta}} \begin{cases} n_\alpha, & \alpha \leq N \\ (n_\alpha + 1), & \alpha > N \end{cases} \quad (6.41)$$

where  $n_\alpha$  are the Bose-Einstein-distribution functions. A bar over an index  $\alpha$  indicates  $\alpha + N$  for  $\alpha \leq N$  and  $\alpha - N$  for  $\alpha > N$  respectively. With this notation the

---

<sup>7</sup>The evaluation of the trace of a commutator is confined to bounded operators which  $H$  and  $P$  are in a finite system.

two-spinor correlation function can be written in the following way

$$\langle B_\alpha^\dagger B_\beta \rangle = f_{\alpha\beta}, \quad (6.42)$$

$$\langle B_\alpha^\dagger B_\beta^\dagger \rangle = g_{\alpha\beta}, \quad (6.43)$$

$$\langle B_\alpha B_\beta \rangle = g_{\bar{\alpha}\bar{\beta}}, \quad (6.44)$$

$$\langle B_\alpha B_\beta^\dagger \rangle = f_{\bar{\alpha}\bar{\beta}}. \quad (6.45)$$

The final result then is

$$\langle jj \rangle(\omega) = \sqrt{2\pi} L_{\alpha\beta} \left[ L_{\bar{\alpha}\bar{\beta}} g_{\alpha\alpha} g_{\bar{\beta}\bar{\beta}} + L_{\beta\alpha} f_{\alpha\alpha} f_{\bar{\beta}\bar{\beta}} \right] \delta(\omega - (z_\alpha E_\alpha - z_\beta E_\beta)). \quad (6.46)$$

As all the energies are larger or equal to zero, only terms where  $z_\alpha E_\alpha$  and  $z_\beta E_\beta$  have the same sign and value survive in the Drude-weight ( $\omega = 0$ ). Then the product of the  $f$  and  $g$  functions is  $n_\alpha(n_\beta + 1)$ . In the case of  $n_\alpha = n_\beta$  one finds

$$n_\alpha(n_\alpha + 1) = -\frac{E_\alpha}{T^2} \frac{\partial n_\alpha}{\partial T}, \quad (6.47)$$

which I found as a prefactor in the diagrammatic evaluation, too. There is a caveat about the evaluation of the Drude-weight. Strictly speaking, a finite Drude-weight can only exist in a system where the currents restoring equilibrium can spatially propagate for an infinite time. Therefore, there is no problem when periodic boundaries are imposed on a finite lattice. Unfortunately, periodic boundaries do not work for the system with a spin-spiral order, because the spin texture on the left and right end of the system can not be matched in general. The Drude-weight can still be extracted in a system with open boundary conditions [142]. In such a system one observes that although the spectral weight at  $\omega = 0$  vanishes, the Drude peak is shifted to finite frequencies. These frequencies correspond to the energies of the magnons with a wavelength which compensate the mismatch at the open boundaries. Hence, the larger the system is, the closer this weight is to  $\omega = \epsilon(k = \mathbf{0}) = 0$ . By comparing analytic results for transport coefficients to numerical results for the same open boundaries, it was shown that by integrating over a small interval in frequency-space, the Drude-weight of an infinite system can be regained.

In Figure 6.10, I show results of the thermal conductivity's  $xx$ -component as a function of the driving frequency for different sizes of a finite  $L \times L$ -square lattice. Here I already included scattering rates as a imaginary addend in the  $\delta$ -functions Lorenzian-representation, i.e. using a broadened magnon-line (for the detailed-scattering rate see equation (6.48)). As a result, the Drude-peak is broadened, too.

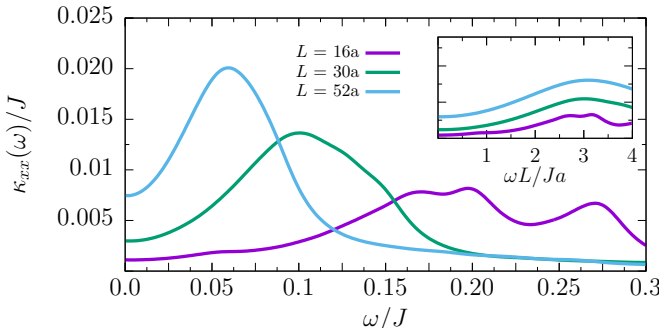


**Figure 6.10.:** Thermal conductivity  $\kappa_{xx}$  as a function of driving frequency  $\omega$  for different dimensions of the system  $L \times L$  (inset: frequency scaled by  $L$ ) at a temperature of  $T = 0.3J$ , a Dzyaloshinskii-Moriya interaction of  $D = 0.1J$ , and the scattering rate in equation (6.48).  $a$  is the length of the magnetic lattice's basis vector.

One can see that the spectral weight moves closer to  $\omega = 0$  as the system's dimension is increased. As can be inferred from the inset in the figure, the shift is linear in  $L$ . In the thermodynamic limit one obtains a broadened Drude-peak centred around  $\omega = 0$ . Throughout the remainder of this chapter I consider a system with dimension  $52a \times 52a$  where  $a$  is the distance between two spins on the lattice. I assume open boundaries in  $x$ -direction and periodic boundary conditions in  $y$ -direction. As a result, there is a single broadened Drude-peak centered around  $\omega = 0$  in the results for  $\kappa_{yy}(\omega)$  for every considered geometry (not shown here). For the two finite components  $\kappa_{xx}$  and  $\kappa_{yy}$ , I integrate the AC-conductivity in the system with open boundary conditions in the interval  $\omega \in [-0.2J, 0.2J]$  in order to find an expression for the DC-conductivity.

## Results

In the following, I present the results for the thermal DC-conductivity. I consider a square-shaped  $L \times L$ -lattice where an electric field (leading to a local DM-interaction  $D$ ) is applied over the complete width  $L = 52a$ , but only over a finite length  $l$ . The numerical results suggest the following classical spin ground state: The spins assume Néel order when there is no DM-interaction between them and rotate along one of the lattice directions when the DM-interaction is finite. In this way, one finds three different regions in the system: a Néel order left of the area where the electric field is applied to, a spiral order in the region with a finite electric field, and a Néel order which is rotated relative to the other one on the right. The spin spiral rotates around the direction parallel to the interface of regions with and without an electric field ( $y$ -direction). As for the homogeneous system, there is an anisotropy between the two crystallographic directions of the magnetic lattice.

Therefore, the  $xx$ -and the  $yy$ -component of the thermal conductivity tensor need to be considered separately.

In order to obtain a finite conductivity, scattering has to be included. Because their calculation from first principles, e.g. from higher order terms in the  $1/S$ -expansion (see chapter 5.3) or magnetoelastic interactions, is involved, I am content with using effective expressions. As in chapter 5.3, I include a temperature-independent scattering rate, as well as a temperature-dependent scattering rate. The former arises, e.g. due to grain-boundary scattering and is most dominant in the low-temperature limit. The temperature-dependent scattering process arises due to scattering of the magnons with other quasi-particles. For a higher temperature, the number of quasi-particles is higher and, hence, this scattering process is less important in the low-temperature limit and dominant in the high-temperature limit. Because the system has a broken translational invariance, the momentum-dependence of the temperature scattering rate can not be included. I, therefore, use a simple expression for the effective scattering rate  $\tau_c^{-1}$  that incorporates both types of scattering:

$$\tau_c^{-1} = \frac{\langle d \rangle}{v} + gT^2 \quad (6.48)$$

with  $\langle d \rangle$  being the mean distance between two impurities,  $v$  the velocity of acoustic magnons and  $g$  is the interaction strength between the magnons and other quasi-particles. Estimations for the former can be found in section 5.2.3 and for the latter I use the same as for the magnon-phonon interaction. The scattering rate is incorporated as an imaginary addend in the argument of the  $\delta$ -distribution in equation (6.46). With this, the thermal conductivity can be calculated via equation (5.39) again. As in chapter 5, the magnitude of the thermal conductivity depends on the ambient temperature  $T$ , in addition to the dependency on the DM-interaction's magnitude  $D$  and the geometry parameter  $l$ . The conductivity is a tensor with three distinct components,  $\kappa_{xx}$ ,  $\kappa_{yy}$ , and  $\kappa_{xy} = \kappa_{yx}$ . Only the first two do not vanish. The main interest is in the  $xx$ -component because in contrast to the  $yy$ -component, here the current has to pass both regions with and without the electric field. Nevertheless, I show the results for all three dependencies  $\kappa(l)$ ,  $\kappa(D)$ , and  $\kappa(T)$  of both components.

The dependency on the length of the intermediate region subjected to the electric field is of particular interest for the design of devices. In reality, only a finite part of the system is contacted. The question can be asked whether the functionality is preserved or even enhanced when the length of this region is reduced. In Figure 6.11, I show the thermal conductivity as a function of the barrier's length  $l$  over which the electric field is applied to. One can see in 6.11(a) that the thermal

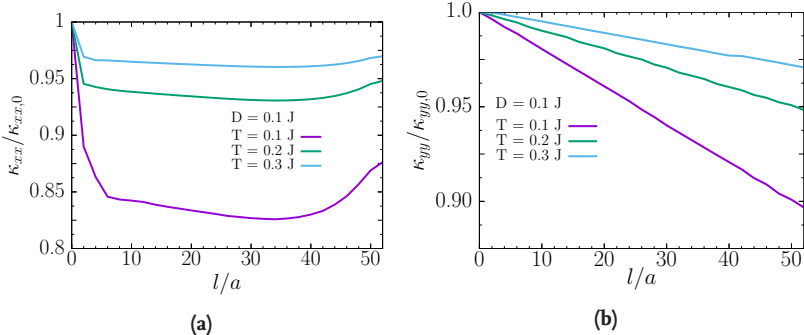


**Figure 6.11.:** Thermal conductivity (a)  $\kappa_{xx}$  and (b)  $\kappa_{yy}$  as a function of the intermediate regions length  $l$  for different DM-interaction strengths  $D$  (normalised to the conductivity at zero field  $\kappa_{xx/yy,0}$ )

transport through the barrier is hindered by the introduction of a small region with a finite electric field. As can be seen in section 6.1, the effect of the field on the thermal transport is the opening of an energy gap for short-wavelength magnons. As a result of this, the heat capacity of these modes is dramatically reduced, i.e. the excitation of these modes becomes more complicated the higher the electric field is. The remainder of the thermal transport is carried by long-wavelength acoustic magnons. When discussing the system's density of states (see Figure 6.9), I find that the excitation spectrum of the magnons in the inhomogeneous system is a mixture of the excitation spectrum of the homogeneous system completely subjected to a finite or vanishing electric field, respectively. This fact is helpful for the interpretation of the thermal conductivity's results.

I argue that the propagation of a short-wavelength magnon through the barrier has to be different from the propagation of a long-wavelength magnon in the  $x$ -direction. If the length of the barrier is smaller or comparable to the magnon's wavelength, fewer spins are flipped inside the region with a finite electric field. Hence, the difference between the energy of a long-wavelength magnon is smaller than for a short-wavelength magnon which corresponds to more spin flips inside the region with a finite electric field. The longer the wavelength of a magnon, the larger the barrier has to be in order to hinder the mode's propagation. For a vanishing electric field, the most important magnons for the thermal transport in the homogeneous system are the ones close to the  $\Gamma$ - and the  $M$ -point. At low temperature, these are either very short ( $M$ -point) or very long ( $\Gamma$ -point). When there is a finite electric field, the gap reduces the contribution of the short-wavelength magnons. Hence, the heat is carried mainly by long-wavelength magnons. These recognise a small barrier to a lesser extent at a lower temperature, while short-wavelength magnons are affected more by a short barrier. For this reason, one can

see that at lower temperature there is a larger dependence of the thermal conductivity on the barrier's length than at higher temperature. For an increasing length of the barrier, the remaining long-wavelength acoustic magnons can propagate better inside the region with a finite electric field, while the excitation of short-wavelength magnons is still hindered there. Hence, the thermal conductivity increases, but does not reach the value which it assumes at vanishing electric field.

I start with the discussion of  $\kappa_{xx}$ . This is the thermal conductivity's component associated with the direction the conditions for the transport are altered most in comparison to the system of section 6.1.3. As for the homogeneous system, the temperature influences the reduction of the thermal conductivity at finite field relative to the one at zero field. At a lower temperature, fewer magnons contribute to the thermal transport at zero field. An electric field opens a gap for optical magnons and reduces their heat capacity. At higher temperature, other magnon modes besides acoustic and optic ones are excited. These are not affected by the electric field, and there is a smaller relative reduction of the thermal conductivity by the electric field at higher temperature. The take-away-message of this is that the length of the barrier is more or less inessential, as long as the electric field is applied over a length greater than a few magnetic lattice constants. The thermal conductivity in an inhomogeneous system is reduced more by the electric field than in a homogeneous system when both are subjected to an electric field of equal magnitude.

In Figure 6.11(b) one can see the  $yy$ -component of the thermal conductivity tensor. Here the heat does not pass through regions with different electric fields. Instead, the heat current always remains either in one of the regions with a vanishing electric field or in the region with a finite electric field. It is apparent that the thermal conductivity decreases linearly with the length of the barrier. Although the mobility of the magnons is not reduced by the electric field in  $y$ -direction, due to the gap the heat capacity is affected in the same way as for the  $x$ -direction. As the length of the region where the electric field is applied to increases, exciting optical magnons in the system becomes more complicated. Because heat is transported separately in the regions with and without an electric field, the overall thermal conductivity  $\kappa_{yy}$  of the whole system is just an average of the conductivities for the individual homogeneous conductivities. In the appendix C I show similar results for a unidirectional staggered DM-vector.

Next, I consider the influence of the DM-interaction's strength on the thermal conductivity. Because the influence of the barrier's length is small for the  $xx$ -component and trivial for the  $yy$ -component, one value of  $l$  is sufficient to get a good impression of the behaviour in other geometries. One can see the results for a system with  $l = 26a$  in Figure 6.12. As for the homogeneous system, the

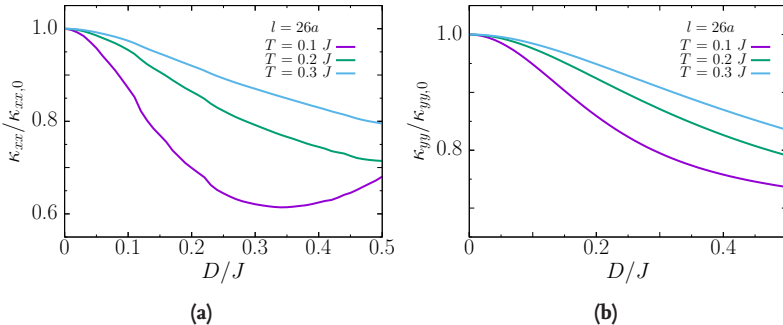


**Figure 6.12.:** Thermal conductivity (a)  $\kappa_{xx}$  and (b)  $\kappa_{yy}$  as a function of the DM-interaction's strength  $D$  (normalised to the conductivity at zero field  $\kappa_{xx/yy,0}$ )

main contribution to the reduction of the thermal conductivity comes from the opening of the gap. When the electric field's strength increases, it becomes harder to excite short-wavelength magnons. Their contribution is missing in the overall conductivity. At higher temperature, more magnon modes are already excited and the decline of the thermal conductivity relative to the conductivity at zero electric field is less steep. As the electric field increases, the gap grows, too. Whereas the mobility of the acoustic magnons is increased in the  $x$ -direction, the mobility is not changed in  $y$ -direction. Hence, the ability of the system to conduct heat along the  $x$ -direction can increase, when the optical magnons are no longer of great importance and a greater gap does not affect the conductivity. In  $y$ -direction, the thermal conductivity keeps on decreasing. All in all, the results are very similar to the ones for the homogeneous system with the electric field being applied to the whole system from section 6.1.3. The differences are, firstly, that due to the inhomogeneity the magnon wavelength is of importance for the thermal transport in  $x$ -direction. Hence, there is an additional reduction in the thermal conductivity due to this effect. Secondly, in contrast to the discussion in section 6.1, scattering rates are temperature-dependent here. Because of the similarities between Figures 6.6 and 6.12, for the temperatures considered so far, this seems to change the results only slightly.

Finally, I present the results for the temperature-dependence of the thermal conductivity in the heterostructure. In Figure 6.13 I show the results for the geometry where half of the system is subjected to an electric field. The low-temperature behaviour shows the characteristic  $T^2$ -law of a 2d-system with an acoustic branch (see Figure 2.1 and the discussion following it). Here the scattering with grain-boundaries is the dominant process which is temperature-independent. At higher temperature, more magnons are excited and can contribute to the thermal transport. The conductivity increases. As the temperature increases, the number of

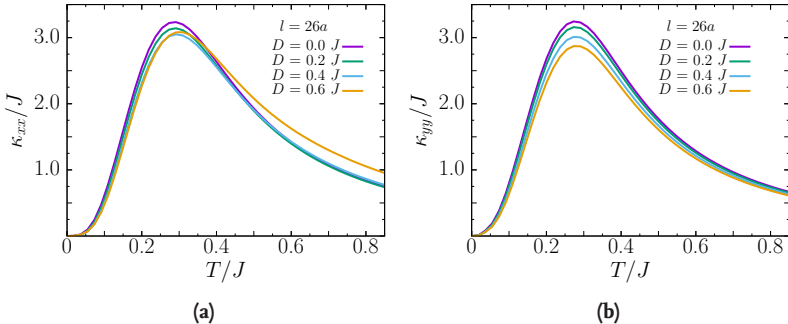


**Figure 6.13.:** Thermal conductivity (a)  $\kappa_{xx}$  and (b)  $\kappa_{yy}$  as a function of the ambient temperature  $T$  for different strengths of the DM-interaction  $D$

other quasi-particles increases, too. Scattering between the magnons and these quasiparticles becomes important, which hinders the magnon's propagation. When the scattering rate exceeds the increase of the magnon heat capacity at a certain temperature, the thermal conductivity assumes a maximum. In Figure 6.13(a) one can see that this maximum shifts to higher temperatures for the conductivity tensor's  $xx$ -component. Such a behaviour can not be observed in Figure 6.13(b) for the  $yy$ -component. As mentioned before, the low-energy excitations' mobility in the  $x$ -direction is only affected by the electric field, but the magnon mobility in  $y$ -direction is unaffected<sup>8</sup>. There it is the opening of the gap that reduces the number of excitable low-energy magnons. This means that the magnons which are important for the transport in  $y$ -direction are still excited at the same temperature as before. Therefore the maximum does not shift.

The mobility of the magnons important for the transport in  $x$ -direction is, in contrast, affected by the electric field. Here the energy of the magnons is increased on average as the acoustic magnon velocity is enhanced by the electric field. Hence, these modes are excited at a higher temperature, i.e. the maximum of the magnon heat capacity shifts to a higher temperature. As a result of this, the maximum of the thermal conductivity is shifted in the same manner. One can also see that for a certain field (e.g.  $D = 0.6 J$ ) and a sufficiently large temperature (e.g.  $T = 0.6 J$ ), the thermal conductivity can be greater than the one at zero field ( $D = 0$ ), i.e. the effect of the gap is compensated by the higher mobility and heat capacity. This fact has to be treated with caution, though. The effective high-temperature scattering rate does not depend on the magnon's wavelength. Because the wavelength of the magnons which transport the majority of the heat at low temperature and the one of the magnons which transport most of the heat at high temperature, is

<sup>8</sup>Here I refer to the acoustic magnons which are present with and without an electric field. The mobility of the acoustic magnon branch which becomes an optic one is obviously affected by the electric field.

very different. Hence, an important factor for the high-temperature behaviour is neglected.

The results illustrated in Figures 6.11 and 6.12 are mostly for temperatures at which the temperature-dependent scattering rate is not the dominant process. At least on a qualitative level, the validity of the results in this low-temperature regime is unaffected by neglecting the momentum-dependence of the scattering rate. The results I show in Figure 6.13 include temperatures where this can not be assumed, though. The high-temperature behaviour in this figure might be altered by the inclusion of a scattering rate that depends on the magnons' wavelength.

## 6.3. Summary

In this chapter I investigate the effect of a spatially confined electric field on the ability of the magnetic system to transport heat. In section 6.1 I analytically calculate the classical spin configuration that minimises the energy when the electric field is not spatially confined and the electric field-induced DM-interaction is only present along one direction. Based on numerical results, I argue that a spin-spiral in one of the crystallographic directions is at least one of many degenerate ground states when the DM-interaction in the other direction is present, too. Using linear spin-wave theory, I discuss the influence of an electric field on the latter. I find that due to the anisotropy of the magnetic ground state, there is a large difference whether magnons propagate along the direction of the spiral or perpendicular to it. While an electric field hardly affects the spectrum in the latter direction, in the other direction the magnon velocity is increased more by it. In addition to this, an energy gap opens for short-wavelength magnons.

At the end of the first section, I calculate the effect of an electric field on the thermal conductivity only considering scattering mechanisms important for the low-temperature behaviour. Here I find that because of the gap and the associate reduction in the magnon's heat capacity as well as mobility, the system's ability to conduct heat is diminished for moderate electric fields. At higher electric fields, the thermal conductivity increases along the  $x$ -direction. This is because after the size of the gap has exceeded a certain temperature-dependent value, the heat capacity of the affected magnons hardly changes. Yet, the mobility of long-wavelength magnons continues to increase with the electric field's magnitude. The thermal conductivity tensor's  $xx$ -component increases for this reason after a certain electric field is exceeded. In the  $y$ -direction the magnon-mobility is not enhanced by an electric field. Hence, the  $yy$ -component continues to decrease for higher magnitudes of the electric field.

With the insights of the homogeneous system, I consider the effect of an electric field that is applied in a confined spatial region in section 6.2. I start by numerically determining the magnetic ground state configuration. Because the  $C_4$ -symmetry is broken by the introduction of an interface between a region with an electric field and one without, in the former region only one of the spiral states which yield minimal energy in the homogeneous system minimises the classical energy in the inhomogeneous system. In the region without an electric field, the spins order in a Néel-like manner. When transitioning from one field region into one with an electric field, the spins start to spiral until the other region without an electric field is reached. Beyond that, the spins keep this rotation relative to the initial Néel-order and order Néel-like again. Additionally, the magnon density of states looks like a combination of the density of states of two homogeneous systems, one with an electric field and one without one (see Figure 6.9). The results for the thermal conductivity corroborate that this interpretation is valid.

For the remainder of this section, I consider the effect of the system's geometry, of the magnitude of the electric field, and of the ambient temperature on the thermal conductivity. The  $xx$ -component of the thermal conductivity tensor is the more interesting one, because the  $yy$ -component is just a superposition of the conductivity at finite and vanishing electric field. The temperature dependence of the thermal conductivity has the  $T^2$ -dependence in the low-temperature limit which is expected, because mostly acoustic magnons with a linear dispersion contribute to the thermal transport and temperature-independent grain-boundary scattering is the dominant scattering process, then. When scattering of the magnons with other quasi-particles becomes important at higher temperature, the thermal conductivity assumes a maximum first, and goes to zero in the high-temperature limit. Hardly any effect of the electric field is visible in the curves, because an electric field mainly affects the low-energy part of the magnon spectrum which is most important at low temperature. In this limit, I observe that the thermal conductivity drops sharply as a function of the barrier's length  $l$ , if the latter is comparable to the magnetic lattice constant  $a$ . Beyond  $l = 8a$  the relative reduction remains more or less constant, but slightly increases when  $l$  becomes comparable to the overall system length. The relative reduction is less pronounced at higher temperature. I explain this by the fact that mostly short-wavelength modes are affected by the barrier and that with increasing temperature the wavelength of the heat carrying modes increases. As a result, the overall effect of the barrier diminishes. I observe this behaviour in the field dependence of the thermal conductivity, too. Here, I find that the thermal conductivity can be reduced by 10-40% by an appropriately

high enough electric field<sup>9</sup> at low temperature.

---

<sup>9</sup>See the discussion below equation (6.18) for a rough estimation of realisable DM-interactions.

## 7. Conclusion

The effect of a magnetic, as well as an electric field on the dynamics of magnetic excitations in insulating quantum magnets is discussed in the literature. There is also a thorough coverage of the spin excitation's contribution to the thermal transport in various types of spin-systems. Spintronic devices which are inhomogeneous systems where external fields are used for switching, i.e. the spin degree of freedom is manipulated, have been developed in the past as well. Based on this, I study the consequences of external fields on the thermal transport by the spin system. My insights can be transferred to gauge whether a field can be used to control the thermal conductivity. The system I look at is a two-dimensional antiferromagnetic square lattice. It is a low-dimensional system where quantum effects are relevant and spin-wave theory still yields good results for the description of the excitations. I investigate the effect of both the magnetic and the electric field on the magnon spectrum and how this transfers to the thermal conductivity, in particular. An electric field can be confined to a much smaller region than is possible for a magnetic field. I consider a heterostructure where the electric field is non-zero only in a small spatial region. This can be realised by putting a material in between the plates of a capacitor. To ensure a large electric field, the material has to be as thin as possible. For the magnetic field, I limit the investigation to a system where the whole system is subjected to a uniform magnetic field.

I calculate the magnon spectrum using linear spin-wave theory and magnon lifetimes using diagrams of three-magnon processes for the magnetic field and effective expressions for the electric field. My focus is on the dependence of the lifetimes on the external field's strength. I use linear response theory to calculate the thermal conductivity. The latter is a function of the ambient temperature and the external field's strength. For the electric field, the length of the region where the electric field is applied to is another parameter potentially affecting the thermal conductivity. I present a method for evaluating the magnon spectrum for this case where translational invariance is broken, i.e. real-space spin-wave theory.

In chapter 5, I investigate the effect of a magnetic field. I determine the classical ground state from minimising the zero order terms in the  $1/S$  expansion as it is common in the literature [45, 119]. I find that the system orders in the Néel

state (spins on neighbouring sites being anti-parallel) in the absence of a magnetic field. The spins start to cant in its direction up to a specific field strength beyond which the system is in the ferromagnetic state. I consider the effects of the magnetic field on the thermal transport for the canted spin order, i.e. strengths of the field between zero and the saturation field. The size of the saturation field is proportional to the exchange interaction. I thoroughly check how the field affects the dispersion of magnons close to high-symmetry points. Without a magnetic field, there are two acoustic magnon branches with a linear dispersion: One at the  $\Gamma$ - and one at the  $M$ -point. A finite magnetic field introduces a preferred direction to the system. Turning all spins by the same angle which corresponds to a magnon of infinite wavelength or zero momentum, now costs energy. As a result, a gap develops at the  $\Gamma$ -point, i.e. the acoustic magnons become optic magnons. Rotating the two-atomic unit cell around the direction of the magnetic field is free, though. The acoustic magnon branch at the  $M$ -point remains acoustic. These results agree with results that can be found in the literature [61].

In a separate section, I look at the dependence of the thermal conductivity on the velocity for a purely acoustic branch, i.e. I neglect its curvature, and on the size of the gap for a completely flat optical magnon branch, respectively. This allows me to get a first impression on the relevance of these two kinds of magnons to the thermal transport. My results suggest that in the low-temperature limit when the gap is larger than the ambient temperature, the acoustic magnons transport the majority of the heat and the thermal conductivity is drastically reduced by the magnetic field as the optic magnons' heat capacity is lowered as well. At the same time, the velocity of the acoustic magnon modes decreases as a function of the magnetic field's strength. The decrease in velocity and mean energy is less important for the contribution of a single acoustic mode than the increase in the number of excitable magnons, though. This means that the magnons' mobility is less important for the thermal conductivity at low temperature than their heat capacity. I corroborate these assumptions by looking at reduced thermal conductivities which only include modes from a small region around the  $\Gamma$ - and the  $M$ -point in the Brillouin-zone in the thermal conductivity's momentum sum. When considering a momentum-independent magnon lifetime which arises, e.g. from grain-boundary scattering, the ratio of these reduced conductivities to the overall conductivity calculated with the sum over the complete Brillouin-zone does not depend on the lifetime. Such momentum-independent scattering rates are dominant in the low-temperature limit.

I find that in zero field magnons close to the  $\Gamma$ -point, as well as magnons close to the  $M$ -point contribute equally to the thermal transport. This is not surprising as both magnon branches are acoustic and have the same velocity. In a non-zero

field, when the magnons around the  $\Gamma$ -point become optic, their contribution to the overall thermal transport diminishes due to the reduction of their heat capacity. Naturally, the contribution of the acoustic magnon modes increases as the contribution of the optic magnons decreases. Because the velocity of the acoustic magnons is hardly affected for a small magnetic field, I observe an initial decrease for the total thermal conductivity, too. At fields comparable to the saturation field, the mobility of magnons further away from the high-symmetry points decreases and their heat capacity increases. At such high magnetic fields, all optical magnon modes are already depolarised at a moderate temperature. The further enlargement of the gap has no effect at all, while the ability of the acoustic magnons to transport heat is enhanced for fields close to the saturation field. The thermal conductivity is increased by magnetic fields comparable to the saturation field.

In the high-temperature limit, scattering of magnons with one another or other quasi-particles is more important than grain-boundary scattering. I include such momentum-dependent scattering rates in the subsequent section. The expressions I use to model the scattering rates stem from effective relations for magnon-phonon interaction [83]. I look at the temperature-dependence of the thermal conductivity in more detail. The behaviour I observe for the acoustic magnons is similar to the contribution of acoustic phonons in regular insulators. At low temperature, the thermal conductivity increases like  $T^d$  (where  $d$  is the dimension of the studied system; in this case  $d = 2$  for the square lattice). At a low temperature, the number of excitable magnons increases faster than the rate they scatter with the phonons. In the high-temperature regime, the number of excited magnons hardly changes as a function of the temperature. The magnon-phonon scattering processes suppress the contribution of all magnon modes and the thermal conductivity goes to zero. At an intermediate temperature, the thermal conductivity necessarily has a maximum. I find that its value, as well as its position depend on the ambient magnetic field's strength<sup>1</sup>. For higher magnetic fields, magnons are shifted to higher energies. With this, the point where the scattering of the modes outperforms the number of newly excitable magnons moves to higher temperature. As a result, the thermal conductivity's maximum is at higher temperature, too. At the same time, the gap reduces the overall number of magnons in the system at a fixed temperature compared to the situation with a vanishing magnetic field. Hence, the value of the maximum is decreasing as a function of the magnetic field. Because of the scattering rate's momentum-dependence, the contribution of magnons further away from the high-symmetry points decreases. The gain in their

---

<sup>1</sup>The value of the grain-boundary scattering rate is kept fixed. The smaller its value, the lower is the temperature at which the thermal conductivity becomes maximal.

mobility at high magnetic fields is more than compensated by the additional scattering. The thermal conductivity diminishes overall with a larger magnetic field.

Inspired by the literature reporting (magnetic) field inducible magnon-magnon scattering processes [45], I include an investigation on its effect for the thermal conductivity. Here, I first reproduce the results for the square-lattice [61]. I find the same sudden appearance of this phenomenon at a specific threshold field and the increase in the number of magnon modes that are affected by it in momentum-space. For fields close to the threshold field, mainly the acoustic magnons at the Brillouin zone's corners are affected, while for higher fields, modes with a longer wavelength start to decay, too. The scattering rates are only present for a non-collinear spin order. The system is in the collinear Néel state without a magnetic field and orders ferromagnetically above the saturation field, the scattering rates vanish. Hence, for fields either close to zero or to the saturation field, the scattering rates go to zero as well.

In the context of field-induced magnon-magnon scattering, only the temperature-independent processes have been discussed before. In this work, I also investigate the influence of the temperature-dependent scattering rates. In contrast to the spontaneous ones, these occur at all finite magnetic fields. For small magnetic fields, magnons in the vicinity of the acoustic branch are exclusively affected by this type of scattering. Because of the small canting angle, the scattering rate is negligible compared to other momentum-dependent scattering processes like magnon-phonon scattering. For higher magnetic fields, the scattering rates become high enough to affect the thermal transport. Surprisingly, although the scattering rates of these processes are proportional to  $B^2$ , I only observe a linear decrease in the thermal conductivity below the threshold field. Responsible for this ostensible inconsistency is the fact that the wavelength of the modes scattered the most becomes longer with increasing field. These modes are not as important for the thermal transport as modes with a shorter wavelength at a fixed temperature. For this reason, the thermal conductivity does not decrease as fast as expected from the sole field dependence of the scattering rates.

At fields high enough to induce spontaneous decay, the associated scattering rates exceed the ones of the temperature-dependent processes. For the thermal conductivity in the presence of a high magnetic field in the low-temperature limit, one can neglect the temperature-dependent magnon-magnon interactions. The effect of the spontaneous magnon decay is much more important. After exceeding the value of the threshold field, I observe a dramatic drop in the thermal conductivity for this reason. The decrease in the thermal conductivity becomes more pronounced at a higher temperature. The reason for this is that the magnon modes primarily affected by spontaneous decay are not excited at a low temperature. At a

higher temperature, more of the magnons contributing to the thermal transport are affected by the spontaneous decay. Hence, the conductivity drops sharper at a higher temperature, when the threshold field for spontaneous decay is exceeded. At a magnetic field close to the saturation field, the thermal conductivity increases again. This is because of the magnon-magnon scattering rate being higher the less collinear the magnetic order is. As I mentioned before, the system orders ferromagnetically when the field exceeds the saturation field. This being a collinear magnetic order, the magnon-magnon scattering rate vanishes.

Inelastic neutron scattering is a reliable source for the detection of spontaneous magnon decay. My results suggest that one can use the sharp drop in the thermal conductivity after exceeding the threshold field, too. For this, the contribution of magnetic excitations to the transport of heat must be dominant or at least relevant. There is a trade-off between the magnitude of the magnetic thermal conductivity and the strength of the magnetic field necessary to induce the spontaneous magnon decay: a large exchange interaction leads to a larger magnetic thermal conductivity, but to a larger threshold field, too. For high- $J$  materials such as cuprates, the magnetic fields necessary to induce the spontaneous decay are unattainable. Organic magnetic materials with only a fraction of the exchange interaction are candidates to observe the sharp reduction in the magnetic thermal conductivity. For magnetic systems that display a non-collinear ordering without an external magnetic field, spontaneous magnon decay occurs at smaller magnetic fields [62, 63]. Transferring the knowledge gained in this work about the field control of magnetic thermal transport on the square lattice to other geometries is not too complicated. It is, therefore, reasonable to assume that the phenomenon can be observed for much smaller fields for these other lattices than in the square lattice. My results further suggest that the magnetic thermal transport can be controlled in practice even if the fields necessary to induce spontaneous magnon decay are not attainable. I find that with a field of about 20% of the field necessary to induce ferromagnetic order in an antiferromagnet, the magnetic thermal conductivity can be reduced by 50%.

Building on results relating the Dzyaloshinskii-Moriya interaction to the electric field [64], I explore its effect on the thermal transport in chapter 6. My focus is on the inhomogeneous application of the electric field, i.e. it is only non-zero in a confined spatial region. As mentioned in the beginning of this conclusion, such a setup can be realised in practice and is of interest for spintronic applications [74]. Because of the inherent dependence of the Dzyaloshinskii-Moriya vector on the exchange path, the mono-directional electric field induces Dzyaloshinskii-Moriya vectors which point in the direction perpendicular to the vector of two interacting spins and to the electric field. Finding the classical ground state of the system

is more complicated than for the system with monodirectional Dzyaloshinskii-Moriya vectors<sup>2</sup>. Hence, I begin the chapter by looking at the system where the electric field is the same everywhere. I am able to analytically determine the classical ground state in the limit where the Dzyaloshinskii-Moriya interaction is only present in one direction. Then, the spins form a spiral along one direction, rotating around the remaining Dzyaloshinskii-Moriya vector. Next, I include the Dzyaloshinskii-Moriya interaction in the second direction. Using different numerical procedures, I determine the spin texture with the smallest classical energy. I compare the energies of the numeric configurations with the energy of the spiral configuration in one of the crystallographic directions. I find that both remain similar for different sizes of the numerical lattice and strength of the Dzyaloshinskii-Moriya interaction. Hence, I conclude that the spiral order is a ground state.

I determine the magnon spectrum in the homogeneous system, using the spiral state as a starting point for the linear spin-wave theory. Due to the anisotropy of the underlying ground state, the excitation spectrum is anisotropic, too. For an increasing electric field, a gap opens for long-wavelength magnons. Acoustic magnons gain mobility in the direction of the spiral ( $x$ -direction) due to the presence of the field. The mobility remains unchanged in the direction perpendicular to the spiral ( $y$ -direction). I find that the conductivity for small field strengths behaves the same in both the  $x$ - and in the  $y$ -direction. The reason for this behaviour is that the thermal conductivity is mainly affected by the dramatic reduction in the magnons' heat capacity where the gap is opened. For higher electric fields, i.e. when the gap is large enough so that the optical magnons no longer affect the thermal transport, the anisotropy of the magnons' mobility increases the thermal conductivity along the  $x$ -direction. The thermal conductivity along the  $y$ -direction, however, keeps on decreasing for increasing magnitude of the field. I explain this behaviour by the anisotropy in the magnon mobility.

Afterwards, I consider the effect of the spatially confined electric field on the thermal transport. I have to numerically determine the spin ground state again for this inhomogeneous system. I use the fact that the Néel state is known to be the ground state at vanishing field. I incrementally increase the field's strength and find the new ground state by adjusting the spherical coordinates of every spin on the lattice, optimising the corresponding energy. Taking this as the starting point for the next higher electric field, I am able to find the spin ground state for an arbitrary value of the field's magnitude. The resulting spin texture shows that in the inhomogeneous system, the degeneracy of the classical ground state is lifted. The system is in a Néel order in the regions where no electric field is applied, and

---

<sup>2</sup>I consider the latter in the appendix C.

assumes a spiral along the direction perpendicular to the interface. As a result, regions free of an electric field which are separated by a region with a finite field have Néel orders which are rotated relative to each other. Both the Néel order, as well as the spiral order can be matched without loosing any energy at the interface. The spin order in all three regions of the inhomogeneous system is the same as for the homogeneous systems.

Next, I determine the excitation spectrum. Because of the broken translational invariance, I have to employ linear spin-wave theory in real-space instead of in momentum-space. I use a numerical diagonalisation procedure developed for bosons [141] to obtain the magnon spectrum. I compare the density of states for a system with no electric field applied at all, a system where a finite field is applied to the whole system, and a system where one half of the system is subjected to an electric field and the other one is not. I find that the magnon spectrum in the inhomogeneous system is a direct combination of the two former cases of homogeneous systems. This result suggests that the opening of the gap for certain magnons in the homogeneous setup also occurs for the inhomogeneous one.

I corroborate this assumption by the results for the thermal conductivity. Qualitatively, the dependence of the thermal conductivity on the electric field's strength remains unchanged with respect to the results for the homogeneous system. The thermal conductivity is reduced along all directions by a small electric field. I explain this behaviour by the opening of a gap again. I consider the dependence of the thermal conductivity on the length of the region where the electric field is applied to, additionally. I find that a barrier of a length comparable to the average magnon's wavelength is enough to induce a similar reduction in the thermal conductivity as for the homogeneous system. This is because at finite electric fields, the excitation of short-wavelength magnons is more difficult than at zero field: for these modes to propagate through the barrier with a finite electric field, many spins need to be flipped which costs more energy in an electric field than without one. For long-wavelength magnons, a much smaller number of spins is flipped inside the barrier. Hence, their propagation is affected less than the shorter-wavelength magnons' propagation. At low temperature, mostly the long-wavelength magnons contribute to the thermal transport and the short-wavelength magnons can not be excited past the barrier. As a result, the thermal conductivity reduces as well. To affect longer-wavelength modes with the electric field, the size of the region where it is applied to has to be increased. At the same time, the energy of modes is changed less by the electric field the longer their wavelength is. Hence, the thermal conductivity changes less the longer the barrier becomes.

Although the square lattice is the only lattice that I consider in this work, I am confident that the results can be easily transferred to other lattices, too. The pro-

cedure I use for real-space linear spin-wave theory can be applied to other lattice geometries without any difficulties. I do not expect there to be any qualitative differences to the square lattice. The principle effects of the fields on the spectrum remain the same, meaning that at one high-symmetry point, a gap is induced and at another one, the velocity of the acoustic mode is changed.

From chapter 6 one can take away the following: I demonstrate how to apply linear spin-wave theory in real-space. I find that it is possible to control the magnetic contribution to thermal transport by an electric field. Best results are achieved by contacting a thin system (large electric field) and applying a voltage of the order of a few volts. By doing so, the contribution of magnetic excitations can be reduced, depending on the ambient temperature, from 10% up to 40%. Comparing the results of the chapter to the proposition of a spin-FET [138], the specifications are similar to the ones given above. There, materials with itinerant magnetism are considered. My results show that there is no reason why such a device can not be realised using materials with localised magnetic moments. As a stand-alone device, the inhomogeneous system can be used as a thermal spin-FET.

**Part III.**

# **Appendix**



# A. Matsubara-Green's functions

In this appendix I introduce Matsubara Green's functions. These are used to calculate finite-temperature correlation functions. I use them in chapter 5 to evaluate the current-current correlations functions and the magnon-self-energies. The first section of this appendix gives a definition and useful properties of the finite-temperature Matsubara-Green's functions. Afterwards I introduce a helpful theorem for diagrammatic evaluation and describe how the latter is carried out. At the end of the appendix, I show how the Matsubara-Green's functions are related to the correlation functions and how to extract one from the other.

## A.1. Definition

It is the main objective of statistical physics to calculate expectation values of observables at finite temperature. To do so, one uses the density operator

$$\varrho = Z^{-1} e^{-\beta K} \quad (\text{A.1})$$

and the partition function

$$Z = \text{Tr} (e^{-\beta K}) \quad (\text{A.2})$$

where  $K$  is the grand-canonical Hamiltonian  $K = H - \mu N$  of a system with Hamiltonian  $H$ , particle number  $N$ , and a chemical potential of  $\mu$ . The density operator allows one to calculate any operator's expectation value. An analogy between the time-evolution of an operator and its finite-temperature expectation value exists. Here the inverse temperature  $\beta$  is interpreted as an imaginary time. Like in the real-time evolution, a Schrödinger, Heisenberg, and Dirac picture exists. To distinguish imaginary- from real-time, I use  $\tau$  for the former and  $t$  for the latter. In the Schrödinger representation, the operators  $O_S$  are time-independent and the time-evolution is contained in the states. In the Dirac or interaction representation, the operators  $O_I$  evolve according to the (grand-canonical) Hamiltonian

$K_0 = H_0 - \mu N$  of the free system or one that can be treated more easily than the system's full Hamiltonian. Operators are transformed from one picture to the other by

$$O_I(\tau) = e^{K_0\tau} O_S e^{-K_0\tau}. \quad (\text{A.3})$$

The transition from the Dirac to the Heisenberg picture, where the full time-dependence is in the operators, is realised by the (imaginary-time) propagator

$$U(\tau) = e^{K_0\tau} e^{-K\tau}, \quad (\text{A.4})$$

via

$$O_H(\tau) = U^\dagger(-\tau) O_I(\tau) U(\tau). \quad (\text{A.5})$$

The (imaginary-time) derivative of the propagator is

$$\frac{\partial}{\partial \tau} U(\tau) = -K_I(\tau) U(\tau) \quad (\text{A.6})$$

where  $K_I = K - K_0$ . This equation is solved by

$$U(\tau) = \sum_{n=0}^{\infty} \frac{(-1)^n}{n!} \int_0^\tau d\tau_1 \cdots \int_0^\tau d\tau_n T_\tau [K_I(\tau_1) \dots K_I(\tau_n)] \quad (\text{A.7})$$

as for real-time evolution<sup>1</sup>. The symbol  $T_\tau$  indicates that the operators are time-ordered with the smallest time on the right and the largest on the left. One defines the single-particle finite-temperature Matsubara Green's function

$$G_{\nu\xi}(x, \tau; x', \tau') = -\text{Tr} \left( \varrho T_\tau \left[ \Psi_{H,\nu}(x, \tau) \Psi_{H,\xi}^\dagger(x', \tau') \right] \right), \quad (\text{A.8})$$

with the creation and annihilation operators  $\Psi_{H,\nu}^\dagger$ ,  $\Psi_{H,\nu}$  for a particle in state  $\nu$ . With these Green's functions one can calculate any one-body operator's expectation value via

$$\langle O \rangle = \mp \int d^3x \lim_{x' \rightarrow x} \lim_{\tau' \rightarrow \tau+0^+} \text{Tr} [O(x) G(x, \tau; x', \tau')]. \quad (\text{A.9})$$

Here the upper sign is for bosons and the lower one is for fermions<sup>2</sup>.

---

<sup>1</sup>One should note, however, that firstly, in the Heisenberg picture  $O_H$  and  $O_H^\dagger$  are not adjoints and secondly, the propagator  $U$  is not unitary. Only after the substitution  $\tau = it$ , they are.

<sup>2</sup>I will stick to this convention for the remainder of this appendix.

In cases where the system is translationally invariant in space and time, the Green's function is only a function of the spatial and temporal distances, i.e.

$\mathcal{G}(x, \tau; x', \tau') = \mathcal{G}(x - x', \tau - \tau')$ . By using the cyclic property of the trace, one can also show that  $\mathcal{G}$  is periodic for bosons and antiperiodic for fermions

$$\mathcal{G}(x, \tau) = \pm \mathcal{G}(x, \tau + \beta). \quad (\text{A.10})$$

Inserting the expression for the density operator and propagator into the Matsubara-Green's function, one obtains [115]

$$\begin{aligned} \mathcal{G}_{\nu\xi}(x, \tau; x', \tau') = & \\ & - \frac{\text{Tr} \left[ e^{-\beta K_0} \sum_{n=0}^{\infty} \frac{(-1)^n}{n!} \int_0^\beta d\tau_1 \dots \int_0^\beta d\tau_n T_\tau \left[ K_I(\tau_1) \dots K_I(\tau_n) \Psi_{H,\nu}(x, \tau) \Psi_{H,\xi}^\dagger(x', \tau') \right] \right]}{\text{Tr} \left[ e^{-\beta K_0} \sum_{n=0}^{\infty} \frac{(-1)^n}{n!} \int_0^\beta d\tau_1 \dots \int_0^\beta d\tau_n T_\tau [K_I(\tau_1) \dots K_I(\tau_n)] \right]} \end{aligned} \quad (\text{A.11})$$

This expression is, like in the real-time formalism at zero-temperature [143–145], the starting point for a diagrammatic evaluation of the Green's functions. The denominator cancels the contribution of all disconnected diagrams and only the numerator has to be evaluated for connected diagrams.

## A.2. Wick's theorem and diagrammatic evaluation

In the zero-temperature formalism, Wick's theorem [146] relates the time-ordered product of operators to a sum of products where the same operators are contracted pairwise and the rest is normal-ordered. Because the ground state expectation values are zero for a normal-ordered term at zero temperature, only fully contracted terms remain. At finite temperature, these terms do not vanish. A generalised analogue to this theorem exists for Matsubara-Green's functions [147–149]. It relates the ensemble average of the time-ordered product to a fully contracted product.

The thermal expectation value of a string of creation and annihilation operators  $\langle ABC \dots F \rangle$  can be manipulated by shifting the operator  $A$  to the end as follows

$$\begin{aligned} \langle ABC \dots F \rangle &= \text{Tr} (\varrho ABC \dots F) \\ &= \text{Tr} (\varrho [A, B]_\mp C \dots F) \pm \text{Tr} (\varrho B [A, C]_\mp \dots F) \\ &\quad + \dots + \text{Tr} (\varrho BC \dots [A, F]_\mp) \pm \text{Tr} (\varrho BC \dots FA). \end{aligned} \quad (\text{A.12})$$

For the last term one can use the relation<sup>3</sup>

$$A(\beta) = e^{\beta K_0} A e^{-\beta K_0} = A e^{\lambda \beta \epsilon_A} \quad \text{or} \quad A\varrho = \varrho A e^{\lambda \beta \epsilon_A} \quad (\text{A.14})$$

to obtain

$$\begin{aligned} & \text{Tr}(\varrho ABC \dots F) \\ &= \frac{1}{1 \mp e^{\lambda \beta \epsilon_A}} ([A, B]_{\mp} \text{Tr}(\varrho C \dots F) \pm [A, C]_{\mp} \text{Tr}(\varrho B \dots F) \dots + [A, F]_{\mp} \text{Tr}(\varrho BC \dots)) \end{aligned} \quad (\text{A.15})$$

With the definition of the contraction

$$\langle AB \rangle = \frac{[A, B]_{\mp}}{1 \mp e^{\lambda \beta \epsilon_A}}, \quad (\text{A.16})$$

and realising that this is the free Matsubara-Green's function  $\mathcal{G}^0 = \langle T_\tau(AB) \rangle$ , one can repeatedly reorder the operators. The ensemble-average then becomes

$$\begin{aligned} \langle ABC \dots F \rangle &= \langle \overbrace{ABC \dots F}^{\square} \rangle + \langle \overbrace{ABC \dots F}^{\square} \rangle + \dots + \langle \overbrace{ABC \dots F}^{\square} \rangle \\ &+ (\text{all other fully contracted terms}). \end{aligned} \quad (\text{A.17})$$

Because ordering the operators with decreasing time changes the sign on both sides, one can assume that the operators are already time-ordered and  $\langle ABC \dots F \rangle$  can be replaced by  $\langle T_\tau(ABC \dots F) \rangle$ . Equation (A.17) is the finite-temperature equivalent of Wick's theorem. The ensemble-average of a product of time-ordered operators can be written as a sum of a product of free Matsubara-Green's functions.

It is advantageous to consider the Fourier transformed Green's functions in the imaginary-time variable  $\tau$ . In this way, different time-orderings of the terms are automatically included [150–152]. Because of their periodicity in the interval  $2\beta$ , the Green's function can be written as a Fourier series<sup>4</sup>

$$\mathcal{G}(x, \tau) = \frac{1}{\beta} \sum_{n=-\infty}^{\infty} e^{-i\omega_n \tau} \mathcal{G}(x, \omega_n) \quad (\text{A.18})$$

---

<sup>3</sup>This relation follows from the creation and annihilation operator's equation of motion

$$A(\tau) = A e^{-\lambda \tau \epsilon_A} \quad (\text{A.13})$$

where  $\epsilon_A$  is the energy of the particle affected by the operator  $A$  and  $\lambda$  is 1 if  $A$  is a creation operator and  $-1$  if it is an annihilation operator.

<sup>4</sup>assuming translational invariance in time

with the Matsubara frequency  $\omega_n = \frac{\pi}{\beta}n$  with  $n$  being an integer. The Fourier coefficient is

$$\begin{aligned}\mathcal{G}(x, \omega_n) &= \frac{1}{2} \int_{-\beta}^{\beta} d\tau e^{i\omega_n \tau} \mathcal{G}(x, \tau) = \frac{1}{2} \int_{-\beta}^0 d\tau e^{i\omega_n \tau} \mathcal{G}(x, \tau) + \frac{1}{2} \int_0^{\beta} d\tau e^{i\omega_n \tau} \mathcal{G}(x, \tau) \\ &= \frac{1}{2} \left( 1 \mp e^{-i\omega_n \beta} \right) \int_0^{\beta} d\tau e^{i\omega_n \tau} \mathcal{G}(x, \tau).\end{aligned}\quad (\text{A.19})$$

Here equation (A.10) was used and the integration range was shifted in the first integral. The bracketed term in front of the integral is only non-zero if  $n$  is even for bosons and odd for fermions, respectively. Hence, the Matsubara sum only runs over even integers for bosons and odd integers for fermions.

With these things at hand, one can evaluate the time-ordered products in equation (A.11) diagrammatically in the following way [114, 115]: One first draws all topological distinct graphs with  $n$  interaction lines and  $2n+1$  directed particle lines. At each vertex, one ensures conservation of momentum and frequency. In the actual calculation, for each interaction line one has a factor of  $V(k)$  (which is the Fourier transformed of the interaction) and for each internal line there is a factor of

$$\mathcal{G}^0(k, \omega_n) = \frac{1}{i\omega_n - (\epsilon_k - \mu)} \quad (\text{A.20})$$

as well as a factor of  $(-8\pi^3 \beta)^{-n} (-1)^F$  for  $F$  closed fermion loops. Whenever a line closes on itself, a convergence factor of  $e^{i\omega_m 0^+}$  is inserted. At last one integrates over all internal momenta and Matsubara frequencies. For the last summation, contour integration over a function with poles at the Matsubara frequencies can be used. It can easily be checked that

$$\sum_{n=-\infty}^{\infty} \frac{e^{i\omega_n \eta}}{i\omega_n - x} = \frac{\beta}{2\pi i} \int_C \frac{dz}{e^{\beta z} \mp 1} \frac{e^{\eta z}}{z - x} \quad (\text{A.21})$$

for the contour  $C$  encircling the imaginary axis clockwise. This contour can be deformed into two parts  $C'$  and  $\Gamma$  like depicted in Figure A.1. The arcs  $\Gamma$  vanish when their radii go to infinity. Hence, only the contour  $C'$  remains. Because the only simple pole is at  $z = x$  one finds

$$\lim_{\eta \rightarrow 0^+} \sum_{n=-\infty}^{\infty} \frac{e^{i\omega_n \eta}}{i\omega_n - x} = \mp \frac{\beta}{e^{\beta x} \mp 1} = \mp \beta n(x) \quad (\text{A.22})$$

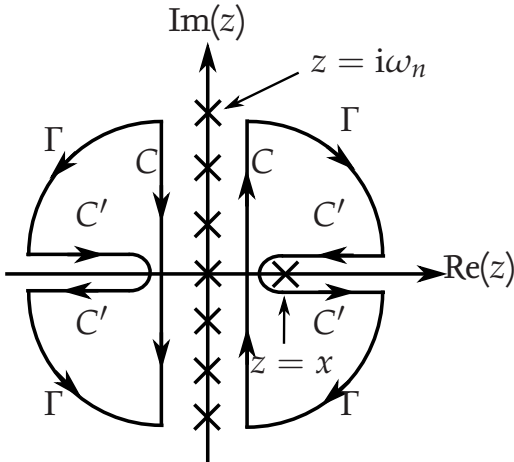


**Figure A.1.:** The Matsubara sums in finite-temperature momentum-space diagrams can be evaluated by contour integration along  $C$  encircling poles at the Matsubara frequencies  $i\omega_n$ . The latter can be deformed into the arcs  $\Gamma$  with a radius going to infinity and  $C'$  going parallel to the real axis and bypassing the pole at  $z = x$ .

where  $n(x)$  is the Bose-Einstein distribution function for bosons and the Fermi-Dirac distribution function for fermions. When calculating the magnon-self-energy in chapter 5, I have to evaluate a Matsubara sum over a product of two magnon-Matsubara-Green's functions. Using the procedure mentioned above, I find

$$-\sum_m \frac{1}{i\omega_m - x} \frac{1}{i(\omega_m \pm \omega_n) - y} = \frac{n(x)}{i\omega_n \pm (y + x)} + \frac{n(\pm y \mp i\omega_n)}{i\omega_n \pm (y + x)}. \quad (\text{A.23})$$

Because magnons are bosons, the Matsubara frequencies are even multiples of  $2\pi/\beta$ . Furthermore,  $n_B(-x) = -(n_B(x) + 1)$ . Hence, the relation simplifies to

$$-\sum_m \frac{1}{i\omega_m - x} \frac{1}{i(\mp\omega_n - \omega_m) - y} = \frac{n_B(x) \pm (n_B(y) + \frac{1}{2}) - \frac{1}{2}}{i\omega_n \pm (y + x)}. \quad (\text{A.24})$$

In a similar fashion one obtains

$$-\sum_m \frac{1}{i\omega_n - x} \frac{1}{i(\omega_n - \omega_m) - y} = \frac{n_B(x) - n_B(y) - 1}{i\omega_n - x + y}. \quad (\text{A.25})$$

### A.3. Relation to real-time Green's functions and transport coefficients

The imaginary-time Matsubara-Green's functions are closely related to real-time retarded Green's functions

$$G_{\nu\xi}^{\text{ret}}(\mathbf{x} - \mathbf{x}', t - t') = -i\theta(t - t') \text{Tr} \left( \varrho \left[ \Psi_{I,\nu}(\mathbf{x}, t), \Psi_{I,\xi}^\dagger(\mathbf{x}', t') \right]_\mp \right) \quad (\text{A.26})$$

where I assumed spatial and temporal translational invariance. This can be expressed in the Källén-Lehmann representation [116, 117], i.e. in the basis  $\{|n\rangle, |m\rangle\}$  of energy, momentum and particle number:

$$G_{\nu\xi}^{\text{ret}}(\mathbf{k}, \omega) = \frac{1}{Z} \sum_{n,m} (2\pi)^3 \langle n | \Psi_\nu | m \rangle \langle m | \Psi_\xi^\dagger | n \rangle \frac{1 \mp e^{-\beta K_m}}{\omega - (K_n - K_m) + i0^+} \delta(\mathbf{k} - \mathbf{p}_n + \mathbf{p}_m). \quad (\text{A.27})$$

$K_n, K_m$  are the eigenvalues of the grand-canonical Hamiltonian  $K$  and  $\mathbf{p}_n, \mathbf{p}_m$  of the momentum operator  $\mathbf{P}$  with respect to the states  $|n\rangle, |m\rangle$ . The imaginary-time Green's function  $\mathcal{G}$  is related via the spectral function  $S$  of the real-time retarded Green's function

$$\begin{aligned} S_{\nu\xi}(\mathbf{k}, \omega) &= -2\text{Im}G_{\nu\xi}^{\text{ret}}(\mathbf{k}, \omega) \\ &= \frac{1}{Z} \sum_{n,m} e^{-\beta K_m} (2\pi)^4 \left( 1 \mp e^{-\beta\omega} \right) \langle n | \Psi_\nu | m \rangle \langle m | \Psi_\xi^\dagger | n \rangle \delta(\mathbf{k} - \mathbf{p}_n + \mathbf{p}_m) \delta(\omega - K_n + K_m) \end{aligned} \quad (\text{A.28})$$

via

$$\mathcal{G}_{\nu\xi}(\mathbf{k}, \omega_n) = \int_{-\infty}^{\infty} \frac{d\omega'}{2\pi} \frac{S_{\nu\xi}(\mathbf{k}, \omega')}{i\omega_n - \omega'}. \quad (\text{A.29})$$

Defining the function

$$\Gamma_{\nu\xi}(\mathbf{k}, z) = \int_{-\infty}^{\infty} \frac{d\omega'}{2\pi} \frac{S_{\nu\xi}(\mathbf{k}, \omega')}{z - \omega'}, \quad (\text{A.30})$$

the retarded Green's function is the boundary value of  $\Gamma$  as  $z$  approaches the real axis from above  $G^{\text{ret}}(\mathbf{k}, \omega) = \Gamma(\mathbf{k}, \omega + i0^+)$ . The Matsubara-Green's functions

yield  $\Gamma(k, z)$  only at the specific points  $z = i\omega_n$ . In order to calculate the retarded correlation functions from the main part, one first evaluates the imaginary-time response coefficients diagrammatically, and then analytically continues these functions to the upper side of the real  $\omega$  axis, treating  $i\omega_n$  as a continuous variable, i.e. by taking the limit  $i\omega_n \rightarrow \omega + i0^+$ .

## B. Current operator from the energy density for an electric field induced Dzyaloshinskii-Moriya interaction

The Hamiltonian of the system in chapter 6 in real-space is

$$H = \frac{SJ}{2} \sum_{\langle i,j \rangle} -\eta_{ij} (b_i^\dagger b_i + b_j^\dagger b_j) + \frac{1}{2} (\eta_{ij} - 1) (b_i^\dagger b_j + \text{h.c.}) + \frac{1}{2} (\eta_{ij} + 1) (b_i b_j + \text{h.c.}) \quad (\text{B.1})$$

with  $\eta_{ij} = \cos \phi_{ij} - (-1)^i \frac{D}{J} \sin \phi_{ij}$ <sup>1</sup> and  $\phi_{ij} = \phi_i - \phi_j$ . A choice for the energy density  $h_l$  so that  $H = \sum_l h_l$  is

$$h_l = \frac{SJ}{2} \sum_{\Delta=\{\pm e_x, \pm e_y\}} \eta_{ll+\Delta} (b_l^\dagger b_l + b_{l+\Delta}^\dagger b_{l+\Delta}) + \frac{(\eta_{ll+\Delta} - 1)}{2} (b_l^\dagger b_{l+\Delta} + \text{h.c.}) + \frac{(\eta_{ll+\Delta} + 1)}{2} (b_l b_{l+\Delta} + \text{h.c.}) \quad (\text{B.2})$$

Therefore the energy current  $j$  can be calculated using the energy polarisation operator  $P = \sum_l h_l l$  through

$$j = i [H, P] = i \sum_{l,m} \mathbf{m} [h_l, h_m] = \frac{i}{2} \sum_{l,m} (\mathbf{m} - \mathbf{l}) [h_l, h_m]. \quad (\text{B.3})$$

---

<sup>1</sup>For the homogeneous system,  $\eta_{ij} = \sqrt{1 + D^2/J^2}$

With the commutators

$$\begin{aligned}
& \sum_{l,m,\delta,\Delta} (\mathbf{m} - \mathbf{l}) \eta_{ll+\delta} \eta_{ll+\Delta} [b_l^\dagger b_l, b_m^\dagger b_m] = 0 \\
& \sum_{l,m,\delta,\Delta} (\mathbf{m} - \mathbf{l}) \eta_{ll+\delta} \eta_{ll+\Delta} [b_l^\dagger b_l, b_{m+\Delta}^\dagger b_{m+\Delta}] = 0 \\
& \sum_{l,m,\delta,\Delta} (\mathbf{m} - \mathbf{l}) \eta_{ll+\delta} \eta_{ll+\Delta} [b_{l+\delta}^\dagger b_{l+\delta}, b_m^\dagger b_m] = 0 \\
& \sum_{l,m,\delta,\Delta} (\mathbf{m} - \mathbf{l}) \eta_{ll+\delta} \eta_{ll+\Delta} [b_{l+\delta}^\dagger b_{l+\delta}, b_{m+\Delta}^\dagger b_{m+\Delta}] = 0 \\
& \sum_{l,m,\delta,\Delta} (\mathbf{m} - \mathbf{l}) \eta_{ll+\delta} (\eta_{ll+\Delta} - 1) [b_l^\dagger b_l, b_{m+\Delta}^\dagger b_m] = \sum_{l,\delta,\Delta} \frac{\Delta}{2} \eta_{ll+\delta} (\eta_{ll+\Delta} - 1) b_l^\dagger b_{l+\Delta} \\
& \sum_{l,m,\delta,\Delta} (\mathbf{m} - \mathbf{l}) \eta_{ll+\delta} (\eta_{ll+\Delta} - 1) [b_l^\dagger b_l, b_m^\dagger b_{m+\Delta}] = - \sum_{l,\delta,\Delta} \frac{\Delta}{2} \eta_{ll+\delta} (\eta_{ll+\Delta} - 1) b_{l+\Delta}^\dagger b_l \\
& \sum_{l,m,\delta,\Delta} (\mathbf{m} - \mathbf{l}) \eta_{ll+\delta} (\eta_{ll+\Delta} - 1) [b_l^\dagger b_l, b_{m+\Delta} b_m] = - \sum_{l,\delta,\Delta} \frac{\Delta}{2} \eta_{ll+\delta} (\eta_{ll+\Delta} + 1) b_l b_{l+\Delta} \\
& \sum_{l,m,\delta,\Delta} (\mathbf{m} - \mathbf{l}) \eta_{ll+\delta} (\eta_{ll+\Delta} - 1) [b_l^\dagger b_l, b_m^\dagger b_{m+\Delta}^\dagger] = \sum_{l,\delta,\Delta} \frac{\Delta}{2} \eta_{ll+\delta} (\eta_{ll+\Delta} + 1) b_{l+\Delta}^\dagger b_l^\dagger \\
& \sum_{l,m,\delta,\Delta} (\mathbf{m} - \mathbf{l}) \eta_{ll+\delta} (\eta_{ll+\Delta} - 1) [b_{l+\delta}^\dagger b_{l+\delta}, b_m^\dagger b_{m+\Delta}] \\
& \quad = \sum_{l,\delta,\Delta} \eta_{ll+\delta} (\eta_{ll+\Delta} - 1) \left[ \frac{\Delta - \delta}{2} b_l^\dagger b_{l+\Delta} + \frac{\delta}{2} b_{l+\Delta}^\dagger b_l \right] \\
& \sum_{l,m,\delta,\Delta} (\mathbf{m} - \mathbf{l}) \eta_{ll+\delta} (\eta_{ll+\Delta} - 1) [b_{l+\delta}^\dagger b_{l+\delta}, b_m^\dagger b_{m+\Delta}] \\
& \quad = \sum_{l,\delta,\Delta} \eta_{ll+\delta} (\eta_{ll+\Delta} - 1) \left[ \frac{\delta - \Delta}{2} b_{l+\Delta}^\dagger b_l - \frac{\delta}{2} b_l^\dagger b_{l+\Delta} \right] \\
& \sum_{l,m,\delta,\Delta} (\mathbf{m} - \mathbf{l}) \eta_{ll+\delta} (\eta_{ll+\Delta} + 1) [b_{l+\delta}^\dagger b_{l+\delta}, b_m b_{m+\Delta}] \\
& \quad = \sum_{l,\delta,\Delta} \eta_{ll+\delta} (\eta_{ll+\Delta} + 1) \left( \delta - \frac{\Delta}{2} \right) b_l b_{l+\Delta} \\
& \sum_{l,m,\delta,\Delta} (\mathbf{m} - \mathbf{l}) \eta_{ll+\delta} (\eta_{ll+\Delta} + 1) [b_{l+\delta}^\dagger b_{l+\delta}, b_{m+\Delta}^\dagger b_m^\dagger] \\
& \quad = \sum_{l,\delta,\Delta} -\eta_{ll+\delta} (\eta_{ll+\Delta} + 1) \left( \delta - \frac{\Delta}{2} \right) b_{l+\Delta}^\dagger b_l^\dagger
\end{aligned}$$

$$\begin{aligned}
 & \sum_{l,m,\delta,\Delta} (\mathbf{m} - \mathbf{l})(\eta_{ll+\delta} - 1)(\eta_{ll+\Delta} - 1) [b_{l+\delta}^\dagger b_l, b_{m+\Delta}^\dagger b_m] \\
 &= \sum_{l,\delta,\Delta} (\eta_{ll+\delta} - 1)(\eta_{ll+\Delta} - 1) \frac{\Delta}{2} b_{l+\Delta}^\dagger b_{l+\delta} \\
 & \sum_{l,m,\delta,\Delta} (\mathbf{m} - \mathbf{l})(\eta_{ll+\delta} - 1)(\eta_{ll+\Delta} - 1) [b_{l+\delta}^\dagger b_l, b_m^\dagger b_{m+\delta}] \\
 &= \sum_{l,\delta,\Delta} (\eta_{ll+\delta} - 1)(\eta_{ll+\Delta} - 1) \frac{\delta - \Delta}{4} b_{l+\Delta}^\dagger b_{l+\delta} \\
 & \sum_{l,m,\delta,\Delta} (\mathbf{m} - \mathbf{l})(\eta_{ll+\delta} - 1)(\eta_{ll+\Delta} + 1) [b_{l+\delta}^\dagger b_l, b_m b_{m+\Delta}] \\
 &= \sum_{l,\delta,\Delta} (\eta_{ll+\delta} - 1)(\eta_{ll+\Delta} + 1) \frac{2\delta - \Delta}{4} b_{l+\delta} b_{l+\Delta} \\
 & \sum_{l,m,\delta,\Delta} (\mathbf{m} - \mathbf{l})(\eta_{ll+\delta} - 1)(\eta_{ll+\Delta} + 1) [b_{l+\delta}^\dagger b_l, b_{m+\Delta}^\dagger b_m^\dagger] \\
 &= \sum_{l,\delta,\Delta} (\eta_{ll+\delta} - 1)(\eta_{ll+\Delta} + 1) \frac{\Delta}{4} b_{l+\delta}^\dagger b_{l+\Delta}^\dagger \\
 & \sum_{l,m,\delta,\Delta} (\mathbf{m} - \mathbf{l})(\eta_{ll+\delta} - 1)(\eta_{ll+\Delta} - 1) [b_l^\dagger b_{l+\delta}, b_m^\dagger b_{m+\Delta}] \\
 &= - \sum_{l,\delta,\Delta} (\eta_{ll+\delta} - 1)(\eta_{ll+\Delta} - 1) \frac{\Delta}{2} b_{l+\Delta}^\dagger b_{l+\delta} \\
 & \sum_{l,m,\delta,\Delta} (\mathbf{m} - \mathbf{l})(\eta_{ll+\delta} - 1)(\eta_{ll+\Delta} + 1) [b_l^\dagger b_{l+\delta}, b_m b_{m+\Delta}] \\
 &= - \sum_{l,\delta,\Delta} (\eta_{ll+\delta} - 1)(\eta_{ll+\Delta} + 1) \frac{\Delta}{4} b_{l+\delta} b_{l+\Delta} \\
 & \sum_{l,m,\delta,\Delta} (\mathbf{m} - \mathbf{l})(\eta_{ll+\delta} + 1)(\eta_{ll+\Delta} + 1) [b_l b_{l+\delta}, b_{m+\Delta}^\dagger b_m^\dagger] \\
 &= \sum_{l,\Delta} (\eta_{ll-\Delta} + 1)(\eta_{ll+\Delta} + 1) \frac{\Delta}{2} b_{l+\Delta}^\dagger b_{l-\Delta} \\
 & \sum_{l,m,\delta,\Delta} (\mathbf{m} - \mathbf{l})(\eta_{ll+\delta} - 1)(\eta_{ll+\Delta} + 1) [b_l^\dagger b_{l+\delta}, b_{m+\Delta}^\dagger b_m^\dagger] \\
 &= \sum_{l,\Delta} (\eta_{ll-\Delta} - 1)(\eta_{ll+\Delta} + 1) \frac{2\delta - \Delta}{4} b_{l+\delta}^\dagger b_{l+\Delta}^\dagger
 \end{aligned}$$

$$\sum_{l,m,\delta,\Delta} (\mathbf{m} - \mathbf{l})(\eta_{ll+\delta} + 1)(\eta_{ll+\Delta} + 1) [b_l b_{l+\delta}, b_{m+\Delta} b_m] = 0$$

$$\sum_{l,m,\delta,\Delta} (\mathbf{m} - \mathbf{l})(\eta_{ll+\delta} + 1)(\eta_{ll+\Delta} + 1) [b_l^\dagger b_{l+\delta}^\dagger, b_{m+\Delta}^\dagger b_m^\dagger] = 0$$

the final expression for the energy current operator is

$$j = \sum_{l,\delta,\Delta} i(\Delta - \delta) \frac{S^2 J^2}{8} \left[ \eta_{ll+\delta}(\eta_{ll+\Delta} - 1) (b_l^\dagger b_{l+\Delta} - b_{l+\Delta}^\dagger b_l) \right.$$

$$- \eta_{ll+\delta}(\eta_{ll+\Delta} + 1) (b_{l+\Delta}^\dagger b_l^\dagger - b_l b_{l+\Delta})$$

$$+ [(\eta_{ll+\delta} - 1)(\eta_{ll+\Delta} - 1) - (\eta_{ll+\delta} + 1)(\eta_{ll+\Delta} + 1)] \frac{b_{l+\delta}^\dagger b_{l+\Delta}}{2}$$

$$\left. - \frac{1}{2}(\eta_{ll+\delta} - 1)(\eta_{ll+\Delta} + 1) (b_{l+\delta}^\dagger b_{l+\Delta}^\dagger - b_{l+\Delta} b_{l+\Delta}) \right] \quad (\text{B.4})$$

# C. Influence of the Dzyaloshinskii-Moriya interaction on the magnonic heat flow

In this appendix I consider the effect of the Dzyaloshinskii-Moriya (DM) interaction on the thermal transport by excitations of the magnetic system. While I look at the control of the DM-interaction by an external electric field in chapter 6, I focus on an intrinsic interaction here, which can be found in materials with a strong spin-orbit interaction, as well as a broken inversion symmetry. The inherent DM-vectors are monodirectional, i.e. they point along one direction throughout the whole system. This is different to the DM-vectors caused by the electric field I consider in chapter 6. As I describe there, the monodirectional electric field produces DM-vectors pointing in the direction perpendicular to the electric field and to the bond between interacting spins. As a result, the magnetic order is different for the intrinsic and for the externally field-induced DM-interaction. In the system with a field-induced DM-interaction one finds a spiral spin order along one of the lattice vectors, while the spins order in a canted manner for the intrinsic DM-interaction.

To start this chapter, I consider the sole effect of the intrinsic DM-interaction, i.e how the thermal transport is altered by it in addition to the usual Heisenberg interaction. Hence, I look at a system with a homogeneous DM-interaction first. I calculate the thermal conductivity as a function of the temperature and the strength of the DM-interaction on the same footing as I do for the system in the presence of a magnetic (chapter 5.2.3) and an electric field (chapter 6.1.3) using effective momentum-independent lifetimes.

Afterwards I consider a system with a limited region subjected to the DM-interaction. The effect of having point defects in a quantum magnet is investigated in [83]. The introduction of a region where an additional interaction is present is a

natural extension of this idea. By inserting a different material with a finite DM-interaction into a material without one, a similar setup as I describe in chapter 6.2 can be realised. Here the inherent DM-interaction's strength can not reach the values which are achievable by using an electric field. The discussion of this system can be seen as a way to explore the influence of three factors to the thermal conductivity: The DM-vectors' orientation, possible transition effects at the boundary between regions with and without DM-interaction, as well as the boundary conditions one uses.

The exchange interaction  $J$  is most certainly different for both materials in reality. For simplicity, I only consider the case where the exchange interaction does not change. Much can be learned from looking at this configuration, though. As for the inhomogeneous system from chapter 6, the spin-wave theory needs to be carried out in real-space instead of in momentum-space, since translational-invariance is broken in such a system. With the exception of the fact that periodic boundary conditions can be employed here, the numerical treatment is identical to the one I describe in chapter 6. The same is true for the evaluation of the current operator. I present the results for the thermal conductivity as a function of the ambient temperature, the size of the intermediate region with finite DM-interaction, as well as its strength, again.

## C.1. Magnonic thermal conductivity in a system with homogeneous Dzyaloshinskii-Moriya interaction

### C.1.1. Magnetic ground state

I study a spin model with nearest neighbour antiferromagnetic Heisenberg exchange  $J > 0$  and DM-interaction  $D$  on a square lattice again. The corresponding Hamiltonian is

$$H = J \sum_{\langle ij \rangle} \mathbf{S}_i^0 \cdot \mathbf{S}_j^0 + \sum_{\langle ij \rangle} \mathbf{D}_{ij} \cdot (\mathbf{S}_i^0 \times \mathbf{S}_j^0). \quad (\text{C.1})$$

As before, I use the superscript 0 to distinguish the spin operators in the laboratory frame from the ones in a rotated frame which I use to simplify the calculation. In section 3.1, I motivate the occurrence of finite DM-interaction in systems with a broken inversion symmetry and strong spin-orbit interaction. I consider such materials where the  $C_4$ -symmetry of the magnetic lattice is preserved like I

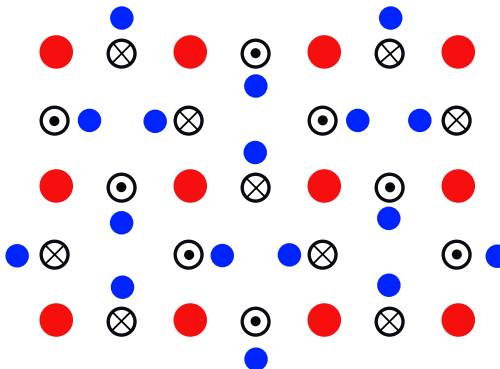


**Figure C.1.:** In a system with finite DM-interaction, the ligand atoms (blue points) are slightly displaced from the center of the magnetic atoms (red points). This leads to a staggered distribution of the DM-vectors ( $\otimes$  indicate that the DMI vector points into the plane, while  $\ominus$  indicate that the vector points out of the magnetic plane).

illustrate in Figure C.1. The red dots represent the magnetic sites involved in the superexchange process and the blue dots are the ligand atoms hosting the virtual state. Such a configuration leads to staggered DM-vectors, i.e. their direction is reversed from one site to another. The DM-interaction is isotropic, because there is no difference between DM-interaction in  $x$ -direction and in  $y$ -direction. Such a behaviour is not observed for the system with a DM-interaction which is induced by an electric field. The DM-vector between a spin pair in  $x$ -direction is perpendicular to the DM-vector between a spin pair in  $y$ -direction when an electric field along the  $z$ -direction induces the DM-interaction.

The general procedure to obtain the magnon spectrum is well established and has been outlined in [68] for the exact same model. I therefore summarise the essential steps only briefly. The laboratory frame of reference is changed so that all spins point in one direction in the new frame (ferromagnetic orientation), first. Spins  $S_i^0$  are ordered in a canted spin configuration in the laboratory frame. The Heisenberg interaction favours a Néel-like classical order on the bipartite square lattice, while the DM-interaction prefers the spins to order perpendicular to each other as well as to the DM-vector. Depending on the DM-interaction's strength, the canting angle is a compromise between both configurations. The general expression for such a change of reference is given by equation (5.2).

Inserting the transformation into the Hamiltonian and only considering the part proportional to  $S^2$ , one obtains the following expression for the classical en-

ergy

$$H^{(0)}/N = -J + \cos^2 \theta_{ij} (2J \cos^2 \phi_{ij} - E \sin 2\phi_{ij}), \quad (\text{C.2})$$

which only depends on the relative angles  $\phi_{ij} := \phi_i - \phi_j$  and  $\theta_{ij} := \theta_i - \theta_j$ . The classical magnetic ground state is the spin texture, which minimises the classical energy. For  $\phi_{ij}$  one finds  $\tan \phi_{ij} = -\frac{D}{J} e^{i\mathbf{r}_{ij} \cdot \mathbf{Q}}$  and  $\theta_{ij} = \pi$ , where  $\mathbf{r}_{ij}$  is the vector pointing to the pair of spins and  $\mathbf{Q} = (\pi, \pi)$ . This means that the spins lie in the plane perpendicular to the DM-vectors. They are canted from the Néel order by an angle which is proportional to the DM-interaction's strength. Because the DM-vector rotates by  $\pi$  from one site to the other, there is no spiral like in the system in the presence of an electric field<sup>1</sup>. Additionally, the canting angle is not anisotropic, i.e. it is the same for an  $x$ -bond as it is for a  $y$ -bond. Hence, the spins can benefit from the DM-interaction by reducing the classical energy along both bond directions. This is a difference between the canted and the spiral spin configuration. As I show next, the magnon excitation spectrum of both configurations is different, too.

### C.1.2. Magnetic excitations

The Hamiltonian becomes:

$$H = \sum_{\langle i,j \rangle} \sqrt{J^2 + D^2} (S_i^x S_j^x - S_i^z S_j^z) - JS_i^y S_j^y, \quad (\text{C.3})$$

when one inserts the optimised rotation of the spin-reference frame. There is no term with an uneven number of magnon creation and annihilation operators after the Holstein-Primakoff transformation is inserted. In contrast to the system in the presence of a magnetic field, those terms are missing although the spin-order is non-collinear, too. The reason for this is that the interaction with the magnetic field involves only the individual spins, while the DM-interaction involves two spins. Therefore, in order to avoid the occurrence of linear terms, all other uneven orders need to be zero, too.

After a Fourier-transformation, the harmonic part of the Hamiltonian is [68]

$$H^{(2)} = 4JS \sum_k A_k a_k^\dagger a_k + \frac{B_k}{2} (a_k a_{-k} + \text{h.c.}). \quad (\text{C.4})$$

---

<sup>1</sup>The sense of the spiral's rotation changes from one site to the other. Hence, spins rotate back and forth in both directions.

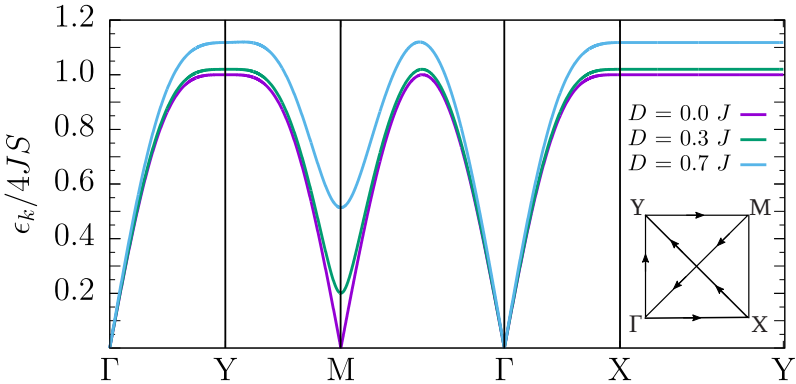


**Figure C.2.:** Magnon dispersion  $\epsilon_k$  for different strengths  $D$  of the DM-interaction along a specific path through the upper right part of the first Brillouin-zone

Here  $A_k = C_1 + \gamma_k C_2$  and  $B_k = -\gamma_k C_3$  with  $C_1 = C_2 + C_3 = \sqrt{1 + (D/J)^2}$ ,  $C_3 - C_2 = 1$ , and  $\gamma_k = \frac{1}{2}(\cos k_x + \cos k_y)$ . As for the other systems, the term is diagonalised by the Bogoliubov transformation in equation (5.17). The result is

$$H^{(2)} = \sum_k \epsilon_k \alpha_k^\dagger \alpha_k + \delta H_0^{(2)}, \quad (\text{C.5})$$

if one chooses  $\tanh 2\theta_k = \frac{B_k}{A_k}$  accordingly. Here  $\delta H_0^{(2)}$  is a constant dispersionless correction to the classical energy. The spin-wave or magnon dispersion is

$$\epsilon_k = 4JS \sqrt{A_k^2 - B_k^2}. \quad (\text{C.6})$$

I show its behaviour on a particular path in the Brillouin zone in Figure C.2. Two regions of the dispersion are of utmost importance for the thermal conductivity  $\kappa$  in the low-temperature limit. A field-dependent gap of width

$\Delta = 4S\sqrt{2}\sqrt{J^2 + D^2 - J\sqrt{J^2 + D^2}}$  opens at the  $M$ -point. One finds a Goldstone mode

$$\begin{aligned} \epsilon_{k \approx 0} &\simeq ck + dk^3, \\ c &= S\sqrt{J^2 + D^2 + J\sqrt{J^2 + D^2}}, \\ d &= -\frac{4S(J^2 + D^2)\sigma + (4\sigma + 1)SJ\sqrt{J^2 + D^2}}{8\sqrt{J^2 + D^2 + J\sqrt{J^2 + D^2}}}, \\ \sigma &= \frac{1}{48}(3 + \cos 4\psi), \end{aligned} \quad (\text{C.7})$$

with group velocity  $c$ , anharmonicity (curvature)  $d$ , and polar coordinates  $(k, \psi)$  in  $k$ -space of the acoustic magnon branch at the  $\Gamma$ -point. In the same manner as I do in section 5.3.2, one can check whether three-magnon interactions are possible for any specific range of the DM-interaction. The general form of the equations is the same. Magnons can only decay into the two-magnon continuum when the ratio of magnon velocity and curvature is positive. Both have, however, an opposite sign for all values of  $D$ . Three-magnon decay is therefore (in the low-temperature limit) also not allowed kinematically. This further corroborates the absence of terms with an uneven number of magnon operators.

One can see that the magnon dispersion is isotropic, i.e. there is no difference between exciting a magnon in  $x$ -direction and in  $y$ -direction. That is not the case for the system with a spiral in one of these directions. Here the staggered spin-order preserves  $C_4$ -symmetry and therefore the excitation spectrum has this symmetry, too. I show that the thermal conductivity is also isotropic for the homogeneous system. Another thing that is different for the system with the monodirectional DM-vectors from the one with anisotropic DM-vectors is the dependence of the optical gap  $\Delta$  on the DM-interaction's strength  $D$ . In Figure C.3 I show this dependence. It is apparent that the gap increases much faster as a function of the DM-interaction's strength for the system with canted spin-order than for the system with a spiral order. I mention again that an explanation is found in the magnetic ground state. For the spiral ordered state, the DM-interaction only affects the energy of spin-pairs in one direction. For the canted structure, the energy of spin-pairs in both directions is lowered by the DM-interaction. It therefore costs more energy to excite a short-wavelength magnon in the former system than in the other. This fact has huge repercussions for the system's ability to transport heat. I discuss this in the next section.

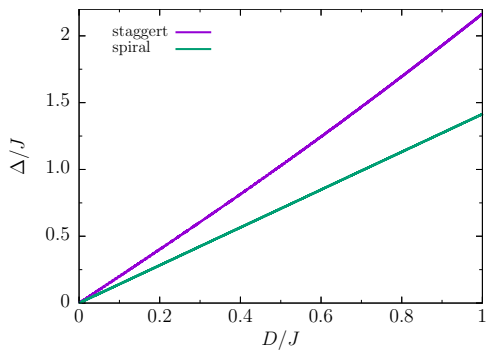


**Figure C.3:** Comparison of the gap  $\Delta$  as a function of the DM-interaction  $D$  in a system with staggered order (due to internal DM-interaction) and a system with spiral order (due to external field-induced DM-interaction)

### C.1.3. Current operator

The problem of deriving an expression for the energy current operator is discussed in chapter 4 (see the discussion of equation 4.5) and in more detail in the beginning of section 5.1.2. In section 6.2.2, I show how to evaluate the current-current correlation function in the real-space representation using numerical results for the eigenenergies and eigenstates. These results are still valid and can be directly transferred to this section. The interested reader can consult these parts if they look for a deeper understanding.

### C.1.4. Thermal conductivity

As for the calculation of the thermal conductivity in section 6.1.3, for the system with anisotropic DM-vectors everywhere, I use the momentum-independent grain-boundary scattering rates of equation (5.43) here. Therefore only the low-temperature behaviour of the thermal conductivity is correctly described. The influence of DM-interaction on the magnon spectrum and the repercussions for the thermal transport, can be investigated best this way. Because the magnon spectrum is the same for magnons moving in the  $x$ -direction and for magnons moving in the  $y$ -direction, I only show one of the thermal conductivity tensor's components. The other looks the same.

The most important mechanism for the DM-interaction to affect the thermal conductivity is by lifting the degeneracy for short- and long-wavelength magnon branches by opening a gap for the former. This means that the energy necessary to excite these modes raises. Their heat capacity at temperatures small compared to the exchange interaction  $J$  is reduced, because it is harder to increase the number

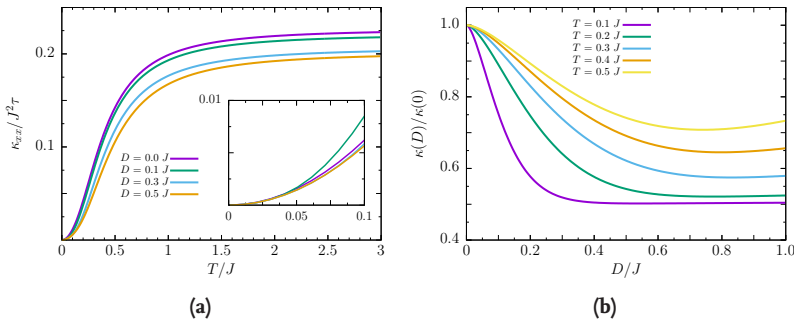


**Figure C.4.:** Thermal Conductivity  $\kappa_{xx}$  (a) as a function of the ambient temperature  $T$  for different DM-interaction strengths  $D$  (the low-temperature behaviour is shown in the inset with the value for the curve with  $D = 0$  divided by two) and (b) as a function of the DM-interaction at a fixed temperature  $T$  (normalised to the conductivity  $\kappa_{xx,0} := \kappa_{xx}(D = 0)$  at zero interaction strength)

of gaped optical magnons. They can be excited and absorb heat at higher temperature, but due to their low mobility, they can not transport it as well as acoustic modes. I find that in the low-temperature limit, the acoustic modes are the most essential ones for the thermal transport. Their mobility, i.e. the magnon velocity, is monotonically increasing with the DM-interaction's strength. This affects the thermal conductivity only when the gap is so large that the magnons' heat capacity is no longer reduced noticeably.

In Figure C.4(a) one can see the thermal conductivity as a function of the ambient temperature for different strengths of the DM-interaction. As for the systems in the presence of a magnetic and an electric field respectively, the acoustic magnons are the most important in the low-temperature limit. One can see the thermal conductivity's behaviour more clearly in the inset of Figure C.4(a). There I divide the thermal conductivity without any DM-interaction by two. The reason for this is that for this kind of system, the spectrum has two acoustic branches which contribute to the same extent. One can see that for very small temperatures all curves lie on top of each other. For the system with  $D = 0.1 J$  magnons above the gap can still be excited at the temperatures shown. For this reason these optical magnons contribute too and the curve lies above the sole acoustic contribution represented by the  $D = 0$ -curve. At the same time, the magnons' velocity is increased by a finite DM-interaction. Exciting magnons further away from the  $\Gamma$ -point takes a higher temperature.

This trade-off between a higher magnon mobility and a corresponding lower heat capacity can influence the conductivity in several ways. One can compare

the insets in Figures C.4(a), 6.5(a), and 6.5(b). For the system with monodirectional DM-vectors, the magnon mobility increases in both crystallographic directions. As a result, the excitation of magnons which transport heat not just along one direction is harder and negates the positive effect of a higher magnon mobility. For the system with anisotropic DM-vectors, the magnon mobility is only enhanced in one direction and is not affected in the other. Hence, the higher mobility outperforms the lower heat capacity and the thermal conductivity increases. For the transport in the perpendicular direction, the mobility is the same, yet the heat capacity decreases. The thermal conductivity decreases as well. This implies that the magnon mobility in the system with monodirectional DM-vectors is more or less unimportant for the conductivity's low-temperature behaviour. However, it affects the conductivity in the high-temperature limit. At these temperatures, almost all magnon modes can be excited. Because of the higher mobility, the thermal conductivity is enhanced. In reality, other scattering mechanisms whose importance increases as a function of the ambient temperature, cancel this effect.

In Figure C.4(b) I show the effect of the DM-interaction by normalising the conductivity  $\kappa(D)$  to the conductivity without DM-interaction  $\kappa(0)$  for a fixed temperature. One can see that for a small DM-interaction, the conductivity decreases faster for lower temperature than for higher temperature. Because mostly the low-energy modes are excited at low temperature, a small DM-interaction is enough to prevent the gapped optical modes from contributing. At a higher temperature, it takes a higher DM-interaction to reduce the number of modes excited above the gap. For high DM-interactions, all optical modes are practically depopulated and acoustic modes make up half of the conductivity at low temperature. One can see that at such temperatures, the conductivity in the high- $D$  limit is reduced to only 50% of its initial value at vanishing DM-interaction. For temperatures below 0.4J, one can see that the curves remain relatively constant after a specific magnitude of the DM-interaction is exceeded. This value increases with temperature. The reason for this is that at higher temperature, magnons inside the gap and further away from the high-symmetry point can still be excited. When the interaction is so high that magnon modes above the gap can not be excited at a certain temperature, the conductivity does not decrease any more. At a temperature above 0.4J, magnons with a mobility which is increased by the DM-interaction can be excited in a larger number. This increases the thermal conductivity a bit, because the increase in the magnons' mobility overcompensates the decrease in their heat capacity.

One can again compare these results to the ones for the system with anisotropic DM-vectors illustrated in Figure 6.6(a) and 6.6(b). For the transport at small  $D$ , all three curves are similar. The conductivity decreases more for the system with mon-

odirectional DM-vectors in comparison to the thermal conductivity of the system with anisotropic DM-vectors. This is due to the gap growing faster as a function of the DM-interaction. Here the process of the gap opening and reducing the heat capacity of the optical magnons is the process that leads to the reduction of the thermal conductivity.

At higher  $D$ , the influence of the magnons' enhanced mobility becomes important. The magnon mobility increases only in one of the directions for the system with anisotropic DM-vectors and in both directions to equal amount for the system with isotropic DM-vectors. Hence, the thermal conductivity evolves differently for both cases. The behaviour of the system with an isotropic dispersion is discussed in the previous paragraphs. Here the increase in magnon mobility and the corresponding increase in their heat capacity compensate each other.

For the system described in the main part, the magnons' mobility is only increased in one direction, but not in the perpendicular direction. For the heat transport, this means that the excitation energy of magnons only increases in the direction where their mobility is enhanced. Therefore, the overall heat capacity decreases less. One can see that the thermal conductivity increases for all temperatures I consider, when the gap is so large that optical magnons play no longer any role in the heat transport. The higher magnon mobility is not beneficial for the thermal transport along the other direction. Contrary, in addition to the reduction in the optical magnons' heat capacity, the acoustic magnons' heat capacity is decreased as well. Hence, the thermal conductivity keeps on decreasing even when optical magnons became unimportant.

## **C.2. Magnonic thermal conductivity in a system with a spatially confined Dzyaloshinskii-Moriya interaction**

An inhomogeneous DM-interaction can be realised for a system with an intrinsic DM-interaction as well: When a magnetic material with inherent DM-interaction is put in between one or two materials without a DM-interaction, there is a heterostructure similar to the one I consider in chapter 6. I assume that all materials have the same exchange interaction  $J$  in this section. My purpose is to not unnecessarily complicate the calculations and be able to compare the results I obtain for the intrinsic DM-interaction to the results for the electric field-induced DM-interaction.

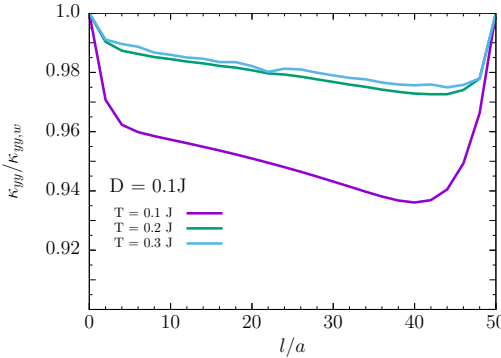


**Figure C.5.:** Thermal conductivity perpendicular to the barrier as a function of its length at different temperatures (normalised to the weighted conductivity  $\kappa_{yy,w}$  in equation (C.8))

The difference between both heterostructures is that the DM-vectors are in-plane for the electric field induced DM-interaction and out-of-plane for the intrinsic DM-interaction. As I show in the previous section, the spin-order inside the region with a finite DM-interaction is different in both systems. I find a spiral spin-order for the electric field-induced DM-interaction in the homogeneous and the inhomogeneous system when the DM-interaction does not vanish. A staggered spin-order is found in the region with non-zero DM-interaction for the system with intrinsic DM-interaction, too. I discuss the influence of the differences that can be observed between both systems' magnon dispersions and their thermal conductivity and are due to the different spin-orders. It is of interest as well, how the spin texture transitions from the Néel order in the regions without a DM-interaction to the canted order in the region with a finite DM-interaction. The influences of both differences can be seen in the thermal conductivity as a function of the ambient temperature  $T$ , the DM-interaction's strength  $D$ , and the length of the intermediate region with finite DM-interaction  $l$ .

The size of the system I consider in this section is  $50a \times 50a$ . I concentrate on the  $xx$ -component of the thermal conductivity's tensor, because it is the most interesting one. Due to symmetry reasons, the  $yy$ -component is the only other finite component. Here the conductivity is more or less an average of the conductivities of the single homogeneous regions weighted by the percentage of sites with a finite DM-interaction and the one where no DM-interaction is present, respectively:

$$\kappa_{ij,w} = \frac{L-l}{L} \kappa_{ij}(l=0) + \frac{l}{L} \kappa_{ij}(l=L). \quad (\text{C.8})$$

This fact can be observed in Figure C.5. I normalised the thermal conductivity's  $yy$ -

component to this weighted conductivity  $\kappa_{ij,w}$ . The deviations from 1 are small. I presume that these differences arise due to boundary effects I discuss in more detail for the  $xx$ -component of the thermal conductivity's tensor.

Before I discuss  $\kappa_{xx}$  as a function of  $D$ ,  $T$ , and  $l$ , I look at its frequency dependence in Figure C.6. I illustrate it for three different values of  $l$  and three values for  $D$ . Contrary to the homogeneous system (see the inset of Figure C.6(a)), which only features the DC-Drude peak, I observe peaks at non-zero  $\omega^2$ . These indicate that the current operator connects magnon modes of different energy when the field is turned on. The introduced intermediate layer acts as a center for inelastic scattering. Since the spin configurations in both regions become more distinct, it becomes harder for spin-waves to penetrate the barrier and propagate in the intermediate region. Therefore, the scattering increases with the DM-interaction's strength. For the lower energy mode of the scattering process to pass the barrier, the temperature needs to be high enough so that the higher energy mode can be excited. Effectively, the excitation energy of the modes is raised and their number is reduced more rapidly with increasing field. It is illuminating to recognise that the mean wavelength of the magnon modes is of the order of 60 sites even at a temperature  $T = 0.1J$  and a DM-interaction  $D = 1J$ . For these parameters, predominantly longer-wavelength magnons should be excited. This means that even in this extreme conditions, the barrier size is within the wavelength of most of the magnon modes contributing to the transport and can be afflicted by scattering.

It is apparent from comparing Figures C.6(a) and C.6(b) that the scattering rates are lower for the system with  $l = 26a$  than in the system with a barrier much shorter than the rest of the system. Due to the periodic boundary conditions, the system does not have a single barrier, but a periodic repetition of these. The leads to the inhomogeneity are large enough to avoid resonance effects for a system with a small or large barrier. In the system where the barrier is of the same length as the leads, resonances occur. This means that a majority of the magnon modes which are important for the thermal transport fit better into this geometry than they fit into others. As a result, magnons can be excited more easily in both parts and scattering rates are reduced. These artificially reduced scattering rates lead to an overestimation of the thermal conductivity. This is seen in some of the results.

In Figure C.7 one sees that it is inessential how long the intermediate layer is or whether the DM-interaction is present for the majority or the minority of the sites.

---

<sup>2</sup>One can compare this behaviour to the homogeneous system in chapter 6. There I observe no peak at  $\omega = 0$ . The reason for the differences is found in the boundary conditions. For the system of chapter 6 I use open boundary conditions and as a result the peak shifts to higher frequencies corresponding to the energies of the magnons with a wavelength which compensate the mismatch at the open boundaries. Since I use closed boundary conditions in this chapter, the peak is concentrated at  $\omega = 0$ .

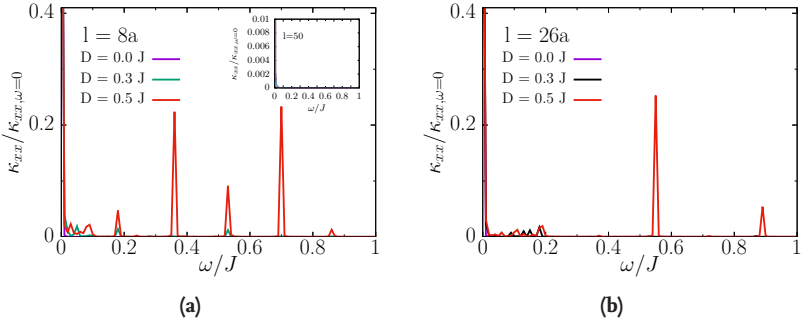


**Figure C.6.:** Thermal conductivity  $\kappa_{xx}$  as a function of frequency  $\omega$  for different length  $l$  of the intermediate barrier (a) a system with a small barrier (in the inset of (a) the AC-conductivity of the homogeneous system is shown) and (b) a system where about half of the system has a finite DM-interaction and the rest has a vanishing DM-interaction (the curves are normalised to the DC-conductivity  $\kappa_{xx}(\omega = 0)$ ). The ambient temperature is  $T = 0.3J$ .

This implies that the main reason for the stark reduction in conductivity is not the DM-interaction alone, but also the introduction of a boundary where a canted spin structure transitions into a collinear one. This corroborates the previous statement about the additional scattering at the barrier increasing the excitation energy of the magnon modes and reducing the thermal conductivity of the system.

An obvious abnormality in my results for the  $\kappa(l)$  curves in Figure C.7 are the systems with lengths of about  $26a$ . I discuss the occurrence of resonances stemming from the use of periodic boundary conditions in the previous paragraphs. The conductivity for this length of the intermediate layer is larger than for any other. Here, due to the assumed boundary conditions, regions of canted and collinear spin configuration of nearly equal size alternate. It seems that for the system with a size of the intermediate layer approximately half of the total number of sites, resonances become important as one can observe a similar behaviour for the systems with  $l = 24a$  and  $l = 28a$  at low temperature. The resonances reduce the scattering at the barrier for certain energy modes. It can be seen in Figure C.6(b) that for  $l = 26a$ , the AC-conductivity has fewer peaks for small  $\omega$  and is missing some of the larger peaks. This suggests that there is less scattering in this geometry.

I do not observe such effects for the system with a spiral order where the DM-interaction does not vanish (see Figure 6.11). For this system I have to use open boundary conditions because the Néel order on the left is rotated against the one on the right. This fact corroborates my statement about the occurrence of resonance effects. Those are averted by open boundary conditions. The thermal con-

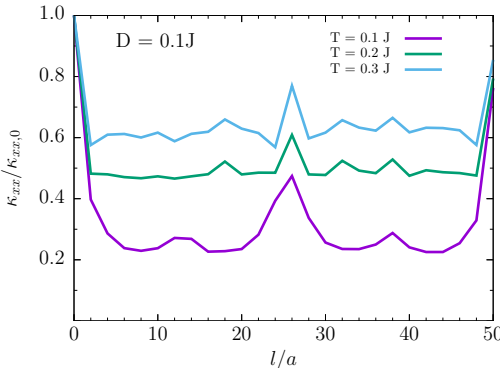


**Figure C.7:** Thermal conductivity  $\kappa_{xx}$  as a function of the length  $l$  of the intermediate barrier at different temperatures  $T$  (normalised by the value at zero DM-interaction  $\kappa_{xx,0}$ )

ductivity for such a system with infinite replicas of a single barrier is much higher than the conductivity of the single barrier alone when these resonances are possible. I am interested in the properties of the latter system and not of the former one. Hence, when one studies the transport in such inhomogeneous systems, one has to make sure that these effects are excluded. As the curves are smoother further away from  $l = 26a$ , longer leads to the inhomogeneity are a measure to avoid them.

In Figure C.8 I show the dependence of the thermal conductivity on the DM-interaction's strength in the barrier for different lengths of the latter. The results I show are for short barriers. These are similar for a system where the majority of the spins are interacting via the DM-interaction. The reasons for this are given in the discussion of Figure C.7. One can see clearly that the conductivity's drop is much sharper for the inhomogeneous systems than for the homogeneous one. Besides hampering the excitation of short-wavelength magnon modes, as I discuss in previous paragraphs, the barrier introduces an additional kind of scattering which further reduces the conductivity. Because the DM-interaction mainly affects short-wavelength magnons, a small inhomogeneity is sufficient to affect the system's ability to transport heat through it.

This behaviour is also observed for the system where the DM-interaction is induced by an external electric field. Here a small inhomogeneity also reduces the thermal conductivity, too. The relative reduction due to the scattering at the barrier is smaller, though. I argue that the reason for this is the spin texture. In the system of the main part, the spiral order in the barrier can be fitted to the Néel order left and right of it without increasing the energy at the boundaries. This is

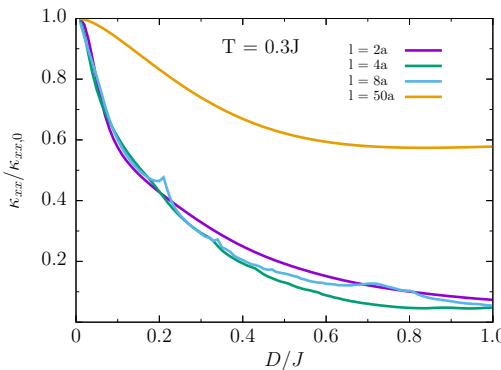


**Figure C.8.:** Thermal conductivity  $\kappa_{xx}$  as a function of the DM-interaction's strength  $D$  for different lengths of the intermediate barrier  $l$  (normalised by the value at zero DM-interaction  $\kappa_{xx,0}$ )

not possible for the staggered order in the system considered in this section. Exciting a magnon at the boundary is therefore harder in the latter system than in the former. Passing the barrier is more complicated and the decrease in the conductivity is more drastic in the system with inherent DM-interaction than for the one with field-induced DM-interaction. Another reason can be that the  $\omega$ -integration which becomes necessary due to the open boundaries, also includes some of the AC-peaks. The integration only extends up to  $\omega = 0.2J$ . In Figure C.6 one can see that the height of the peaks is quite small (of the order of a few percent of the DC-conductivity) and can not explain the difference of about 30% between the relative reduction of the conductivity in both systems.

I also observe certain bumps in the curves in Figure C.8, e.g. at  $D \approx 0.2J$  and  $D \approx 0.7J$ , for the system with  $l = 8$ . These can be explained by resonances again. For the inhomogeneous system it seems, there is a certain interval for the DM-interaction where modes important for the transport are not scattered and can then be excited at lower temperature. The reason for that is possibly that at these fields many of the modes 'fit' into the barrier while they do not before and after. Other modes, however, that are not important because the temperature is too low to excite them, do not fit and scattering at the barrier increases for these. At higher temperature, these modes are important for the transport, however, and the conductivity is reduced.

The temperature dependence of the thermal conductivity is shown in Figure C.9. One can see that the introduction of the inhomogeneity drastically reduces the ability of the system to transport heat. Especially the low-temperature behaviour is affected. This implies that the barrier has an effect on the low-energy spec-

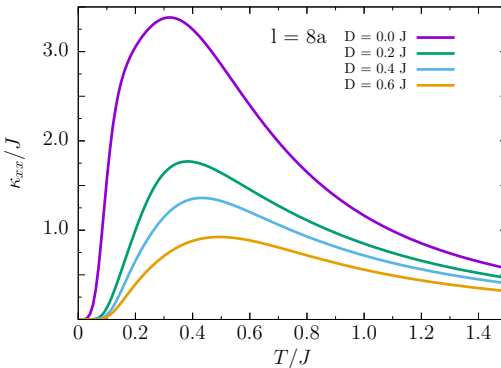


**Figure C.9:** Thermal conductivity  $\kappa_{xx}$  as a function of temperature  $T$  for different magnitudes of the DM-interaction  $D$  which is present over a length  $l$  in a system of total length  $L = 50a$  ( $a$  is the magnetic lattice constant)

trum in particular. As for the homogeneous system, the DM-interaction reduces the contribution of the short-wavelength magnons by reducing their heat capacity and mobility. At the boundaries of the barrier, exciting magnons is further complicated, since there is an energy loss at the boundary of the regions with a finite DM-interaction and the one without. This apparently increases the energy necessary for the excitation of magnons with a long-wavelength, too. The higher the DM-interaction's strength, the greater is the energy loss in the interface. This might be an additional, unintended effect of the periodic boundary conditions. Having many small barriers might affect the long-wavelength magnons' excitation, too. I argue, however, that the effect can be explained by the difference in the magnons' heat capacity in the regions with and without finite DM-interaction.

One can see that the maximum of the conductivity shifts to higher temperatures. This is in accordance with the claim that the excitation energy of magnon modes is enhanced. The peak does not shift when the scattering rate of certain modes is increased, because these are still excited at the same temperature. Only their contribution decreases. When the average energy for the excitation of a magnon increases, it takes a higher temperature to excite it and the maximum of the conductivity shifts. The shift in the conductivity's maximum is less pronounced for the system where the DM-interaction is induced by an electric field (see Figure 6.13) in comparison to the system considered in this chapter. As mentioned before, here the spin-orders in the different homogeneous regions can be fitted together without any energy loss. Therefore, the energy necessary for the excitation of a magnon beyond the interface does not change in the system with a spiral-order as much as it does for the system with canted spin-order. The low-energy spectrum

in the latter configuration is not affected as much as it is for the former canted spin structure. At the same time, the magnon mobility in the spiral-spin ordered system is only affected along the direction perpendicular to the interface. For the system considered in this chapter with monodirectional DM-vectors, the magnon mobility changes in both directions as a function of the DM-interaction's strength. The magnon heat capacity is higher at low temperature for the former system than for the latter. For this reason, the low-temperature behaviour of both systems is so different. One can see by comparing Figure C.4(b) with 6.5(a), that for the homogeneous system the low-temperature behaviour is already affected more greatly by the DM-interaction in the system with staggered spin order than in the system with spiral spin-order. The presence of the barrier only enhanced the effect. It is therefore plausible that the alteration of the low-temperature behaviour is not solely an artefact of the periodic boundary conditions.

### C.3. Summary

While I look at the influence of an electric field-induced DM-interaction in chapter 6 on the thermal transport, I show how the thermal conductivity is influenced by an inherent DM-interaction in this appendix. I consider a homogeneous as well as an inhomogeneous setup with the DM-interaction being present in this appendix, too. A crucial difference between both systems is that the former has an anisotropic DM-interaction and the latter has DM-vectors that are collinear throughout the whole lattice. As a result, the magnetic ground state is different. The system I consider in the main part orders in a spiral along one of the DM-interactions and in a Néel-like manner in the other direction. A spin-order which is canted from the Néel state and lies in the plane perpendicular to the DM-interaction is found for the system I consider here. As a result, the magnon excitation spectrum is different in both systems. For the system with anisotropic DM-vectors, the long-wavelength magnons' mobility is only enhanced in one direction, while it is increased in both directions for the system with monodirectional DM-vectors. A gap opens in both systems for the short-wavelength magnons. The size of this gap depends on the DM-interaction's strength. For the system where the DM-interaction is induced by the electric field, the gap increases not as much as a function of the DM-interaction's strength as it does in the system of this appendix. I stress the fact that the inherent DM-interaction is not as large as the DM-interaction induced by an electric field can become. The results of this section should only be considered for the purpose of comparison to the results of the main part.

The opening of the gap is the most dominant process for the reduction of the

thermal conductivity in both systems in the low-temperature limit. Since the gap grows faster as a function of the DM-interaction's strength in the system I consider here, the thermal conductivity decreases more with the DM-interaction's strength than in the system of the main part. Qualitatively, there is no difference for small DM-interaction strengths, however. For values where the gap is large enough so that optical magnons are unimportant for the thermal transport, the effect of the DM-interaction on the magnon mobility becomes important. Then, since the heat capacity decreases as fast as the mobility increases in the system with monodirectional DM-vectors, the thermal conductivity is unaffected in the low-temperature limit. For the system with anisotropic DM-vectors, the mobility increases faster in one direction and slower in the other direction than the heat capacity. Hence, the conductivity is enhanced along one direction and diminishes in the other when the DM-interaction's strength increases.

For the inhomogeneous system, I find that the effect of the barrier is more important in the system with monodirectional DM-vectors than in the system with anisotropic ones. The reason for this is most likely the fact that the optimal spin textures in the homogeneous system without and with DM-interaction can not be fitted together in the canted configuration, but can be fitted together in the spin-spiral configuration. As a result, it is harder to excite magnons in the interface of these regions. The thermal conductivity is further reduced. Because I use periodic boundary conditions for this chapter's system and open boundaries for the system in the main part, I obtain the DC-conductivity in different ways. For the periodic system, I use the value at  $\omega = 0$  of the AC-conductivity, while I integrate the AC-conductivity in a small interval for the system with open boundaries. I observe spikes in the results for the system with periodic boundaries and argue that they are a result of resonance effects. As the thermal conductivity of a system is overestimated due to these, geometries have to be avoided where they can occur. Mainly, resonances are observed in a system where the number of sites with a finite DM-interaction is equal to the number of sites without a DM-interaction. This means that the leads to the inhomogeneity need to be much larger than the size of the former.

Apart from such artefacts, I find that a small barrier is sufficient to diminish the thermal conductivity as much or even more than for the homogeneous system. The reason for this is that mainly short-wavelength magnons are affected by the DM-interaction-induced gap. This means that a short region where the excitation of magnons is complicated, is enough so that those can sense the barrier. Because these magnons contribute heavily to the thermal transport in systems without a DM-interaction, the opening of the gap dramatically reduces the system's ability to transport heat. I find this behaviour in the system with a electric field-induced

DM-interaction as well.



# Bibliography

- [1] S. Manipatruni, D. E. Nikonov, C.-C. Lin, T. A. Gosavi, H. Liu, B. Prasad, Y.-L. Huang, E. Bonturim, R. Ramesh, and I. A. Young, *Nature* **565**, 35 (2019).
- [2] A. Serga, A. Chumak, and B. Hillebrands, *Journal of Physics D: Applied Physics* **43**, 264002 (2010).
- [3] T. Schneider, A. A. Serga, B. Leven, B. Hillebrands, R. L. Stamps, and M. P. Kostylev, *Applied Physics Letters* **92**, 022505 (2008).
- [4] Y. Kajiwara, K. Harii, S. Takahashi, J.-i. Ohe, K. Uchida, M. Mizuguchi, H. Umezawa, H. Kawai, K. Ando, K. Takanashi, *et al.*, *Nature* **464**, 262 (2010).
- [5] V. Kruglyak, S. Demokritov, and D. Grundler, *Journal of Physics D: Applied Physics* **43**, 264001 (2010).
- [6] M. Kostylev, A. Serga, T. Schneider, B. Leven, and B. Hillebrands, *Applied Physics Letters* **87**, 153501 (2005).
- [7] A. V. Chumak, A. A. Serga, and B. Hillebrands, *Nature communications* **5**, 1 (2014).
- [8] K.-i. Uchida, J. Xiao, H. Adachi, J.-i. Ohe, S. Takahashi, J. Ieda, T. Ota, Y. Kajiwara, H. Umezawa, H. Kawai, *et al.*, *Nature materials* **9**, 894 (2010).
- [9] G. E. Bauer, E. Saitoh, and B. J. Van Wees, *Nature materials* **11**, 391 (2012).
- [10] A. Khitun, M. Bao, and K. L. Wang, *Journal of Physics D: Applied Physics* **43**, 264005 (2010).
- [11] P. Pirro, V. I. Vasyuchka, A. A. Serga, and B. Hillebrands, *Nature Reviews Materials* , 1 (2021).
- [12] P. Trempler, R. Dreyer, P. Geyer, C. Hauser, G. Woltersdorf, and G. Schmidt, *Applied Physics Letters* **117**, 232401 (2020).

- [13] G. Schmidt, C. Hauser, P. Trempler, M. Paleschke, and E. T. Papaioannou, *physica status solidi (b)* **257**, 1900644 (2020).
- [14] B. Lenk, H. Ulrichs, F. Garbs, and M. Münzenberg, *Physics Reports* **507**, 107 (2011).
- [15] A. Kimel, B. Ivanov, R. Pisarev, P. Usachev, A. Kirilyuk, and T. Rasing, *Nature Physics* **5**, 727 (2009).
- [16] T. L. Gilbert, *IEEE Transactions on Magnetics* **40**, 3443 (2004).
- [17] C. Hess, *Physics Reports* (2019).
- [18] Y. Nakamura, S. Uchida, T. Kimura, N. Motohira, K. Kishio, K. Kitazawa, T. Arima, and Y. Tokura, *Physica C: Superconductivity* **185**, 1409 (1991).
- [19] C. Hess, B. Büchner, U. Ammerahl, L. Colonescu, F. Heidrich-Meisner, W. Brenig, and A. Revcolevschi, *Phys. Rev. Lett.* **90**, 197002 (2003).
- [20] M. Hofmann, T. Lorenz, K. Berggold, M. Grüninger, A. Freimuth, G. S. Uhrig, and E. Brück, *Phys. Rev. B* **67**, 184502 (2003).
- [21] X. F. Sun, S. Komiya, J. Takeya, and Y. Ando, *Phys. Rev. Lett.* **90**, 117004 (2003).
- [22] X. F. Sun, J. Takeya, S. Komiya, and Y. Ando, *Phys. Rev. B* **67**, 104503 (2003).
- [23] K. Berggold, T. Lorenz, J. Baier, M. Kriener, D. Senff, H. Roth, A. Severing, H. Hartmann, A. Freimuth, S. Barilo, and F. Nakamura, *Phys. Rev. B* **73**, 104430 (2006).
- [24] S. A. Friedberg and D. Douthett, *Physica* **24**, S176 (1958).
- [25] B. Dreyfus and F. Zadworny, *Journal de Physique et le Radium* **23**, 490 (1962).
- [26] R. Berman, *Thermal Conduction in Solids* (Clarendon Press, Oxford, 1976).
- [27] J. M. Ziman, *Electrons and phonons: the theory of transport phenomena in solids* (Oxford university press, 2007).
- [28] H. Fröhlich and W. Heitler, *Proceedings of the Royal Society of London. Series A-Mathematical and Physical Sciences* **155**, 640 (1936).
- [29] B. Lüthi, *Journal of Physics and Chemistry of Solids* **23**, 35 (1962).
- [30] R. Douglass, *Phys. Rev.* **129**, 1132 (1963).

- [31] J. Rives, G. Dixon, and D. Walton, *Journal of Applied Physics* **40**, 1555 (1969).
- [32] D. Walton, J. Rives, and Q. Khalid, *Phys. Rev. B* **8**, 1210 (1973).
- [33] X. Zotos, F. Naef, and P. Prelovsek, *Phys. Rev. B* **55**, 11029 (1997).
- [34] K. Kudo, S. Ishikawa, T. Noji, T. Adachi, Y. Koike, K. Maki, S. Tsuji, and K. Kummagai, *Journal of Low Temperature Physics* **117**, 1689 (1999).
- [35] A. Sologubenko, K. Gianno, H. Ott, U. Ammerahl, and A. Revcolevschi, *Phys. Rev. Lett.* **84**, 2714 (2000).
- [36] C. Hess and C. Baumann and U. Ammerahl and B. Büchner and F. Heidrich-Meisner and W. Brenig and A. Revcolevschi, *Phys. Rev. B* **64**, 184305 (2001).
- [37] A. Sologubenko, E. Felder, K. Gianno, H. Ott, A. Vietkine, and A. Revcolevschi, *Phys. Rev. B* **62**, R6108 (2000).
- [38] A. Sologubenko, K. Gianno, H. Ott, A. Vietkine, and A. Revcolevschi, *Physical Review B* **64**, 054412 (2001).
- [39] M. Yamashita, N. Nakata, Y. Senshu, M. Nagata, H. M. Yamamoto, R. Kato, T. Shibauchi, and Y. Matsuda, *Science* **328**, 1246 (2010).
- [40] Y. Tokiwa, T. Yamashita, M. Udagawa, S. Kittaka, T. Sakakibara, D. Terazawa, Y. Shimoyama, T. Terashima, Y. Yasui, T. Shibauchi, *et al.*, *Nature communications* **7**, 1 (2016).
- [41] Y. Kasahara, K. Sugii, T. Ohnishi, M. Shimozawa, M. Yamashita, N. Kurita, H. Tanaka, J. Nasu, Y. Motome, T. Shibauchi, and Y. Matsuda, *Phys. Rev. Lett.* **120**, 217205 (2018).
- [42] R. Henrich, M. Roslova, A. Isaeva, T. Doert, W. Brenig, B. Büchner, and C. Hess, *Physical Review B* **99**, 085136 (2019).
- [43] M. I. Kaganov and A. V. Chubukov, *Soviet Physics Uspekhi* **30**, 1015 (1987).
- [44] S. Tyc and B. I. Halperin, *Phys. Rev. B* **42**, 2096 (1990).
- [45] M. E. Zhitomirsky and A. L. Chernyshev, *Review Modern Physics* **85**, 219 (2013).
- [46] A.M. Kosevich, *The Crystal Lattice: Phonons, Solitons, Dislocations, Superlattices* (Wiley Verlag, Weinheim, 2006).
- [47] E. Lifshitz and L. Pitaevskii, *Statistical Physics II* (Pergamon, Oxford, 1980).

- [48] C. Pethick and H. Smith, *Bose-Einstein Condensation in Dilute Gases* (Cambridge University Press, Cambridge, 2008).
- [49] M. B. Stone, I. Zaliznyak, T. Hong, C. L. Broholm, and D. H. Reich, *Nature* **440**, 187 (2006).
- [50] T. Masuda, A. Zheludev, H. Manaka, L.-P. Regnault, J.-H. Chung, and Y. Qiu, *Phys. Rev. Lett.* **96**, 047210 (2006).
- [51] T. Masuda, S. Kitaoka, S. Takamizawa, N. Metoki, K. Kaneko, K. C. Rule, K. Kiefer, H. Manaka, and H. Nojiri, *Phys. Rev. B* **81**, 100402 (2010).
- [52] J. Oh, M. D. Le, J. Jeong, J. h. Lee, H. Woo, W.-Y. Song, T. G. Perring, W. J. L. Buyers, S.-W. Cheong, and J.-G. Park, *Phys. Rev. Lett.* **111**, 257202 (2013).
- [53] K. W. Plumb, K. Hwang, Y. Qiu, L. W. Harriger, G. E. Granroth, A. I. Kolesnikov, G. J. Shu, F. C. Chou, C. Rüegg, Y. B. Kim, *et al.*, *Nature Physics* (2015).
- [54] J. Ma, Y. Kamiya, T. Hong, H. B. Cao, G. Ehlers, W. Tian, C. D. Batista, Z. L. Dun, H. D. Zhou, and M. Matsuda, *Phys. Rev. Lett.* **116**, 087201 (2016).
- [55] T. Hong, Y. Qiu, M. Matsumoto, D. Tennant, K. Coester, K. Schmidt, F. Awwadi, M. Turnbull, H. Agrawal, and A. Chernyshev, *Nature communications* **8**, 15148 (2017).
- [56] M. E. Zhitomirsky and A. L. Chernyshev, *Phys. Rev. Lett.* **82**, 4536 (1999).
- [57] B. C. Sales, M. Lumsden, S. E. Nagler, D. Mandrus, and R. Jin, *Phys. Rev. Lett.* **88**, 095901 (2002).
- [58] A. L. Chernyshev and M. E. Zhitomirsky, *Phys. Rev. Lett.* **97**, 207202 (2006).
- [59] I. Y. Korenblit, A. Aharony, and O. Entin-Wohlman, *Phys. Rev. B* **75**, 174420 (2007).
- [60] A. Kreisel, F. Sauli, N. Hasselmann, and P. Kopietz, *Phys. Rev. B* **78**, 035127 (2008).
- [61] M. Mourigal, M. E. Zhitomirsky, and A. L. Chernyshev, *Phys. Rev. B* **82**, 144402 (2010).
- [62] P. A. Maksimov, M. E. Zhitomirsky, and A. L. Chernyshev, *Phys. Rev. B* **94**, 140407 (2016).

- [63] P. A. Maksimov and A. L. Chernyshev, Phys. Rev. B **93**, 014418 (2016).
- [64] T. Liu and G. Vignale, Phys. Rev. Lett. **106**, 247203 (2011).
- [65] T. Moriya, Phys. Rev. Lett. **4**, 228 (1960).
- [66] I. E. Dzyaloshinskii, Soviet Physics JETP **19**, 960 (1964).
- [67] L. Shekhtman, O. Entin-Wohlman, and A. Aharony, Phys. Rev. Lett. **69**, 836 (1992).
- [68] A. L. Chernyshev, Phys. Rev. B **72**, 174414 (2005).
- [69] V. Dmitrienko, E. Ovchinnikova, S. Collins, G. Nisbet, G. Beutier, Y. Kvashnin, V. Mazurenko, A. Lichtenstein, and M. Katsnelson, Nature physics **10**, 202 (2014).
- [70] S. Singh, S. W. D' Souza, J. Nayak, E. Suard, L. Chapon, A. Senyshyn, V. Petricek, Y. Skourski, M. Nicklas, C. Felser, and S. Chadov, Nature Communications **7**, 12671 (2016).
- [71] X. Cao, K. Chen, and D. He, Journal of Physics: Condensed Matter **27**, 166003 (2015).
- [72] H. Katsura, N. Nagaosa, and A. V. Balatsky, Phys. Rev. Lett. **95**, 057205 (2005).
- [73] X. Zhang, T. Liu, M. E. Flatté, and H. X. Tang, Phys. Rev. Lett. **113**, 037202 (2014).
- [74] R. Cheng, M. W. Daniels, J.-G. Zhu, and D. Xiao, Scientific reports **6**, 24223 (2016).
- [75] G. Slack and R. Newman, Phys. Rev. Lett. **1**, 359 (1958).
- [76] H. Rosenberg and B. Sujak, Philosophical Magazine **5**, 1299 (1960).
- [77] I. Morton and H. Rosenberg, Phys. Rev. Lett. **8**, 200 (1962).
- [78] B. Dreyfus, A. Lacaze, and F. Zadworny, Comptes rendus hebdomadaires des séances de l'académie des sciences **254**, 3337 (1962).
- [79] J. Brock and D. Huntley, Canadian Journal of Physics **46**, 2231 (1968).
- [80] R. Berman, J. Brock, and D. Huntley, Physics Letters **3**, 310 (1963).

- [81] S. A. Friedberg and E. D. Harris, (1963).
- [82] R. E. Peierls, *Quantum theory of solids* (Clarendon Press, 1996).
- [83] W. Brenig and A. L. Chernyshev, Phys. Rev. Lett. **110**, 157203 (2013).
- [84] J. Kanamori, Progress of Theoretical Physics **30**, 275 (1963).
- [85] M. C. Gutzwiller, Phys. Rev. Lett. **10**, 159 (1963).
- [86] J. Hubbard, Proceedings of the Royal Society of London. Series A. Mathematical and Physical Sciences **276**, 238 (1963).
- [87] J. Hubbard, Proceedings of the Royal Society of London. Series A. Mathematical and Physical Sciences **277**, 237 (1964).
- [88] J. Hubbard, Proceedings of the Royal Society of London. Series A. Mathematical and Physical Sciences **281**, 401 (1964).
- [89] J. Hubbard, Proceedings of the Royal Society of London. Series A. Mathematical and Physical Sciences **285**, 542 (1965).
- [90] J. Hubbard, Proceedings of the Royal Society of London. Series A. Mathematical and Physical Sciences **296**, 82 (1967).
- [91] J. Hubbard, Proceedings of the Royal Society of London. Series A. Mathematical and Physical Sciences **296**, 100 (1967).
- [92] A. Auerbach, *Interacting electrons and quantum magnetism* (Springer Science & Business Media, 2012).
- [93] N. F. Mott, Proceedings of the Physical Society. Section A **62**, 416 (1949).
- [94] N. Mott, Philosophical Magazine **6**, 287 (1961).
- [95] P. W. Anderson, Phys. Rev. **115**, 2 (1959).
- [96] P. W. Anderson, in *Solid state physics*, Vol. 14 (Elsevier, 1963) pp. 99–214.
- [97] M. Cryot, Solid State Communications **8**, 1255 (1970).
- [98] P. Fazekas, *Lecture notes on electron correlation and magnetism*, Vol. 5 (World scientific, 1999).
- [99] J. M. Ziman, *Elements of advanced quantum theory* (Cambridge University Press, 1969).

- [100] P. W. Anderson, Phys. Rev. **86**, 694 (1952).
- [101] M. Trif, F. Troiani, D. Stepanenko, and D. Loss, Phys. Rev. B **82**, 045429 (2010).
- [102] J. Nossa, M. Islam, C. M. Canali, and M. Pederson, Phys. Rev. B **85**, 085427 (2012).
- [103] N. D. Mermin and H. Wagner, Phys. Rev. Lett. **17**, 1133 (1966).
- [104] I. J. Junger, D. Ihle, and J. Richter, Physical Review B **80**, 064425 (2009).
- [105] G. Toulouse, in *Modern trends in the theory of condensed matter* (Springer, 1980) pp. 195–203.
- [106] Y. Nambu, Phys. Rev. **117**, 648 (1960).
- [107] J. Goldstone, Il Nuovo Cimento (1955-1965) **19**, 154 (1961).
- [108] J. Goldstone, A. Salam, and S. Weinberg, Phys. Rev. **127**, 965 (1962).
- [109] W. Nolting, *Fundamentals of Many-body Physics* (Springer, 2008).
- [110] Mahan, G. D., *Many Body Physics* (Plenum, New York, 1981).
- [111] H. Mori, Progress of Theoretical Physics **28**, 763 (1962).
- [112] R. d. L. Kronig, Josa **12**, 547 (1926).
- [113] H. A. Kramers, in *Atti Cong. Intern. Fisica (Transactions of Volta Centenary Congress) Como*, Vol. 2 (1927) pp. 545–557.
- [114] A. A. Abrikosov, L. P. Gorkov, I. E. Dzialochinski, and R. A. Silverman, *Methods of quantum field theory in statistical physics* (Dover Publications, John Wiley & Sons, 1961).
- [115] A. L. Fetter and J. D. Walecka, *Quantum theory of many-particle systems* (Courier Corporation, 2012).
- [116] G. Källén, Helvetica Physica Acta. **25**, 417 (1952).
- [117] H. Lehmann, Il Nuovo Cimento (1943-1954) **11**, 342 (1954).
- [118] M. E. Zhitomirsky and T. Nikuni, Phys. Rev. B **57**, 5013 (1998).
- [119] S. Eggert, O. F. Syljuåsen, F. Anfuso, and M. Andres, Phys. Rev. Lett. **99**, 097204 (2007).

- [120] F. J. Dyson, Phys. Rev. **102**, 1217 (1956).
- [121] S. Maleev, Sov. Phys. JETP **6**, 776 (1958).
- [122] D. C. Mattis, *The theory of magnetism made simple: an introduction to physical concepts and to some useful mathematical methods* (World Scientific Publishing Company, 2006).
- [123] T. Holstein and H. Primakoff, Phys. Rev. **58**, 1098 (1940).
- [124] C. Landee and M. Turnbull, Molecular Crystals and Liquid Crystals Science and Technology. Section A. Molecular Crystals and Liquid Crystals **335**, 193 (1999).
- [125] X. Wan, T. A. Maier, and S. Y. Savrasov, Physical Review B **79**, 155114 (2009).
- [126] G. Liu and J. Greedan, Journal of Solid State Chemistry **114**, 499 (1995).
- [127] P. R. Hammar, D. C. Dender, D. H. Reich, A. Albrecht, and C. Landee, Journal of applied physics **81**, 4615 (1997).
- [128] S. J. Rettig, R. C. Thompson, J. Trotter, and S. Xia, Inorganic chemistry **38**, 1360 (1999).
- [129] J. Bardeen, L. N. Cooper, and J. R. Schrieffer, Phys. Rev. **106**, 162 (1957).
- [130] J. Valatin, Il Nuovo Cimento (1955-1965) **7**, 843 (1958).
- [131] N. Bogoljubov, V. V. Tolmachov, and D. Širkov, Fortschritte der Physik **6**, 605 (1958).
- [132] B. S. Shastry, Phys. Rev. B **73**, 085117 (2006).
- [133] J. Oh, M. D. Le, H.-H. Nahm, H. Sim, J. Jeong, T. Perring, H. Woo, K. Nakajima, S. Ohira-Kawamura, Z. Yamani, et al., Nature communications **7**, 13146 (2016).
- [134] W. H. Press, S. A. Teukolsky, W. T. Vetterling, and B. P. Flannery, *Numerical recipes 3rd edition: The art of scientific computing* (Cambridge university press, 2007).
- [135] A. L. Chernyshev and W. Brenig, Phys. Rev. B **92**, 054409 (2015).
- [136] N. Barbero, T. Shiroka, C. P. Landee, M. Pikulski, H.-R. Ott, and J. Mesot, Physical Review B **93**, 054425 (2016).

- [137] I. M. Miron, G. Gaudin, S. Auffret, B. Rodmacq, A. Schuhl, S. Pizzini, J. Vogel, and P. Gambardella, *Nature materials* **9**, 230 (2010).
- [138] A. Hirohata and J. Kim, *6 Optically induced and detected spin current* (London, UK: Oxford Univ. Press, 2012).
- [139] S. Maekawa, S. O. Valenzuela, E. Saitoh, and T. Kimura, *Spin current*, Vol. 22 (Oxford University Press, 2017).
- [140] N. B. Perkins, G.-W. Chern, and W. Brenig, *Physical Review B* **87**, 174423 (2013).
- [141] J. Colpa, *Physica A: Statistical Mechanics and its Applications* **93**, 327 (1978).
- [142] M. Rigol and B. S. Shastry, *Physical Review B* **77**, 161101 (2008).
- [143] F. Mandl and G. Shaw, *Quantum field theory* (John Wiley & Sons, 2010).
- [144] R. D. Klauber, *Student friendly quantum field theory: basic principles & quantum electrodynamics* (Sandtrove Press, 2013).
- [145] T. Lancaster and S. J. Blundell, *Quantum field theory for the gifted amateur* (OUP Oxford, 2014).
- [146] G.-C. Wick, *Phys. Rev.* **80**, 268 (1950).
- [147] T. Matsubara, *Progress of theoretical physics* **14**, 351 (1955).
- [148] M. Gaudin, *Nuclear Physics* **15**, 89 (1960).
- [149] T. Evans and D. Steer, *Nuclear Physics B* **474**, 481 (1996).
- [150] A. Abrikosov, L. Gorkov, and I. Dzyaloshinskii, *Sov. Phys. JETP* **9**, 636 (1959).
- [151] E. Fradkin, *Sov. Phys. JETP* **9**, 912 (1959).
- [152] P. C. Martin and J. Schwinger, *Phys. Rev.* **115**, 1342 (1959).



# **Selbstständigkeitserklärung**

Hiermit erkläre ich, dass ich die vorliegende Arbeit selbstständig angefertigt, nicht anderweitig zu Prüfungszwecken vorgelegt und keine anderen als die angegebenen Hilfsmittel verwendet habe. Sämtliche wissentlich verwendete Textausschnitte, Zitate oder Inhalte anderer Verfasser wurden ausdrücklich als solche gekennzeichnet.

Leipzig, den 25. Februar 2023

---

Benjamin Köhler